Fraunhofer Institut
Techno- und
Wirtschaftsmathematik

M. Krekel, J. Wenzel

A unified approach to Credit Default Swaption and Constant Maturity Credit Default Swap valuation

Berichte des Fraunhofer ITWM, Nr. 96 (2006)

ISSN 1434-9973

Bericht 96 (2006)

Die Veröffentlichungen in der Berichtsreihe des Fraunhofer ITWM können bezogen werden über:

Fraunhofer-Institut für Techno- und
Wirtschaftsmathematik ITWM
Fraunhofer-Platz 1

67663 Kaiserslautern
Germany

Telefon: +49 (0) 6 31/3 16 00-0
Telefax: +49 (0) 6 31/3 16 00-10 99
E-Mail: info@itwm.fraunhofer.de
Internet: www.itwm.fraunhofer.de

Vorwort

Das Tätigkeitsfeld des Fraunhofer-Instituts für Techno- und Wirtschaftsmathematik ITWM umfasst anwendungsnahe Grundlagenforschung, angewandte Forschung sowie Beratung und kundenspezifische Lösungen auf allen Gebieten, die für Techno- und Wirtschaftsmathematik bedeutsam sind.

In der Reihe »Berichte des Fraunhofer ITWM« soll die Arbeit des Instituts kontinuierlich einer interessierten Öffentlichkeit in Industrie, Wirtschaft und Wissenschaft vorgestellt werden. Durch die enge Verzahnung mit dem Fachbereich Mathematik der Universität Kaiserslautern sowie durch zahlreiche Kooperationen mit internationalen Institutionen und Hochschulen in den Bereichen Ausbildung und Forschung ist ein großes Potenzial für Forschungsberichte vorhanden. In die Berichtreihe sollen sowohl hervorragende Diplom- und Projektarbeiten und Dissertationen als auch Forschungsberichte der Institutsmitarbeiter und Institutsgäste zu aktuellen Fragen der Techno- und Wirtschaftsmathematik aufgenommen werden.

Darüber hinaus bietet die Reihe ein Forum für die Berichterstattung über die zahlreichen Kooperationsprojekte des Instituts mit Partnern aus Industrie und Wirtschaft.

Berichterstattung heißt hier Dokumentation des Transfers aktueller Ergebnisse aus mathematischer Forschungs- und Entwicklungsarbeit in industrielle Anwendungen und Softwareprodukte – und umgekehrt, denn Probleme der Praxis generieren neue interessante mathematische Fragestellungen.

Prof. Dr. Dieter Prätzel-Wolters
Institutsleiter

Kaiserslautern, im Juni 2001

A unified approach to Credit Default Swaption and Constant Maturity Credit Default Swap valuation

Martin Krekel (HypoVereinsbank München)
email: Martin.Krekel@hvb.de
Jörg Wenzel (Fraunhofer ITWM Kaiserslautern)
email: joerg.wenzel@itwm.fraunhofer.de

October 12, 2006

Kaiserslautern, Germany

Abstract

In this paper we examine the pricing of arbitrary credit derivatives with the Libor Market Model with Default Risk. We show, how to setup the Monte Carlo-Simulation efficiently and investigate the accuracy of closed-form solutions for Credit Default Swaps, Credit Default Swaptions and Constant Maturity Credit Default Swaps. In addition we derive a new closed-form solution for Credit Default Swaptions which allows for time-dependent volatility and abitrary correlation structure of default intensities.[1]

Keywords: LIBOR market model, credit risk, Credit Default Swaption, Constant Maturity Credit Default Swap

JEL classification: C31, G32

[1] The views and opinions expressed in this paper are those of the authors alone acting in their personal capacity and do not reflect the views, opinions or policies of Fraunhofer ITWM or HypoVereinsbank AG. Neither Fraunhofer ITWM nor HypoVereinsbank AG accepts any legal liability or responsibility for the accuracy, completeness or functionality of any information disclosed or described in this paper.

Contents

1 Introduction

Libor market models have become a standard model for the pricing of interest rate derivatives. The recent introduction of more instruments depending on both, interest rates and credit events, made it necessary to introduce a similar model in the credit derivatives world, see Schönbucher (2000). Such a model transfers the advantages of a Libor market model to the setting of default events and credit derivatives.

The purpose of this paper is threefold. First we consider a Monte Carlo implementation of Schönbucher's original model, using default free forward rates and discrete default intensities as model primitives. In Section **2.3** we derive the complete dynamics of the model and in Section **3.2** we collect prices for payoffs contingent on several credit events.

Second we use the implementation to value Credit Default Swaptions (CDSwaptions) and Constant Maturity Credit Default Swaps (CMCDS). In both cases, to increase accuracy of the Monte Carlo simulation, we use closed form solutions due to Schönbucher (2004) and Brigo (2005), respectively as control variates. We obtain prices for CDSwaptions and CMCDS. The results of these investigations are summarized and compared to Schönbucher's and Brigo's closed formulas in Sections **5.3** and **5.4**.

Third, in Section **5.3**, we derive a new pricing formula for CDSwaptions in the case of time varying volatilities and decorrelated discrete default intensities. We compare this formula to Schönbucher's and to prices obtained using Monte Carlo simulation.

We also investigate the influence of correlation of default intensities and risk-free interest rates on prices of credit derivatives.

2 Notation and model setup

2.1 Default model, bond prices, and basic rates

The model is set in a filtered probability space $(\Omega, (\mathcal{F}_t), \mathbf{Q})$, where the filtration satisfies the usual conditions and $\mathbf{Q}$ is the spot martingale measure. stochastic processes are adapted to $(\mathcal{F}_t)$. Given a tenor date T_k, with slight abuse of notation, we also write $\mathcal{F}_k$ instead of $\mathcal{F}_{T_k}$.

The default time is given by a stopping time τ. Default is triggered by the first jump of a Cox process N. The survival indicator function is denoted by I and is one before default and jumps to zero at the time of default, i. e.

$$I(t) = \chi_{\{\tau<t\}}.$$

Payoffs occur at discrete dates $T_0 = 0, T_1, \ldots, T_n$. The distance between two tenor dates is $\delta_k := T_{k+1} - T_k$ and the function $\kappa(t) := \min\{k : t < T_k\}$ is the next tenor date after t.

At time t, default-free zero coupon bond prices maturing at T_k are denoted by

$$B_k(t).$$

Defaultable zero coupon bond prices maturing at T_k are

$$I(t)\overline{B}_k(t).$$

These bonds have zero recovery in default and the default event, given by I and the pre-default price, given by $\overline{B}_k$ are separated.

The default-risk factors at time t for maturity T_k are

$$D_k := \frac{\overline{B}_k}{B_k}.$$

These separate the default risk from standard discounting with default-free interest rates. One can show that $D_k(0)$ is the survival probability until T_k under $\mathbf{P}_k$, that is

$$\mathbf{P}_k(\tau > T_k) = D_k(0).$$

In the case of independence it turns out that the same holds for any of the forward measures $\mathbf{P}_i$ with $i \geq k$, to be introduced in Section **2.2**.

The default-free effective forward rate over the period $[T_k, T_{k+1}]$ as seen from t is

$$F_k := \frac{1}{\delta_k}\Big(\frac{B_k}{B_{k+1}} - 1\Big).$$

Similarly the defaultable effective forward rate is

$$\overline{F}_k := \frac{1}{\delta_k}\Big(\frac{\overline{B}_k}{\overline{B}_{k+1}} - 1\Big).$$

The forward credit spread S_k is the difference between defaultable and default-free effective forward rate, that is

$$S_k = \overline{F}_k - F_k. \tag{1}$$

The discrete-tenor forward default intensity over $[T_k, T_{k+1}]$ as seen from t is

$$H_k := \frac{1}{\delta_k}\Big(\frac{D_k}{D_{k+1}} - 1\Big).$$

2.2 Forward measures and dynamics of risk free rates

Associated with the numeraire B_k is the T_k-*forward measure* $\mathbf{P}_k$. It is defined by the property that all discounted prices S/B_k of securities S (in particular of all the zero bonds $B_1, \ldots, B_n$) are martingales. In order to change numeraires between the different B_k, the density

$$\frac{d\mathbf{P}_k}{d\mathbf{P}_{k+1}} = \frac{B_k}{B_{k+1}} \cdot \frac{B_{k+1}(0)}{B_k(0)} = \frac{1 + \delta_k F_k}{1 + \delta_k F_k(0)}$$

will be used.

Under $\mathbf{P}_{k+1}$ the process B_k/B_{k+1} must be a martingale, hence also F_k must be a martingale. Assuming a lognormal volatility distribution, we therefore have

$$\frac{dF_k}{F_k} = \sigma_k^F \, dW_{k+1} \tag{2}$$

for a vector of d independent $\mathbf{P}_{k+1}$-Brownian motions W_{k+1} and deterministic, possibly time dependent volatilities σ_k^F. The suitable dimension d will be specified later. Usually we will have 2 factors, one driving the interest rates F_k and one driving the discrete default intensities H_k.

Since at time T_i the bonds B_j with $j < i$ have expired already, the measures $\mathbf{P}_j$ with $j < i$ cannot be used to price payoffs occurring at T_i. On the other hand,

using a measure $\mathbf{P}_j$ with $j > i$ to price payoffs occurring at T_i adds superfluous volatility to calculation and thus decreases the accuracy of the Monte Carlo simulation. Therefore payoffs at time T_i should be priced if possible under the measure $\mathbf{P}_i$.

To this end, we want to specify the dynamics of F_k under a generic measure $\mathbf{P}_i$. Under such a measure the forward rates F_k have drifts $\mu^F_{k,i}$, depending on the index k of the rate F_k and on the index i of the measure $\mathbf{P}_i$, such that

$$\frac{dF_k}{F_k} = \mu^F_{k,i}\, dt + \sigma^F_k\, dW_i,$$

where W_i is a $\mathbf{P}_i$-Brownian motion. To obtain the drifts $\mu^F_{k,i}$, we use Equation (2) and Girsanov's theorem to find that for a $\mathbf{P}_k$-Brownian motion W_k the equation

$$dW_{k+1} = \frac{\delta_k F_k}{1+\delta_k F_k}\sigma^F_k\, dt + dW_k \tag{3}$$

defines a $\mathbf{P}_{k+1}$-Brownian motion W_{k+1}. Iterative application of this formula yields the drift under the measure $\mathbf{P}_i$ for any i.

2.3 Survival measures and dynamics of risky rates

Associated with the numeraire $I\overline{B}_k$ is another measure $\overline{\mathbf{P}}_k$, the T_k-*survival measure*. It is used to price defaultable payoffs at T_k. These survival measures are not equivalent to the measures $\mathbf{P}_k$, since they attach zero probability to events after default. They are however absolutely continuous to the $\mathbf{P}_k$ and therefore Girsanov's theorem still applies.

We obtain the density

$$\frac{d\overline{\mathbf{P}}_k}{d\mathbf{P}_k} = I \cdot \frac{\overline{B}_k}{B_k} \cdot \frac{B_k(0)}{\overline{B}_k(0)} = I\frac{D_k}{D_k(0)}. \tag{4}$$

The survival measure technique is explained in more detail in Schönbucher (2004) and Schönbucher (2003).

Note that it is not appropriate to specify the dynamics of the risky interest rates $\overline{F}_k$ directly in a similar fashion to (2), since then it cannot be ensured that we always have $\overline{F}_k \geq F_k$. Therefore the following two ways of specifying the dynamics of the defaultable interest rates can be used.

(1) The discrete default intensities H_k have lognormal volatility distribution.
(2) The forward credit spreads S_k have lognormal volatility distribution.

Choosing the first alternative above, we assume a lognormal volatility structure for the H_k as follows

$$\frac{dH_k}{H_k} = \mu_k^H\, dt + \sigma_k^H\, dW_n, \tag{5}$$

for deterministic, possibly time dependent d-dimensional volatility vectors σ_k^H.

We can also write down the dynamics of the risky forward rates $\overline{F}_k$ and the spreads S_k, but their volatilities are now longer deterministic. The following relations allow to calculate the volatility parameters $\sigma_k^{\overline{F}}$ and σ_k^S from given volatilities σ_k^H and σ_k^F.

Fact: Writing

$$\frac{d\overline{F}_k}{\overline{F}_k} = \mu_k^{\overline{F}}\, dt + \sigma_k^{\overline{F}}\, dW_n, \tag{6}$$

and

$$\frac{dS_k}{S_k} = \mu_k^S\, dt + \sigma_k^S\, dW_n, \tag{7}$$

we have

$$\overline{F}_k \sigma_k^{\overline{F}} = F_k \sigma_k^F + S_k \sigma_k^S, \tag{8}$$

$$\sigma_k^H = \sigma_k^S - \frac{\delta_k F_k}{1+\delta_k F_k}\sigma_k^F, \tag{9}$$

$$\overline{F}_k \sigma_k^{\overline{F}} = (1+\delta_k F_k) H_k \sigma_k^H + (1+\delta_k H_k) F_k \sigma_k^F. \tag{10}$$

Proof: From the definitions

$$d\overline{F}_k = dF_k + dS_k = (F_k \mu_k^F + S_k \mu_k^S)\, dt + (F_k \sigma_k^F + S_k \sigma_k^S)\, dW_n. \tag{11}$$

Comparing the volatility terms in (6) and (11) yields (8).

In order to connect the volatilities of H_k and S_k, we use the definitions in Section **2.1** to see that

$$1+\delta_k H_k = \frac{D_k}{D_{k+1}} = \frac{\overline{B}_k}{\overline{B}_{k+1}} \cdot \frac{B_{k+1}}{B_k} = \frac{1+\delta_k \overline{F}_k}{1+\delta_k F_k} = 1 + \frac{\delta_k S_k}{1+\delta_k F_k}.$$

Therefore

$$H_k = \frac{S_k}{1+\delta_k F_k} \tag{12}$$

and it follows that the log-volatility of H_k is the difference of the log-volatility of S_k and $1+\delta_k F_k$. Now

$$\frac{d(1+\delta_k F_k)}{1+\delta_k F_k} = \frac{\delta_k F_k}{1+\delta_k F_k}\mu_k^F\, dt + \frac{\delta_k F_k}{1+\delta_k F_k}\sigma_k^F\, dW_n. \tag{13}$$

So that (5) gives (9).

Finally, inserting (12) and (9) into (8), we obtain (10). □

If we want to find a Brownian motion under $\overline{\mathbf{P}}_k$, by Girsanov's theorem, we have to find the log-volatility of the density $d\overline{\mathbf{P}}_k/d\mathbf{P}_k$, that is essentially the volatility of $\log(ID_k)$, see (4). Namely, defining σ_k^D as the volatility of $\log(ID_k)$ by

$$\frac{d(ID_k)}{ID_k} = \mu_k^D\, dt + \sigma_k^D\, dW_k,$$

Girsanov's theorem says that

$$d\overline{W}_k := -\sigma_k^D\, dt + dW_k \tag{14}$$

defines a $\overline{\mathbf{P}}_k$-Brownian motion $\overline{W}_k$. See (Rebonato, 1998, App. A.8) for a non-technical explanation of Girsanov's theorem.

Similarly as before, it follows that given a $\overline{\mathbf{P}}_k$-Brownian motion $\overline{W}_k$ a $\overline{\mathbf{P}}_{k+1}$-Brownian motion $\overline{W}_{k+1}$ is defined by

$$d\overline{W}_{k+1} = \frac{\delta_k \overline{F}_k}{1+\delta_k \overline{F}_k}\sigma_k^{\overline{F}}\, dt + d\overline{W}_k. \tag{15}$$

Under the T_{k+1}-survival measure the process $\overline{B}_k/\overline{B}_{k+1}$ must be a martingale, hence also $\overline{F}_k$ must be a martingale and it follows that

$$\frac{d\overline{F}_k}{\overline{F}_k} = \sigma_k^{\overline{F}}\, d\overline{W}_{k+1}.$$

Now note that

$$\frac{\delta_k \overline{F}_k}{1+\delta_k \overline{F}_k}\sigma_k^{\overline{F}} = \frac{H_k\delta_k}{1+\delta_k H_k}\sigma_k^H + \frac{F_k\delta_k}{1+\delta_k F_k}\sigma_k^F,$$

therefore we can find a recursion formula for the σ_k^D using (3) and (15) as

$$\sigma_k^D - \sigma_{k+1}^D = \frac{\delta_k H_k}{1+\delta_k H_k}\sigma_k^H. \tag{16}$$

Apparently $\sigma_0^H = 0$, hence $\sigma_0^D = 0$ so that

$$\sigma_k^D = -\sum_{j=0}^{k-1} \frac{\delta_j H_j}{1+\delta_j H_j}\sigma_j^H. \tag{17}$$

It is now easy to write down the dynamics of F_k and H_k under $\overline{\mathbf{P}}_{k+1}$ as follows:

$$dF_k = F_k\sigma_k^F\sigma_{k+1}^D\,dt + F_k\sigma_k^F\,d\overline{W}_{k+1},$$
$$dH_k = -\frac{F_k}{1+\delta_k F_k}\big((1+\delta_k H_k)\sigma_{k+1}^D + \delta_k H_k\sigma_k^H\big)\sigma_k^F\,dt + H_k\sigma_k^H\,d\overline{W}_{k+1}.$$

In order to derive the dynamics under a generic measure $\overline{\mathbf{P}}_i$, we use

$$d\overline{W}_{k+1} = d\overline{W}_k + \frac{\delta_k\overline{F}_k}{1+\delta_k\overline{F}_k}\sigma_k^{\overline{F}}\,dt$$

to obtain a $\overline{\mathbf{P}}_{k+1}$-Brownian motion.

To obtain shorter formulas, we use throughout the notations

$$f_k = \delta_k F_k, \quad \overline{f}_k = \delta_k\overline{F}_k, \quad h_k = \delta_k H_k, \text{ and } \quad s_k = \delta_k S_k.$$

These quantities are connected by the formulas

$$\overline{f}_k = f_k + h_k(1+f_k), \qquad \overline{f}_k\sigma_k^{\overline{F}} = (1+f_k)h_k\sigma_k^H + (1+h_k)f_k\sigma_k^F,$$
$$s_k = h_k(1+f_k), \qquad \sigma_k^S = \sigma_k^H + \frac{f_k}{1+f_k}\sigma_k^F,$$

which can be used to eliminate s_k and $\overline{f}_k$.

We also write

$$\Sigma_{l,m}^F := \sum_{j=l}^{m-1}\frac{f_j}{1+f_j}\sigma_j^F \quad \text{and} \quad \Sigma_{l,m}^H := \sum_{j=l}^{m-1}\frac{h_j}{1+h_j}\sigma_j^H.$$

These are the essential building stones of the drift corrections and can be seen as weighted integrated volatilities.

Then under a generic measure $\overline{\mathbf{P}}_i$ the dynamics of f_k and h_k are given by

$$\frac{df_k}{f_k} = \big(-\Sigma_{0,i}^H\sigma_k^F - \Sigma_{k+1,i}^F\sigma_k^F\big)\,dt + \sigma_k^F\,d\overline{W}_i, \tag{18}$$
$$\frac{dh_k}{h_k} = \Big(\frac{f_k}{1+f_k}\frac{1+h_k}{h_k}\Sigma_{0,k}^H\sigma_k^F - \Sigma_{k+1,i}^H\sigma_k^H - \Sigma_{k+1,i}^F\sigma_k^H\Big)\,dt + \sigma_k^H\,d\overline{W}_i,$$

if $k+1 \le i$ and

$$\frac{df_k}{f_k} = \big(-\Sigma_{0,i}^H\sigma_k^F + \Sigma_{i,k+1}^F\sigma_k^F\big)\,dt + \sigma_k^F\,d\overline{W}_i, \tag{19}$$
$$\frac{dh_k}{h_k} = \Big(\frac{f_k}{1+f_k}\frac{1+h_k}{h_k}\Sigma_{0,k}^H\sigma_k^F + \Sigma_{i,k+1}^H\sigma_k^H + \Sigma_{i,k+1}^F\sigma_k^H\Big)\,dt + \sigma_k^H\,d\overline{W}_i,$$

if $k+1 > i$.

In the best possible of all worlds, for simulation, the measure $\overline{\mathbf{P}}_i$ should be chosen such that $i = k+1$. Then f_k and h_k are «nearly» martingales and the dynamics simplifies significantly:

$$\frac{df_k}{f_k} = -\Sigma^H_{0,k+1}\sigma^F_k\,dt + \sigma^F_k\,d\overline{W}_{k+1},$$
$$\frac{dh_k}{h_k} = \frac{f_k}{1+f_k}\frac{1+h_k}{h_k}\Sigma^H_{0,k}\sigma^F_k\,dt + \sigma^H_k\,d\overline{W}_{k+1}$$

However, this will not always be possible. If e. g. the payoff at time T_i depends on several or all of the rates $F_0,\ldots,F_{n-1}$, the simulation of $F_0,\ldots,F_{n-1}$ should be done under the measure $\overline{\mathbf{P}}_i$. The remaining drift terms in the above equations can only be avoided if we assume independence of interest rates and default, as we will see in the next section.

Simulation under independence

If default and riskless forward rates are independent, then $\sigma^H_k\sigma^F_j = 0$ for all k, j, which also means that all the mixed products of $\Sigma^H_{\cdot,\cdot}\sigma^F_\cdot$ and $\Sigma^F_{\cdot,\cdot}\sigma^H_\cdot$ are zero, see Section **2.4**. Therefore the dynamics of h_k and f_k under the measure $\overline{\mathbf{P}}_i$ simplifies to:

$$\frac{df_k}{f_k} = \Sigma^F_{k+1,i}\sigma^F_k\,dt + \sigma^F_k\,d\overline{W}_i,$$
$$\frac{dh_k}{h_k} = -\Sigma^H_{k+1,i}\sigma^H_k\,dt + \sigma^H_k\,d\overline{W}_i \tag{20}$$

if $k+1 \le i$ and

$$\frac{df_k}{f_k} = \Sigma^F_{i,k+1}\sigma^F_k\,dt + \sigma^F_k\,d\overline{W}_i,$$
$$\frac{dh_k}{h_k} = \Sigma^H_{i,k+1}\sigma^H_k\,dt + \sigma^H_k\,d\overline{W}_i \tag{21}$$

if $k+1 > i$.

2.4 Correlation and calibration

For implementation purposes, we will use two Brownian motions, one driving the risk-free interest rates F_k (which are hence assumed to be perfectly correlated), and one driving the default intensities H_k (which are hence also perfectly correlated).

Besides calibration of the default-free part of the model (which determines σ^F_k),

defaultable bond prices $\overline{B}_k$ can be calibrated to observed defaultable bond prices, default swap rates and asset swap rates, which gives parameters $\sigma_k^{\overline{F}}$ and hence also σ_k^H. Finally parameters σ_k^D can be obtained from the recursion formula (16).

Once all the volatilities are specified, the drifts follow from the respective change of measure formulas.

The expected recovery rate R is needed as an input, too. We will assume a given constant expected recovery rate R.

Assuming independence of default-free bond prices and time of default under this model means that the volatility vectors σ_k^F of all forward rates F_k are orthogonal to the volatility vectors σ_l^H of the default intensities H_l, that is $\sigma_k^F \sigma_l^H = 0$ for all $k, l = 1, 2, \ldots, n$. In particular, one can think of σ_k^F having zero second component and σ_l^H having zero first component, so that the F_ks are driven by one Brownian motion and the H_ks are driven by another independent Brownian motion. The correlation of dependent defaults is then influenced by the size of the (non-zero) first component of σ_k^H.

3 General payoffs

3.1 Zero bonds

To price a defaultable payoff X at time T_k, its price $p(0)$ at time $T_0 = 0$ is calculated under the terminal survival measure $\overline{\mathbf{P}}_n$ as

$$p(0) = \mathbb{E}^{\overline{\mathbf{P}}_n}\Big[X \cdot \frac{\overline{B}_n(0)}{\overline{B}_n(T_k)}\Big].$$

In particular the prices of defaultable zero bonds can be recovered as

$$\begin{aligned}
\overline{B}_k(0) &= \mathbb{E}^{\overline{\mathbf{P}}_n}\Big[\frac{\overline{B}_n(0)}{\overline{B}_n(T_k)}\Big] \\
&= \overline{B}_n(0)\mathbb{E}^{\overline{\mathbf{P}}_n}\big[(1+\overline{f}_{n-1}(T_k)) \cdot \cdots \cdot (1+\overline{f}_k(T_k))\big] \\
&= \overline{B}_n(0)\mathbb{E}^{\overline{\mathbf{P}}_n}\big[(1+h_{n-1}(T_k)) \cdot \cdots \cdot (1+h_k(T_k)) \\
&\qquad\qquad (1+f_{n-1}(T_k)) \cdot \cdots \cdot (1+f_k(T_k))\big].
\end{aligned}$$

This formula can be used as a test for the accuracy of a Monte Carlo implementation. See Section **4**.

3.2 Defaultable payoffs

The following formulas show that the model can be used to price arbitrary payoffs depending on default or survival of the reference party. Note that the payoffs X can depend on all forward rates $F_0, \ldots, F_{n-1}$ as well as on the default intensities $H_0, \ldots, H_{n-1}$ and therefore also on observed bond prices $B_1, \ldots, B_n$ and $\overline{B}_1, \ldots, \overline{B}_n$.

The proofs of these formulas can be found in (Schönbucher, 2000, Proposition 3 and Appendix).

Proposition:

(1) *The price at time* 0 *of a contract paying at* T_{k+1} *the amount* X *if no default happened before* T_{k+1} *or* 0 *if a default happened before* T_{k+1} *is*

$$\overline{B}_n(0)\mathbb{E}^{\overline{\mathbf{P}}_n}\Big[\frac{X}{\overline{B}_n(T_{k+1})}\Big] = \overline{B}_{k+1}(0)\mathbb{E}^{\overline{\mathbf{P}}_{k+1}}[X].$$

(2) *The price at time* 0 *of a contract paying at* T_{k+1} *the amount* $X(T_k)$ *if no default happened before* T_k *or* 0 *if a default happened before* T_k *is*

$$\overline{B}_n(0)\mathbb{E}^{\overline{\mathbf{P}}_n}\Big[\frac{X}{\overline{B}_n(T_{k+1})}(1+h_k(T_k))\Big] = \overline{B}_{k+1}(0)\mathbb{E}^{\overline{\mathbf{P}}_{k+1}}\big[X(1+h_k(T_k))\big].$$

(3) *The price at time* 0 *of a contract paying at* T_{k+1} *the amount* $X(T_k)$ *if a default happened between* T_k *and* T_{k+1} *or* 0 *if no default happened between* T_k *and* T_{k+1} *is*

$$\overline{B}_n(0)\mathbb{E}^{\overline{\mathbf{P}}_n}\Big[\frac{X}{\overline{B}_n(T_{k+1})}h_k(T_k)\Big] = \overline{B}_{k+1}(0)\mathbb{E}^{\overline{\mathbf{P}}_{k+1}}\big[Xh_k(T_k)\big]$$

Note that defaults or their probabilities need not be modeled directly but are incorporated into the formulas by simulating under the *survival* measure. This approach contrasts the one taken in Bennani and Dahan (2004) for multi name credit derivatives, where besides the processes h_k so called default accumulator processes ε_k are simulated under the forward measures $\mathbf{P}_k$ to obtain default times.

3.3 Defaultable payoffs under independence

If the payoffs X in the previous section depend only on $F_0, \ldots, F_{n-1}$ and not on $H_0, \ldots, H_{n-1}$ and if default intensities and interest rates are independent we can significantly simplify the formulas of the previous section.

(1) *The price at time* 0 *of a contract paying at* T_{k+1} *the amount* X *if no default happened before* T_{k+1} *or* 0 *if a default happened before* T_{k+1} *is*

$$\overline{B}_{k+1}(0)\mathbb{E}^{\mathbf{P}_{k+1}}[X].$$

(2) *The price at time* 0 *of a contract paying at* T_{k+1} *the amount* $X(T_k)$ *if no default happened before* T_k *or* 0 *if a default happened before* T_k *is*

$$\overline{B}_{k+1}(0)\mathbb{E}^{\mathbf{P}_{k+1}}[X](1+\delta_k H_k(0)).$$

(3) *The price at time* 0 *of a contract paying at* T_{k+1} *the amount* $X(T_k)$ *if a default happened between* T_k *and* T_{k+1} *or* 0 *if no default happened between* T_k *and* T_{k+1} *is*

$$\overline{B}_{k+1}(0)\mathbb{E}^{\mathbf{P}_{k+1}}[X]\delta_k H_k(0).$$

4 Monte Carlo setup

We priced several credit derivatives using a Monte Carlo pricer based on this model using real world data. We usually used quarterly tenor dates and for the discretization of the Euler scheme put ten to twenty intermediate time steps between these tenor dates.

As we also found, a simulation under the terminal survival measure T_n yields very high variance, forcing us to use a high number of MC runs to obtain a reasonable accuracy. Therefore we usually priced all payoffs simulating under the T_k-survival measure where T_k is the date the payoff occurs at T_k. Even if this involves multiple simulations for each payoff date $T_1, \ldots, T_n$ this method turns out to yield the same accuracy faster than using only the single terminal measure.

Using control variates increases accuracy by a factor of four to five, thus speeding up calculation by 15 to 25 times.

As input for our model we use the tenor dates, riskless and risky zero bond prices, volatilities for the default intensities and interest rates, a given correlation between interest rates and default, and a constant recovery rate. All other parameters are obtained from these input values. As we will show the volatility of interest rates has only a negligible effect on prices of standard derivatives. Under the assumptions of zero interest rate volatility simulation can be done much faster and it takes about 3 to 4 seconds to price a CDSwaption or around 20 seconds to price a CMCDS with accuracy of 1% of the price.

The initial values $h_k(0)$ and $f_k(0)$ are obtained directly from initial zero bond prices using the definition, while default intensities $h_k(t)$ and forward rates $f_k(t)$ are obtained from equations (18) and (19) in the dependent or (20) and (21) in the independent case using a standard log-Euler scheme. We also tried a predictor-corrector algorithm but found, that it does not yield much enhancement.

As tenor dates, we used quarterly dates starting from today. The initial risky and riskless zero bond prices were given as in the following table.

Date	$B_k(0)$	$\overline{B}_k(0)$	Date	$B_k(0)$	$\overline{B}_k(0)$
today	1.000000000	1.000000000	63m	0.837825795	0.796597667
3m	0.993864466	0.993656891	66m	0.830042391	0.785064871
6m	0.986772847	0.986360812	69m	0.822199336	0.773574888
9m	0.979314304	0.978355834	72m	0.814364493	0.762191393
12m	0.971434331	0.969926913	75m	0.806864865	0.751303738
15m	0.964246967	0.961710691	78m	0.799057422	0.740138004
18m	0.956337173	0.952732155	81m	0.791094000	0.728841693
21m	0.948187661	0.943510892	84m	0.783413581	0.718027315
24m	0.940271501	0.934576615	87m	0.776250081	0.707632008
27m	0.932511725	0.925077675	90m	0.768387240	0.696437380
30m	0.924582647	0.915444248	93m	0.760789961	0.685713550
33m	0.916471618	0.905664707	96m	0.753064353	0.674972498
36m	0.908505453	0.896043345	99m	0.745614342	0.664575413
39m	0.900697577	0.885303735	102m	0.738173761	0.654281514
42m	0.892784470	0.874490739	105m	0.730798658	0.644139329
45m	0.884786790	0.863626517	108m	0.723345606	0.633982566
48m	0.876813834	0.852851627	111m	0.716117224	0.624192080
51m	0.869122271	0.841735229	114m	0.708811279	0.614385254
54m	0.861186494	0.830342540	117m	0.701526132	0.604649098
57m	0.853276128	0.819058887	120m	0.694246572	0.595007846
60m	0.845320657	0.807816030			

Table 1 Initial zero bond prices used for MC simulation

5 Closed form solutions and numerical results

5.1 Forward Credit Default Swaps (CDS)

A forward Credit Default Swap (forward CDS) starting at T_k consists of two payment legs

(1) the fixed, or premium leg, paying $s\delta_i$ at T_{i+1} for all $i = k, \ldots, n-1$, if no default happened before T_{i+1} and

(2) the floating, credit, or protection leg, paying $(1-R)$ at T_{i+1} for all $i = k, \ldots, n-1$, if a default happened between T_i and T_{i+1}.

Here s is the CDS spread and R is the recovery rate.

The value at any time $t \leq T_k$ of the fixed leg of a forward CDS is therefore

$$V_{premium}(t) = s \sum_{i=k}^{n-1} \delta_i \overline{B}_{i+1}(t).$$

The value at time t of the i-th payment of the floating leg of the forward CDS is given by payoff (3) discussed in Section **3.2** as

$$(1-R)\overline{B}_{i+1}(t)\mathbb{E}^{\overline{\mathbf{P}}_{i+1}}[h_i(T_i)|\mathcal{F}_t].$$

Therefore the value of the floating leg of the forward CDS is

$$V_{credit}(t) = (1-R) \sum_{i=k}^{n-1} \overline{B}_{i+1}(t)\mathbb{E}^{\overline{\mathbf{P}}_{i+1}}[h_i(T_i)|\mathcal{F}_t]. \tag{22}$$

Under the assumption of independence we have seen that h_i is in fact a martingale under $\overline{\mathbf{P}}_{i+1}$ and therefore $\mathbb{E}^{\overline{\mathbf{P}}_{i+1}}[h_i(T_i)|\mathcal{F}_t] = h_i(t)$ and it follows that

$$V_{credit}(t) = (1-R)\sum_{i=k}^{n-1} \overline{B}_{i+1}(t)h_i(t).$$

The (k,n)-forward swap rate $\overline{s}_{k,n}$ is the rate of a forward CDS starting at T_k and running for $n-k$ periods, such that the value of the premium leg equals the value of the credit leg. It is given as

$$\overline{s}_{k,n}(t) = (1-R)\frac{\sum_{i=k}^{n-1} \overline{B}_{i+1}(t)\mathbb{E}^{\overline{\mathbf{P}}_{i+1}}\big[h_i(T_i)\big|\mathcal{F}_t\big]}{\sum_{i=k}^{n-1}\delta_i\overline{B}_{i+1}(t)}. \tag{23}$$

Using the notation

$$\overline{w}_i(t) = \frac{\overline{B}_{i+1}(t)}{\sum_{j=k}^{n-1}\delta_j\overline{B}_{j+1}(t)},$$

we can rewrite this formula as

$$\overline{s}_{k,n}(t) = (1-R)\sum_{i=k}^{n-1}\overline{w}_i(t)\mathbb{E}^{\overline{\mathbf{P}}_{i+1}}\big[h_i(T_i)\big|\mathcal{F}_t\big].$$

In particular the $(k,k+1)$-forward swap rate is

$$\overline{s}_{k,k+1}(t) = (1-R)E^{\overline{\mathbf{P}}_{k+1}}\big[H_k(T_k)\big|\mathcal{F}_t\big],$$

which under the assumption of independence equals $(1-R)H_k(t)$.

To examine the actual dependence of $\overline{s}_{k,n}$ on the interest rate volatility, we next derive an approximation for $\mathbb{E}^{\overline{\mathbf{P}}_{i+1}}[h_i(T_i)|\mathcal{F}_t]$; see (Schönbucher, 2000, Proposition 3).

Proposition: We assume that
(1) $\sigma_i^D = \sigma_i^D(t)$ is constant between t and T_i, see (17) on page 6 for the definition of σ_i^D
(2) $\sigma_i^F/(1+f_i) = \sigma_i^F/(1+f_i(t))$ is constant.
Under these assumptions for $\Delta_t = T_i - t \geq 0$ we get

$$\begin{aligned}\mathbb{E}^{\overline{\mathbf{P}}_{i+1}}[h_i(T_i)|\mathcal{F}_t] &= h_i(t)\exp\Big(\frac{\Delta_t\sigma_i^D(t)\sigma_i^F}{1+f_i(t)}\Big) + \overline{f}_i(t)\left(1-\exp\Big(\frac{\Delta_t\sigma_i^D(t)\sigma_i^F}{1+f_i(t)}\Big)\right)\\ &= h_i(t) + f_i(t)\big(1+h_i(t)\big)\left(1-\exp\Big(\frac{\Delta_t\sigma_i^D(t)\sigma_i^F}{1+f_i(t)}\Big)\right).\end{aligned}$$

In the case of non-constant, time-dependent volatilities, the products

$$\Delta_t \sigma_j^H \sigma_i^F$$

have to be replaced by the integrals

$$\int_t^{T_i} \sigma_j^H(s)\sigma_i^F(s)\,ds = \sum_{l=k}^{i-1} \delta_l \sigma_j^H(T_l)\sigma_i^F(T_l).$$

where for the last equality we assumed that volatilities remain constant between tenor dates.

Proof: First observe that by a change of measure

$$\overline{B}_{i+1}(t)\mathbb{E}^{\overline{\mathbf{P}}_{i+1}}[1+h_i(T_i)|\mathcal{F}_t] = \overline{B}_i(t) - \overline{B}_i(t)\mathbb{E}^{\overline{\mathbf{P}}_i}\Big[\frac{f_i(T_i)}{1+f_i(T_i)}\Big|\mathcal{F}_t\Big].$$

Therefore we focus on $\mathbb{E}^{\overline{\mathbf{P}}_i}\big[f_i(T_i)/(1+f_i(T_i))\big|\mathcal{F}_t\big]$. Switching to the measure $\mathbf{P}_i$ yields

$$\mathbb{E}^{\overline{\mathbf{P}}_i}\Big[\frac{f_i(T_i)}{1+f_i(T_i)}\Big|\mathcal{F}_t\Big] = \frac{1}{I(t)D_i(t)}\mathbb{E}^{\mathbf{P}_i}\Big[\frac{f_i(T_i)}{1+f_i(T_i)}I(T_i)D_i(T_i)\Big|\mathcal{F}_t\Big].$$

Now $I\cdot D_i = I\overline{B}_i/B_i$ as well as $f_i/(1+f_i) = 1 - B_{i+1}/B_i$ are martingales under $\mathbf{P}_i$ so that the dynamics of their product essentially depends on their respective log-volatilities. The log-volatility of $I\cdot D_i$ is σ_i^D and was already calculated in (17), while the log-volatility of $f_i/(1+f_i)$ can be found via Itô's formula as $\sigma_i^F/(1+f_i)$.

Note that the conditional expectation of a lognormal process X with (non-stochastic) drift μ and (non-stochastic) log-volatility σ is given as

$$\mathbb{E}[X(T)|\mathcal{F}_t] = X(t)\exp\Big(\int_t^T \mu(s)\,ds\Big).$$

Also, the drift of the product of two lognormal martingales is given as the product of their respective log-volatilities, which easily follows from Itô again. To get a non-stochastic drift, we have however to assume that this product of the log-volatilities of $f_i/(1+f_i)$ and of $I\cdot D_i$ is constantly equal to $\sigma_i^F\sigma_i^D(t)/(1+f_i(t))$. Also, in order to be able to evaluate the expectation, we need non-stochastic volatility of the product process, which essentially amounts to the assumptions of constant drifts σ_i^D and $\sigma_i^F/(1+f_i)$.

This yields

$$\mathbb{E}^{\mathbf{P}_i}\Big[\frac{f_i(T_i)}{1+f_i(T_i)}I(T_i)D_i(T_i)\Big|\mathcal{F}_t\Big] = \frac{f_i(t)}{1+f_i(t)}I(t)D_i(t)\exp\Big(\frac{(T_i-t)\sigma_i^D(t)\sigma_i^F}{1+f_i(t)}\Big).$$

Putting everything together, the claimed formula follows. □

Note that in case of independence we have $\sigma_i^H \sigma_i^F = 0$ so that $\sigma_i^D(t)\sigma_i^F = 0$ for all t and all the exponentials in the formula above equal 1, so in this special case the formula reduces to the known fact that h_i is a martingale under $\overline{\mathbf{P}}_{i+1}$.

We next price a five year CDS with quarterly payments, starting today for the issuer described at the end of Section **4**. The volatility of the discrete default intensities $|\sigma^H|$ was usually held at 60%, if not otherwise stated. For the recovery rate we chose a fixed value of 40%.

Since the influence of correlation is very small, we had to obtain small standard deviation and a high number of runs for the Monte Carlo implementation. So we used a Monte Carlo simulation with $200\,000$ runs and 20 intermediate time steps between tenor dates in the Euler scheme. We also use the uncorrelated case as a control variate. Calculation of one CDS rate took about four hours in the correlated cases.

The next table shows CDS rates depending on the correlation of default and interest rates

$$\rho = \frac{\sigma^F \sigma^H}{|\sigma^F| \cdot |\sigma^H|}$$

for different interest rate volatilities $|\sigma^F|$ and volatilities of default intensities $|\sigma^H|$ calculated exactly with a Monte Carlo Simulation (MC) and with the help of the closed form approximation formula proved above (CF). The standard deviation of the Monte Carlo Simulation is given as $\pm StandardDeviation$.

$\lvert\sigma^F\rvert$ | $\lvert\sigma^H\rvert$	$\rho = -100\%$	$\rho = -50\%$	$\rho = 0\%$	$\rho = +50\%$	$\rho = +100\%$
10% | 60%	$0.519\%\pm0.002\%$	$0.521\%\pm0.001\%$	$0.523\%\pm0.000\%$	$0.526\%\pm0.001\%$	$0.531\%\pm0.002\%$
CF:	0.520%	0.522%	0.523%	0.525%	0.527%
40% | 60%	$0.510\%\pm0.002\%$	$0.516\%\pm0.001\%$	$0.523\%\pm0.000\%$	$0.534\%\pm0.001\%$	$0.553\%\pm0.002\%$
CF:	0.508%	0.516%	0.523%	0.531%	0.539%
10% | 120%	$0.525\%\pm0.015\%$	$0.514\%\pm0.009\%$	$0.523\%\pm0.000\%$	$0.532\%\pm0.009\%$	$0.534\%\pm0.013\%$
CF:	0.516%	0.520%	0.523%	0.527%	0.531%
40% | 120%	$0.512\%\pm0.015\%$	$0.505\%\pm0.009\%$	$0.523\%\pm0.000\%$	$0.551\%\pm0.010\%$	$0.587\%\pm0.014\%$
CF:	0.492%	0.508%	0.523%	0.539%	0.553%

Table 2 MC simulation results for CDS rates depending on correlation of interest rates and default intensities

The graph on page 16 shows the results of the Monte Carlo Simulation, where the standard deviation is given in the error bars.

It can be seen from the MC results, that the influence of correlation on the CDS rate is very small. In particular for negative correlation, which can be observed in the market (see (Longstaff and Schwartz, 1995, p. 808)), even for a 120% default intensity volatility and 40% interest rate volatility and correlation of -100% the CDS rate deviates only by one basis point from the CDS rate for the uncorrelated case. The closed formula captures the correct tendency of

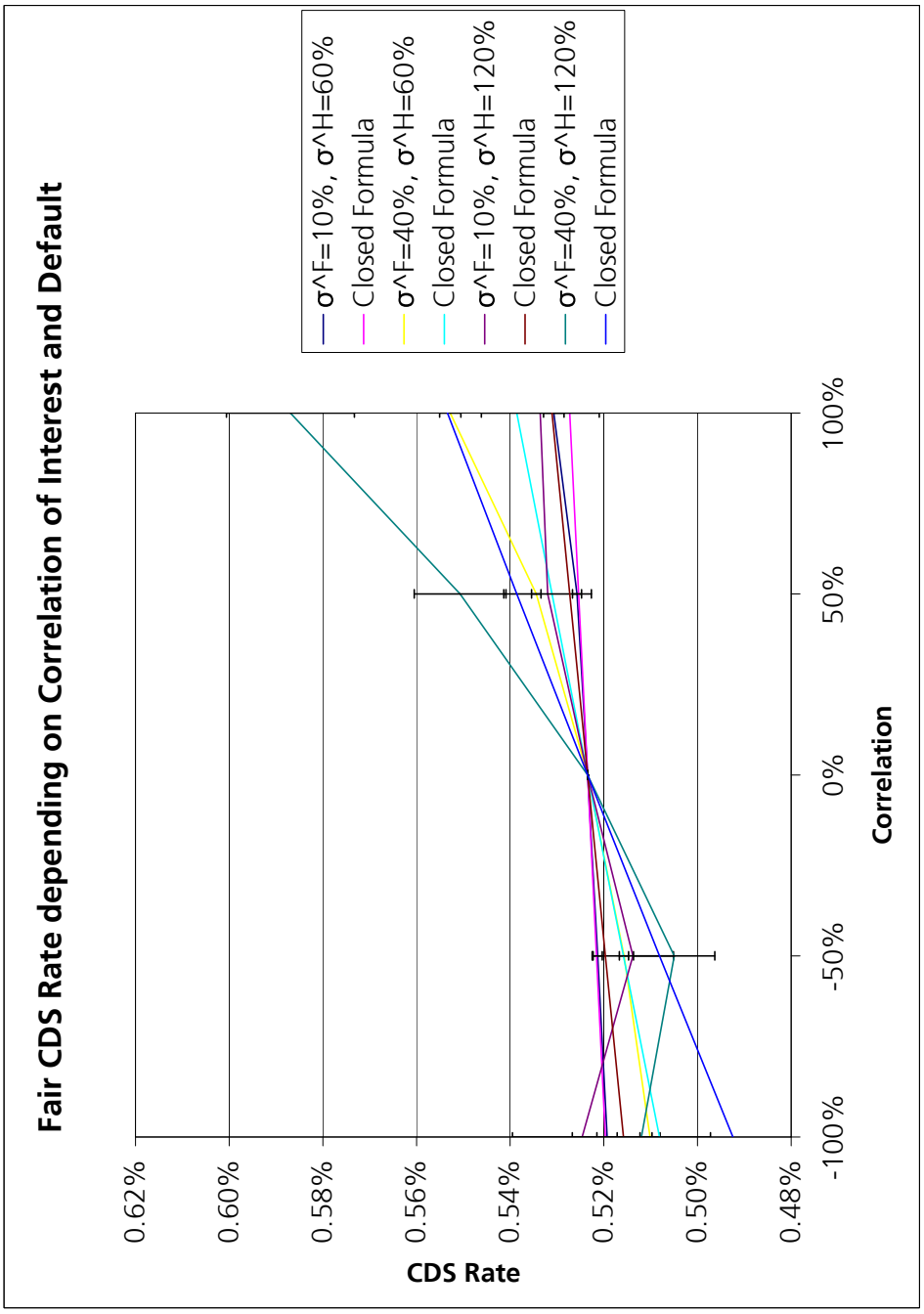

Figure 1 CDS rates depending on correlation of interest rates and default intensities

deviation from the uncorrelated case, but especially for negative correlations the error introduced by the closed formula approximation is the same order of magnitude as the deviation from the uncorrelated case. Summarizing, it does not seem to be useful to take correlation of interest rates and defaults into account when calculating CDS rates.

5.2 Credit Default Swaptions (CDSwaptions)

A Credit Default Swaption (CDSwaption) is an option on a forward starting CDS.

The payoff function of the Credit Default Swaption Call at T_k is $V_{credit}(T_k) - V_{premium}(T_k)$ if this value is positive and 0 otherwise. That is

$$\begin{aligned}
V^{call}_{swaption}(T_k) &= \big(V_{credit}(T_k) - V_{premium}(T_k)\big)^+ \\
&= \Big((1-R)\sum_{i=k}^{n-1} \overline{B}_{i+1}(T_k)\mathbb{E}^{\overline{\mathbf{P}}_{i+1}}[h_i(T_i)|\mathcal{F}_k] - s\sum_{i=k}^{n-1}\delta_i\overline{B}_{i+1}(T_k)\Big)^+ \\
&= \sum_{i=k}^{n-1}\delta_i\overline{B}_{i+1}(T_k)\Big((1-R)\frac{\sum_{i=k}^{n-1}\overline{B}_{i+1}(T_k)\mathbb{E}^{\overline{\mathbf{P}}_{i+1}}[h_i(T_i)|\mathcal{F}_k]}{\sum_{i=k}^{n-1}\delta_i\overline{B}_{i+1}(T_k)} - s\Big)^+ \\
&= \sum_{i=k}^{n-1}\delta_i\overline{B}_{i+1}(T_k)\big(\overline{s}_{k,n}(T_k) - s\big)^+.
\end{aligned}$$

Hence the value of the swaption at time $T_0 = 0$ is

$$\begin{aligned}
V^{call}_{swaption}(0) &= \mathbb{E}^{\overline{\mathbf{P}}_k}\Big[\sum_{i=k}^{n-1}\delta_i\overline{B}_{i+1}(T_k)\big(\overline{s}_{k,n}(T_k) - s\big)^+\Big]\overline{B}_k(0) \\
&= \sum_{i=k}^{n-1}\delta_i\overline{B}_{i+1}(0)\mathbb{E}^{\overline{\mathbf{P}}_{i+1}}\big[\big(\overline{s}_{k,n}(T_k) - s\big)^+\big].
\end{aligned}$$

Under several assumptions, namely
(1) independence,
(2) homogeneous and constant volatility, $\sigma^H = \sigma^H_i$ for all i,
(3) default intensities only driven by *one* Brownian motion, and
(4) the weights $\overline{w}_i$ are constant over time,
Schönbucher (2000), Schönbucher (2003), and Schönbucher (2004) derives a closed form solution as follows.

Firstly it follows from assumption (1) that

$$\overline{s}_{k,n}(T_k) = (1-R)\sum_{i=k}^{n-1}\overline{w}_i(T_k)h_i(T_k).$$

Next, from condition (4) we get

$$\overline{s}_{k,n}(T_k) = (1-R)\sum_{i=k}^{n-1} \overline{w}_i(0) h_i(T_k), \tag{24}$$

which implies for the dynamics of $\overline{s}_{k,n}$ that

$$d\overline{s}_{k,n} = (1-R)\sum_{i=k}^{n-1} \overline{w}_i(0) dh_i.$$

The Swaption can now be priced under the measure $\overline{\mathbf{P}}^s$ associated with the numeraire $X(t) = I(t)\sum_{i=k}^{n-1} \delta_i \overline{B}_{i+1}(t)$. The density process of this numeraire is

$$\frac{d\overline{\mathbf{P}}_{i+1}}{d\overline{\mathbf{P}}^s} = \frac{I\overline{B}_{i+1}}{\overline{B}_{i+1}(0)} \cdot \frac{\sum_{j=k}^{n-1} \delta_j \overline{B}_{j+1}(0)}{I\sum_{j=k}^{n-1} \delta_j \overline{B}_{j+1}} = \frac{\overline{w}_i}{\overline{w}_i(0)}.$$

Therefore, under assumption (4) the density process is constant over time and there is no drift correction when changing measure from $\overline{\mathbf{P}}_{i+1}$ to $\overline{\mathbf{P}}^s$, that is, under $\overline{\mathbf{P}}^s$ the intensities h_i are driftless:

$$d\overline{s}_{k,n} = (1-R)\sum_{i=k}^{n-1} \overline{w}_i(0) h_i \sigma_i^H \, dW.$$

Finally from assumptions (2) and (3) it follows that

$$\frac{d\overline{s}_{k,n}}{\overline{s}_{k,n}} = \sigma^H \, dW,$$

that is $\overline{s}_{k,n}$ is lognormal with volatility σ^H.

It now follows from

$$V^{call}_{swaption}(0) = \mathbb{E}^{\overline{\mathbf{P}}^s}\left[\left(\overline{s}_{k,n}(T_k) - s\right)^+\right] \sum_{i=k}^{n-1} \delta_i \overline{B}_{i+1}(0), \tag{25}$$

using the standard Black-Scholes formula that

$$V^{call}_{swaption}(0) = \sum_{i=k}^{n-1} \delta_i \overline{B}_{i+1}(0)\big(\overline{s}_{k,n}(0) N(d_1) - sN(d_2)\big), \tag{26}$$

where

$$d_{1,2} = \frac{\ln(\overline{s}_{k,n}(0)/s) \pm (\sigma^H)^2 T_k/2}{\sigma^H \sqrt{T_k}}.$$

Weakening assumption (2), the case of time dependent volatilities can be treated by using

$$(\sigma^H)^2 T_k = \int_0^{T_k} \sigma^H(t)^2 \, dt = \sum_{l=0}^{k-1} \delta_l \sigma^H(T_l)^2,$$

where for the last equality, we assumed that the volatility remains constant between tenor dates T_l. The case of inhomogeneous volatilities will be covered in the next section.

As a consequence, we can use for our calculations a control variate, satisfying assumptions (1) through (4) and using the closed form solution (26) as correction value.

For this control variate, we simulate the intensities H_i under the swap measure $\overline{\mathbf{P}}^s$ and have to take into account, that there is no drift under this measure.

Note that this formula does not involve the volatility structure of default-free interest rates F_i, although even in what we call here the «independent» case, there is a slight dependence of CDSwaption prices on these interest rate volatilities. As Monte Carlo shows however, this dependence is almost negligible. Only for interest rate volatilities far above 100% we could observe an increase of CDSwaption prices by more than one basis point.

Table 3 shows CDSwaption prices calculated with Monte Carlo (exact prices MC) and with the approximating closed formula (CF) depending on the volatility parameter σ^H.

As a basis for these calculations, we used the same issuer as in Section **5.1** and priced an option on a five year CDS starting in one year from today with quarterly payments and strike set at 0.8%. All other parameters are the same as before. In particular we used a Monte Carlo simulation with $2\,000\,000$ runs and 20 intermediate time steps, which took about one hour.

The difference between Closed form solution and Monte Carlo result is also shown in the next graph on page 20. The standard deviations of the Monte Carlo simulation are given as error bars. Since we violate only condition (4) of the assumptions for the closed form formula, this difference is indeed very small, in the order of less than one basis point.

5.3 CDSwaptions under decorrelation of default intensities

Next we derive a formula similar to (26) but using multiple driving Brownian motions for the default intensities H_i and also inhomogeneous, time-dependent

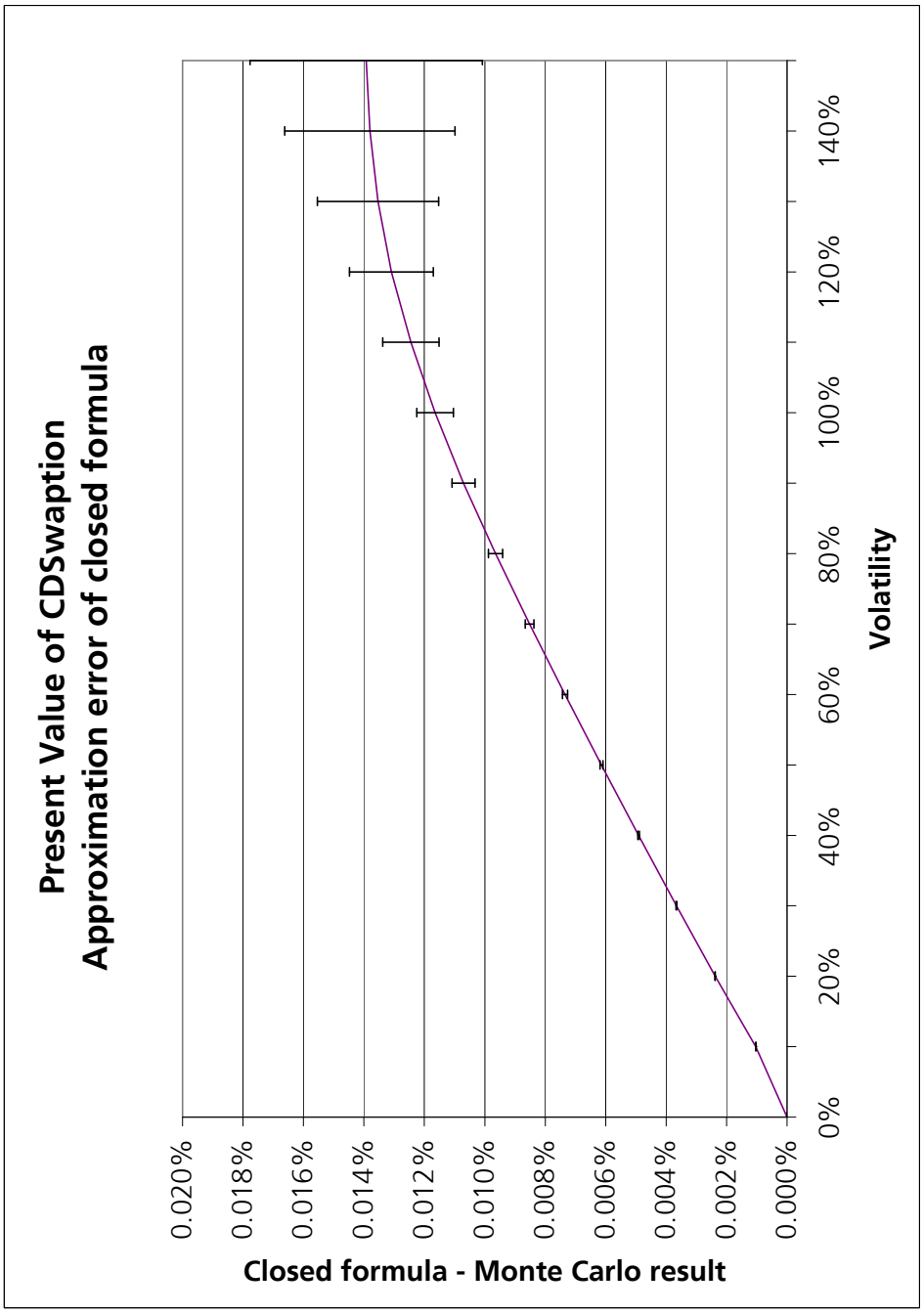

Figure 2 CDSwaption PV — approximation error of closed formula depending on volatility of default intensities

σ^H	Swaption call price	σ^H	Swaption call price
0%	MC: $0.000\%_{\pm 0.000\%}$	80%	MC: $0.935\%_{\pm 0.000\%}$
	CF: 0.000%		CF: 0.945%
10%	MC: $0.054\%_{\pm 0.000\%}$	90%	MC: $1.057\%_{\pm 0.000\%}$
	CF: 0.056%		CF: 1.067%
20%	MC: $0.175\%_{\pm 0.000\%}$	100%	MC: $1.175\%_{\pm 0.001\%}$
	CF: 0.177%		CF: 1.187%
30%	MC: $0.303\%_{\pm 0.000\%}$	110%	MC: $1.291\%_{\pm 0.001\%}$
	CF: 0.306%		CF: 1.304%
40%	MC: $0.431\%_{\pm 0.000\%}$	120%	MC: $1.404\%_{\pm 0.001\%}$
	CF: 0.436%		CF: 1.417%
50%	MC: $0.560\%_{\pm 0.000\%}$	130%	MC: $1.513\%_{\pm 0.002\%}$
	CF: 0.566%		CF: 1.527%
60%	MC: $0.687\%_{\pm 0.000\%}$	140%	MC: $1.620\%_{\pm 0.003\%}$
	CF: 0.694%		CF: 1.634%
70%	MC: $0.812\%_{\pm 0.000\%}$	150%	MC: $1.723\%_{\pm 0.004\%}$
	CF: 0.821%		CF: 1.737%

Table 3 MC simulation results for present value of CDSwaption calls depending on volatility of default σ^H

volatilities σ_i^H for the different i. This will in particular be useful when using e. g. hump shaped volatility structures.

We assume that the default intensities have lognormal volatility structure

$$\frac{dh_k}{h_k} = \mu_k^H \, dt + \sigma_k^H \, d\overline{W}_n,$$

for deterministic n-dimensional volatility vectors σ_k^H and a vector of n independent Brownian motions $(\overline{W}_{n,0}, \ldots, \overline{W}_{n,n-1})$ under the terminal survival measure $\overline{\mathbf{P}}_n$. By a suitable Cholesky decomposition, we can assume that the volatility vectors $\sigma_k^H = (\sigma_{k,0}^H, \ldots, \sigma_{k,n-1}^H)$ have lower triangular form, i. e. $\sigma_{k,j}^H = 0$ for $j > k$. Moreover, the instantaneous correlation of the returns of h_i and h_j is given as

$$\rho_{ij} = \frac{\sigma_i^H \sigma_j^H}{|\sigma_i||\sigma_j|}, \tag{27}$$

where $\sigma_i^H \sigma_j^H$ denotes the scalar product of the volatility vectors σ_i^H and σ_j^H and $|\sigma_i^H| = \sqrt{\sigma_i^H \sigma_i^H}$ is the Euclidean norm of σ_i^H.

Recall that the dynamics of h_k under a different measure $\overline{\mathbf{P}}_i$ are given by

$$\frac{dh_k}{h_k} = \mu_{k,i}^H \, dt + \sigma_k^H \, d\overline{W}_i,$$

where under independence of interest rates and defaults by (20)

$$\mu^H_{k,i} = -\sum_{j=k+1}^{i-1} \frac{h_j}{1+h_j}\sigma^H_j\sigma^H_k$$

if $k+1 \le i$ and by (21)

$$\mu^H_{k,i} = \sum_{j=i}^{k} \frac{h_j}{1+h_j}\sigma^H_j\sigma^H_k$$

if $k+1 > i$.

The following assumptions and approximations will be used
(1) interest rates and defaults are independent,
(2) the weights $\overline{w}_i$ are constant over time,
(3) furthermore we will approximate the sum of lognormal processes by a lognormal process with the same mean and variance.

Proposition 1: Under the assumptions above, we obtain for the price of the Credit Default Swaption Call

$$V^{call}_{swaption}(0) = \sum_{i=k}^{n-1} \delta_i \overline{B}_{i+1}(0)\big(\overline{s}_{k,n}(0)N(d_1) - sN(d_2)\big),$$

where

$$d_{1,2} = \frac{\ln(\overline{s}_{k,n}(0)/s) \pm \sigma^2/2}{\sigma},$$

and

$$\sigma^2 = \ln\left(\frac{\sum_{i,j=k}^{n-1}\overline{w}_i(0)\overline{w}_j(0)h_i(0)h_j(0)\exp\left(\int_0^{T_k}\sigma^H_i(s)\sigma^H_j(s)\,ds\right)}{\sum_{i,j=k}^{n-1}\overline{w}_i(0)\overline{w}_j(0)h_i(0)h_j(0)}\right)$$
$$= \ln\left(\frac{\sum_{i,j=k}^{n-1}\overline{B}_{i+1}(0)\overline{B}_{j+1}(0)h_i(0)h_j(0)\exp\left(\int_0^{T_k}\sigma^H_i(s)\sigma^H_j(s)\,ds\right)}{\sum_{i,j=k}^{n-1}\overline{B}_{i+1}(0)\overline{B}_{j+1}(0)h_i(0)h_j(0)}\right).$$

Proof: Using assumption (2), we obtain as before formula (25), but this time $\overline{s}_{k,n}$ is not lognormal itself under $\overline{\mathbf{P}}^s$ but is a sum of the lognormal intensities h_i which are driftless under $\overline{\mathbf{P}}^s$. We now approximate $\overline{s}_{k,n}(T_k)$ by a random variable X with the same first and second moment, but whose logarithm *is* normally distributed

$$\ln(X) \sim N(\mu, \sigma^2).$$

This method is known as moment matching or Levy approximation; see Levy (1992).

Now since under $\overline{\mathbf{P}}^s$ the forward rate $\overline{s}_{k,n}$ is driftless, we obtain for the first

moment of $\overline{s}_{k,n}(T_k)$ the value

$$\mathbb{E}^{\overline{\mathbf{P}}^s}[\overline{s}_{k,n}(T_k)] = \overline{s}_{k,n}(0),$$

for the second moment however get from the dynamics

$$\frac{dh_i}{h_i} = \sigma_i^H \, d\overline{W}^s$$

that

$$\mathbb{E}^{\overline{\mathbf{P}}^s}\big[h_i(T_k)h_j(T_k)\big] = h_i(0)h_j(0)\exp\Big(\int_0^{T_k} \sigma_i^H(s)\sigma_j^H(s)\,ds\Big),$$

which yields the more complicated expression

$$\mathbb{E}^{\overline{\mathbf{P}}^s}[\overline{s}_{k,n}(T_k)^2] = (1-R)^2 \sum_{i,j=k}^{n-1} \overline{w}_i(0)\overline{w}_j(0)h_i(0)h_j(0)\exp\Big(\int_0^{T_k} \sigma_i^H(s)\sigma_j^H(s)\,ds\Big).$$

On the other hand, the first two moments of X are

$$\begin{aligned}\mathbb{E}^{\overline{\mathbf{P}}^s}[X] &= \exp(\mu + \sigma^2/2),\\ \mathbb{E}^{\overline{\mathbf{P}}^s}[X^2] &= \exp(2\mu + 2\sigma^2).\end{aligned}$$

Matching the moments provides the formulas

$$\begin{aligned}\mu &= \ln(\overline{s}_{k,n}(0)) - \frac{1}{2}\sigma^2,\\ \sigma^2 &= \ln\left(\frac{\sum_{i,j=k}^{n-1} \overline{w}_i(0)\overline{w}_j(0)h_i(0)h_j(0)\exp(\sigma_i^H\sigma_j^H T_k)}{\overline{s}_{k,n}(0)^2}\right).\end{aligned}$$

Now, replacing $\overline{s}_{k,n}(T_k)$ by X in (25) yields

$$V_{call}^{swaption} = \sum_{i=k}^{n-1} \delta_i \overline{B}_{i+1}(0)\mathbb{E}^{\overline{\mathbf{P}}^s}[(X-s)^+].$$

which easily evaluates to the desired formula using

$$\ln(X) \sim N(\mu, \sigma^2)$$

and the expressions above for μ and σ^2.

□

Note that if $\sigma_i^H = \sigma^H$ is the same for all i we obtain

$$\sigma^2 = (\sigma^H)^2 T_k$$

and Schönbucher's formula follows.

Also, using the relation between correlation and volatility vectors (27), we can write the value of σ^2 as

$$\sigma^2 = \ln\left(\frac{\sum_{i,j=k}^{n-1} \overline{B}_{i+1}(0)\overline{B}_{j+1}(0)h_i(0)h_j(0)\exp(\rho_{ij}|\sigma_i^H||\sigma_j^H|T_k)}{\sum_{i,j=k}^{n-1} \overline{B}_{i+1}(0)\overline{B}_{j+1}(0)h_i(0)h_j(0)}\right).$$

And if all the intensities are perfectly correlated ($\rho_{ij} = 1$), we get

$$\sigma^2 = \ln\left(\frac{\sum_{i,j=k}^{n-1} \overline{B}_{i+1}(0)\overline{B}_{j+1}(0)h_i(0)h_j(0)\exp(|\sigma_i^H||\sigma_j^H|T_k)}{\sum_{i,j=k}^{n-1} \overline{B}_{i+1}(0)\overline{B}_{j+1}(0)h_i(0)h_j(0)}\right).$$

We further remark, that one can in fact derive a similar formula using the survival measures $\overline{\mathbf{P}}_i$ instead of the CDS-measure $\overline{\mathbf{P}}^s$. Then the resulting formula also involves the drifts $\mu_{k,i}^H$ at time 0.

Proposition 2: Assuming moreover constant drift terms $\mu_{k,i}^H$, we obtain for the price of the Credit Default Swaption Call

$$V_{swaption}^{call}(0) = \sum_{i=k}^{n-1} \delta_i \overline{B}_{i+1}(0)\big(M_i N(d_i^1) - sN(d_i^2)\big),$$

where

$$d_i^{1,2} = \frac{\ln(M_i/s) \pm \sigma_i^2/2}{\sigma_i},$$

$$M_i = (1-R)\sum_{j=k}^{n-1} c_{i,j}(T_k),$$

and

$$\sigma_i^2 = \ln\left(\frac{\sum_{l,j=k}^{n-1} c_{i,j}(T_k)c_{i,l}(T_k)\exp(\sigma_l^H \sigma_j^H T_k)}{\sum_{l,j=k}^{n-1} c_{i,j}(T_k)c_{i,l}(T_k)}\right),$$

and

$$c_{i,j}(T_k) = \overline{w}_j(0)h_j(0)\exp(\mu_{j,i+1}^H T_k).$$

A proof can be found in Acar (2006).

The disadvantage of the last formula is of course, that it does not recover Schönbucher's original formula for CDSwaptions if all the volatilities are constant and equal.

Finally we derive yet another approximation formula for the CDSwaption value, which corresponds to the one given in (Brigo and Mercurio, 2001, Prop. 6.13.1, p. 248) as Rebonato's formula in the setting of interest rate swaps.

To this end, we approximate $\overline{s}_{k,n}$ itself by a lognormal process by making the volatility of $\log(\overline{s}_{k,n})$ deterministic. Note that

$$\frac{d\overline{s}_{k,n}}{\overline{s}_{k,n}} = \sum_{i=k}^{n-1} \frac{\overline{w}_i(0)h_i}{\overline{s}_{k,n}} \sigma_i^H \, d\overline{W}^s. \tag{28}$$

Now approximating (as before for the $\overline{w}_i$'s) the fractions in the expression above by their initial value at time zero, makes $\overline{s}_{k,n}$ a lognormal process with volatility

$$\sigma^2 = \frac{\sum_{i,j=k}^{n-1} \overline{w}_i(0)\overline{w}_j(0)h_i(0)h_j(0) \int_0^{T_k} \sigma_i^H(s)\sigma_j^H(s)\, ds}{\sum_{i,j=k}^{n-1} \overline{w}_i(0)\overline{w}_j(0)h_i(0)h_j(0)}.$$

The approximation error should be small, at least for small deviations from a perfectly correlated default intensity structure.

Proposition 3: Using the approximation above leads to the following closed form valuation formula for CDSwaptions:

$$V_{swaption}^{call}(0) = \sum_{i=k}^{n-1} \delta_i \overline{B}_{i+1}(0)\big(\overline{s}_{k,n}(0)N(d_1) - sN(d_2)\big),$$

where

$$d_{1,2} = \frac{\ln(\overline{s}_{k,n}(0)/s) \pm \sigma^2/2}{\sigma},$$

and

$$\sigma^2 = \frac{\sum_{i,j=k}^{n-1} \delta_i\delta_j\overline{w}_i(0)\overline{w}_j(0)H_i(0)H_j(0) \int_0^{T_k} \sigma_i^H(s)\sigma_j^H(s)\, ds}{\sum_{i,j=k}^{n-1} \delta_i\delta_j\overline{w}_i(0)\overline{w}_j(0)H_i(0)H_j(0)}.$$

Proof: The proof is a direct application of Black's option pricing formula using Equation (28). □

We compared all four formulas (Schönbucher's original and the ones derived in Propositions 1 to 3) to the real value of a CDSwaption using Monte Carlo under different term structures of volatilities. The volatilities are given by the formula

$$\sigma_n^H(t) = \gamma_1 \exp(-\gamma_2(T_n - t))(1 + \gamma_3(T_n - t)))$$

with the two scenarios
(1) $\gamma_1 = 0.015$, $\gamma_2 = 0.4$, and $\gamma_3 = 50$,

(2) $\gamma_1 = 0.03$, $\gamma_2 = 0.6$, and $\gamma_3 = 25$,
giving hump shaped volatility structures as shown on page 29. The volatilities are assumed to depend only on time to expiration, so that $\sigma_i^H(T_k) = \sigma_n^H(T_{n+k-i})$ and stay constant between tenor dates. Except for the now varying volatility structures, we used the same setting as in Section **5.2**. In Schönbucher's formula (26) we used the average of all tenor volatilities at time T_l as volatility parameter $\sigma^H(T_l)$.

The comparison of the results can be found in the following table and the approximation errors are plotted in the charts on pages 30–31.

Strike	Swaption price	CF (26)	CF Prop. 1	CF Prop. 2	CF Prop. 3
0.0%	3.260%±0.000%	3.260%	3.260%	3.267%	3.260%
0.1%	2.827%±0.000%	2.826%	2.826%	2.834%	2.826%
0.2%	2.397%±0.000%	2.396%	2.398%	2.405%	2.397%
0.3%	1.988%±0.000%	1.985%	1.991%	1.999%	1.991%
0.4%	1.622%±0.000%	1.614%	1.629%	1.635%	1.627%
0.5%	1.310%±0.000%	1.297%	1.318%	1.324%	1.316%
0.6%	1.052%±0.000%	1.035%	1.062%	1.067%	1.060%
0.7%	0.843%±0.000%	0.822%	0.853%	0.858%	0.851%
0.8%	0.675%±0.000%	0.653%	0.686%	0.690%	0.684%
0.9%	0.542%±0.000%	0.519%	0.552%	0.556%	0.550%
1.0%	0.436%±0.000%	0.413%	0.446%	0.449%	0.444%
1.1%	0.352%±0.000%	0.329%	0.361%	0.364%	0.359%
1.2%	0.285%±0.000%	0.264%	0.293%	0.296%	0.291%
1.3%	0.232%±0.000%	0.212%	0.239%	0.241%	0.237%
1.4%	0.189%±0.000%	0.171%	0.196%	0.197%	0.194%
1.5%	0.155%±0.000%	0.138%	0.181%	0.162%	0.159%
1.6%	0.127%±0.000%	0.112%	0.133%	0.134%	0.131%
1.7%	0.105%±0.000%	0.092%	0.110%	0.111%	0.108%
1.8%	0.087%±0.000%	0.075%	0.091%	0.092%	0.090%
1.9%	0.072%±0.000%	0.062%	0.076%	0.077%	0.075%
2.0%	0.060%±0.000%	0.051%	0.064%	0.064%	0.063%
2.1%	0.050%±0.000%	0.042%	0.053%	0.054%	0.052%
2.2%	0.042%±0.000%	0.035%	0.045%	0.045%	0.044%
2.3%	0.036%±0.000%	0.029%	0.038%	0.038%	0.037%
2.4%	0.030%±0.000%	0.024%	0.032%	0.032%	0.031%
2.5%	0.025%±0.000%	0.020%	0.027%	0.028%	0.027%
2.6%	0.022%±0.000%	0.017%	0.023%	0.023%	0.023%
2.7%	0.018%±0.000%	0.014%	0.020%	0.020%	0.019%
2.8%	0.016%±0.000%	0.012%	0.017%	0.017%	0.017%
2.9%	0.013%±0.000%	0.010%	0.015%	0.015%	0.015%
3.0%	0.011%±0.000%	0.009%	0.013%	0.013%	0.012%

Table 4 MC simulation results and closed formulas for variable volatility structure $\sigma_n^H(t) = 0.015\exp(-0.4(T_n - t))(1 + 50(T_n - t))$

Strike	Swaption price	CF (26)	CF Prop. 1	CF Prop. 2	CF Prop. 3
0.0%	3.259%±0.000%	3.260%	3.260%	3.260%	3.260%
0.1%	2.826%±0.000%	2.826%	2.826%	2.827%	2.826%
0.2%	2.393%±0.000%	2.393%	2.393%	2.394%	2.393%
0.3%	1.960%±0.000%	1.961%	1.960%	1.961%	1.960%
0.4%	1.530%±0.000%	1.536%	1.532%	1.533%	1.532%
0.5%	1.123%±0.000%	1.141%	1.128%	1.129%	1.128%
0.6%	0.772%±0.000%	0.803%	0.780%	0.780%	0.778%
0.7%	0.501%±0.000%	0.540%	0.508%	0.509%	0.507%
0.8%	0.310%±0.000%	0.350%	0.316%	0.316%	0.314%
0.9%	0.186%±0.000%	0.221%	0.189%	0.189%	0.187%
1.0%	0.109%±0.000%	0.136%	0.110%	0.110%	0.108%
1.1%	0.063%±0.000%	0.083%	0.063%	0.063%	0.062%
1.2%	0.036%±0.000%	0.050%	0.035%	0.035%	0.034%
1.3%	0.021%±0.000%	0.030%	0.020%	0.020%	0.019%
1.4%	0.012%±0.000%	0.018%	0.011%	0.011%	0.011%
1.5%	0.007%±0.000%	0.011%	0.006%	0.006%	0.006%
1.6%	0.004%±0.000%	0.006%	0.003%	0.003%	0.003%
1.7%	0.002%±0.000%	0.004%	0.002%	0.002%	0.002%
1.8%	0.001%±0.000%	0.002%	0.001%	0.001%	0.001%
1.9%	0.001%±0.000%	0.001%	0.001%	0.001%	0.001%
2.0%	0.001%±0.000%	0.001%	0.000%	0.000%	0.000%
2.1%	0.000%±0.000%	0.001%	0.000%	0.000%	0.000%
2.2%	0.000%±0.000%	0.000%	0.000%	0.000%	0.000%

Table 5 MC simulation results and closed formulas for variable volatility structure $\sigma_n^H(t) = 0.03\exp(-0.6(T_n - t))(1 + 25(T_n - t))$

As one can see, formula (26) in general has the highest deviation (up to four bp) from the true (MC) swaption price. Also in general, the formula proved in Proposition 3 meets best the true value. The highest deviation occurs if the option is at the money, that is if the strike is close to the fair CDS spread. If the option is far out of or in the money, all deviations converge to zero except for the one in Proposition 2, which does not recover the true swaption price for strike zero.

We also tested the closed formulas against varying volatility. To this end, we chose the volatility structure given by (1) above and varied γ_1 from 0 to 0.06 with a fixed strike of 0.8%. The resulting approximation errors of the different formulas can be found in the chart on page 32. Again, the formula in Proposition 3 turns out to be the best approximation. Summarizing, this formula yields the best fit to the true value of a CDSwaption.

γ_1	Swaption price	CF (26)	CF Prop. 1	CF Prop. 2	CF Prop. 3
0.000	$0.000\%_{\pm 0.000\%}$	0.000%	0.000%	0.000%	0.000%
0.005	$0.172\%_{\pm 0.000\%}$	0.164%	0.174%	0.174%	0.174%
0.010	$0.424\%_{\pm 0.000\%}$	0.408%	0.430%	0.432%	0.429%
0.015	$0.675\%_{\pm 0.000\%}$	0.653%	0.686%	0.690%	0.684%
0.020	$0.920\%_{\pm 0.000\%}$	0.892%	0.937%	0.946%	0.932%
0.025	$1.156\%_{\pm 0.001\%}$	1.123%	1.181%	1.195%	1.171%
0.030	$1.381\%_{\pm 0.003\%}$	1.344%	1.415%	1.437%	1.399%
0.035	$1.597\%_{\pm 0.006\%}$	1.554%	1.638%	1.670%	1.614%
0.040	$1.801\%_{\pm 0.011\%}$	1.751%	1.848%	1.893%	1.815%
0.045	$1.990\%_{\pm 0.017\%}$	1.934%	2.044%	2.104%	2.001%
0.050	$2.176\%_{\pm 0.026\%}$	2.103%	2.224%	2.304%	2.171%
0.055	$2.357\%_{\pm 0.037\%}$	2.258%	2.388%	2.492%	2.326%
0.060	$2.531\%_{\pm 0.050\%}$	2.399%	2.534%	2.667%	2.465%

Table 6 MC simulation results and closed formulas for different values of γ_1 and volatility structure $\sigma_n^H(t) = \gamma_1 \exp(-0.4(T_n - t))(1 + 50(T_n - t))$

In the final paragraph of this section we briefly address the problem of correlation of interest rates and default. As pointed out e. g. in (Longstaff and Schwartz, 1995, p. 808) this correlation is negative in general. Our graph on page 34 shows the dependence of CDSwaption prices on the correlation parameter

$$\rho = \frac{\sigma^F \sigma^H}{|\sigma^F| \cdot |\sigma^H|}$$

for different interest rate volatilities $|\sigma^F|$ of 10% and 40% and volatilities of discrete default intensities $|\sigma^H|$ of 60% and 120%. Again, all other parameters are chosen as in Section **5.2**. MC calculation of these values in our implementation is very slow, since we have to calculate a conditional expectation and do this by simple recalculation in each path. Calculation time thus depends quadratic on the number of simulation. We used $10\,000$

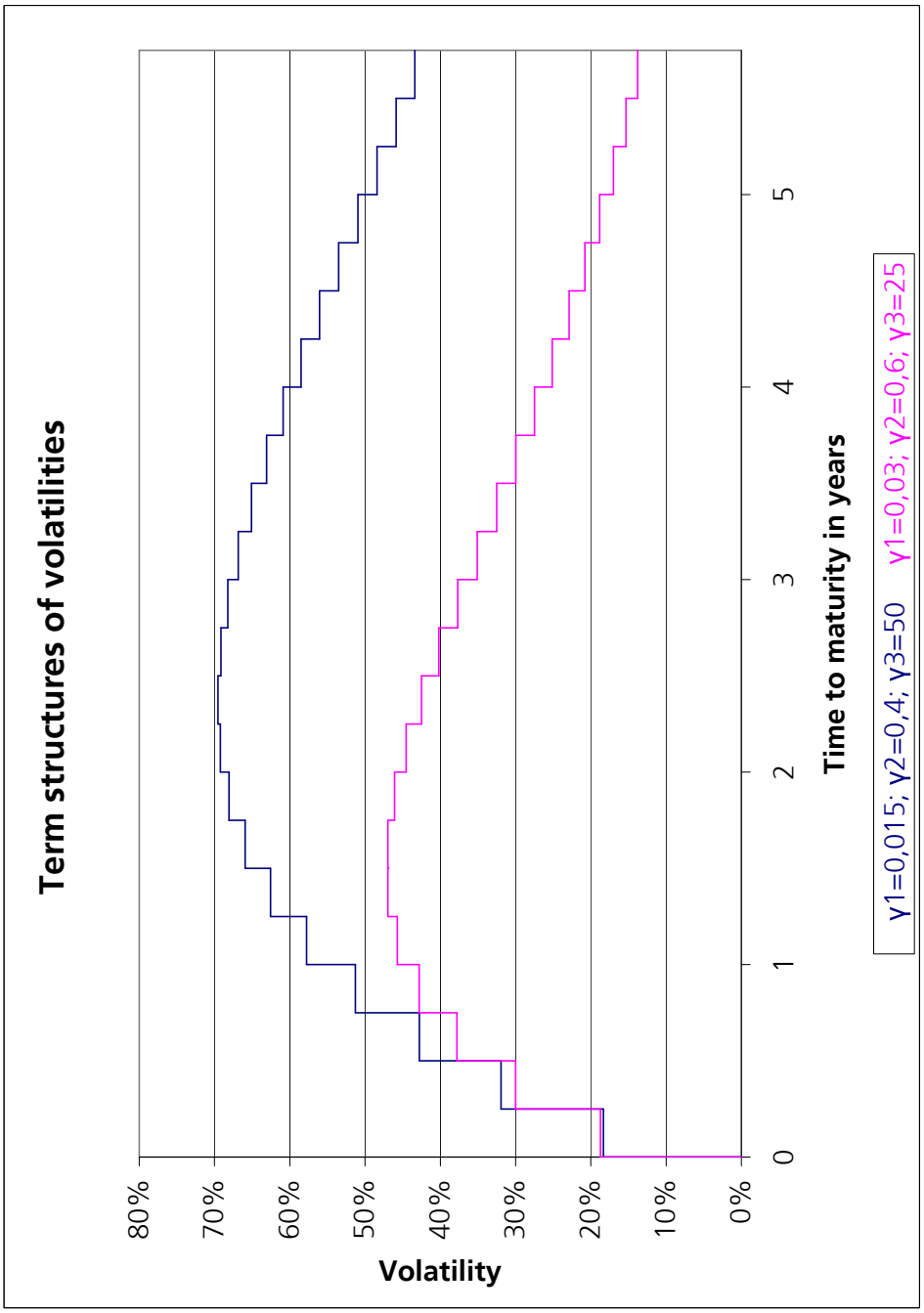

Figure 3 Term structures of volatilities of default intensities

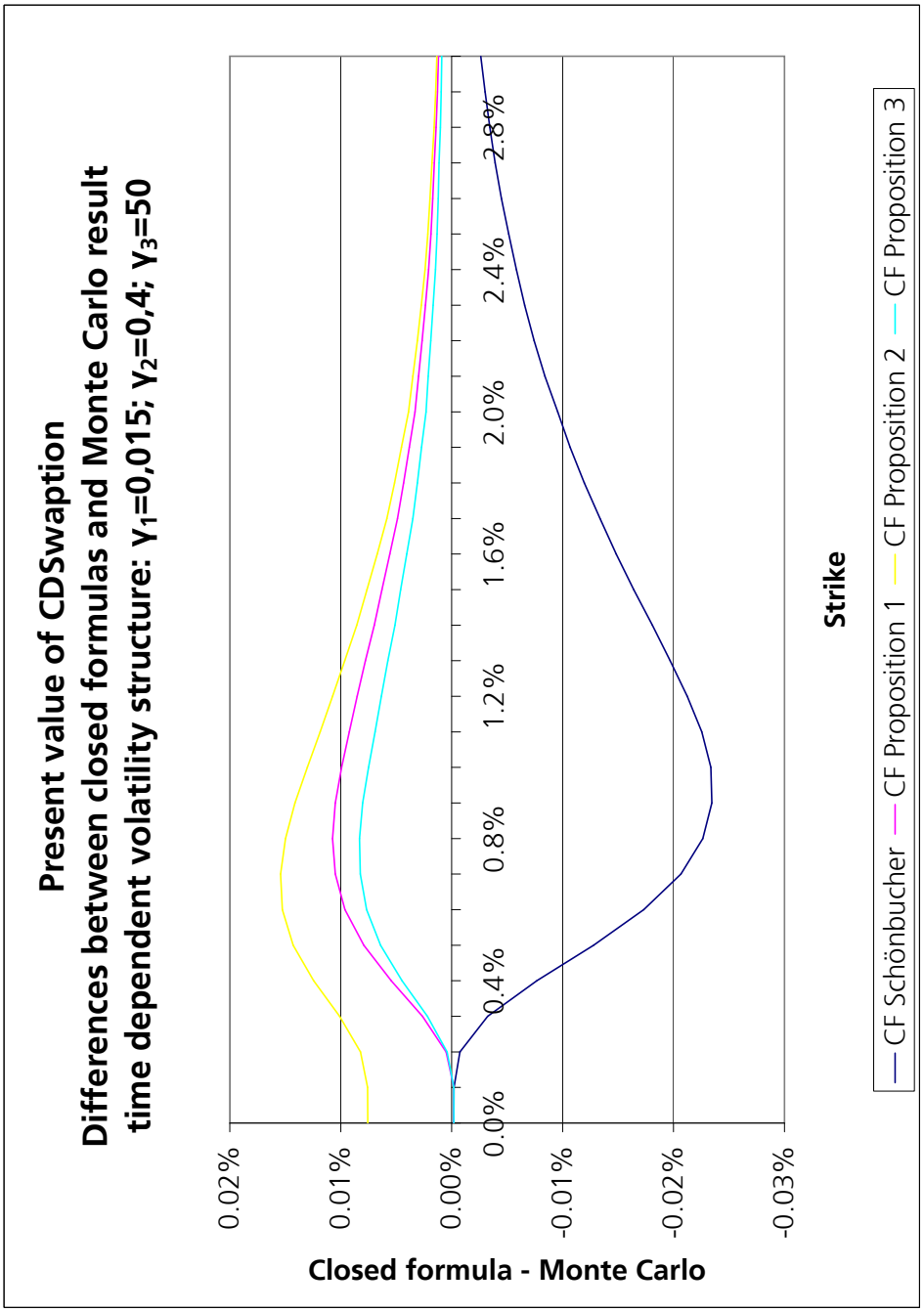

Figure 4 CDSwaption PV — approximation error using $\sigma_n^H(t) = 0.015\exp(-0.4(T_n - t))(1 + 50(T_n - t))$

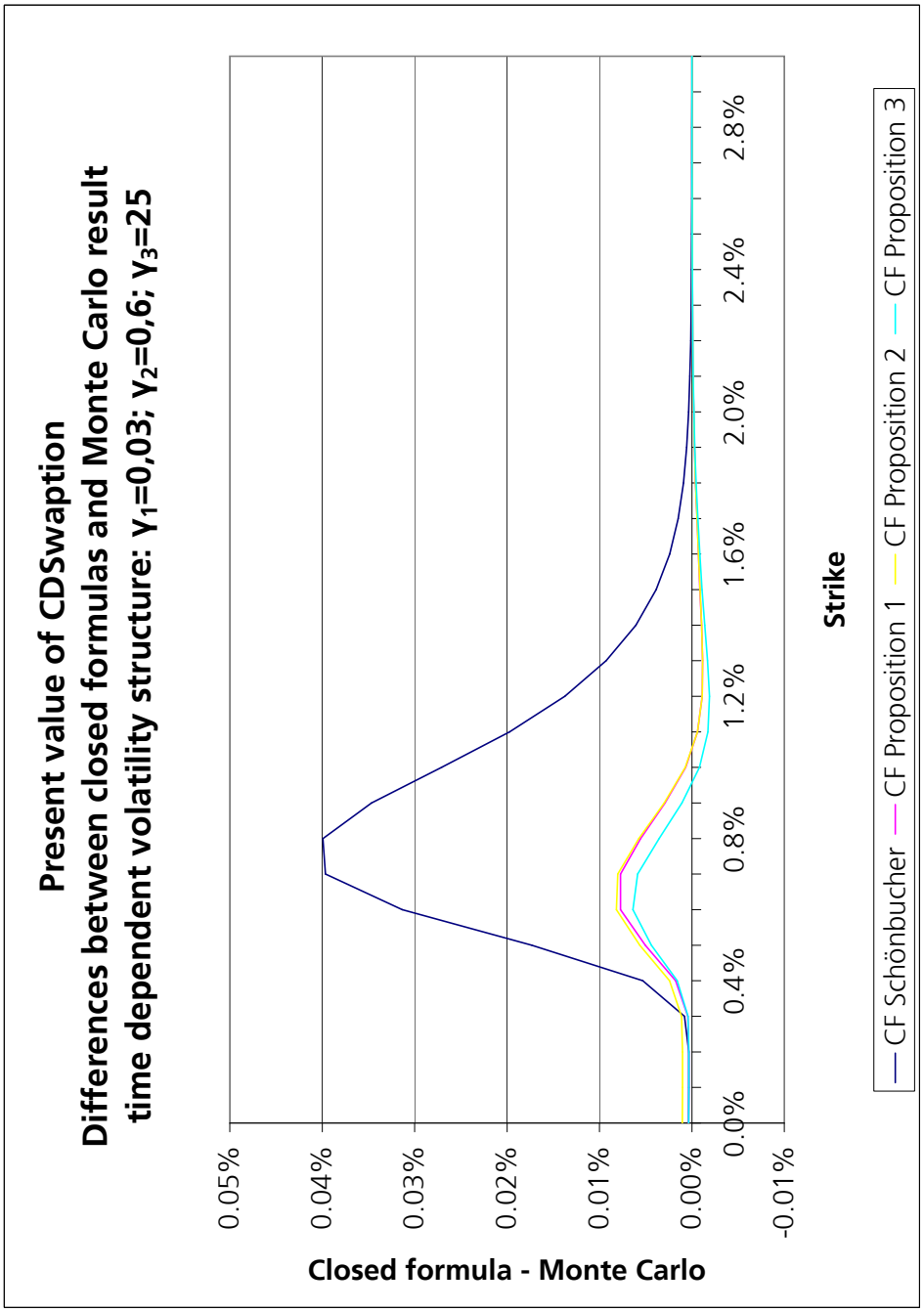

Figure 5 CDSwaption PV — approximation error using $\sigma_n^H(t) = 0.03\exp(-0.6(T_n - t))(1 + 25(T_n - t))$

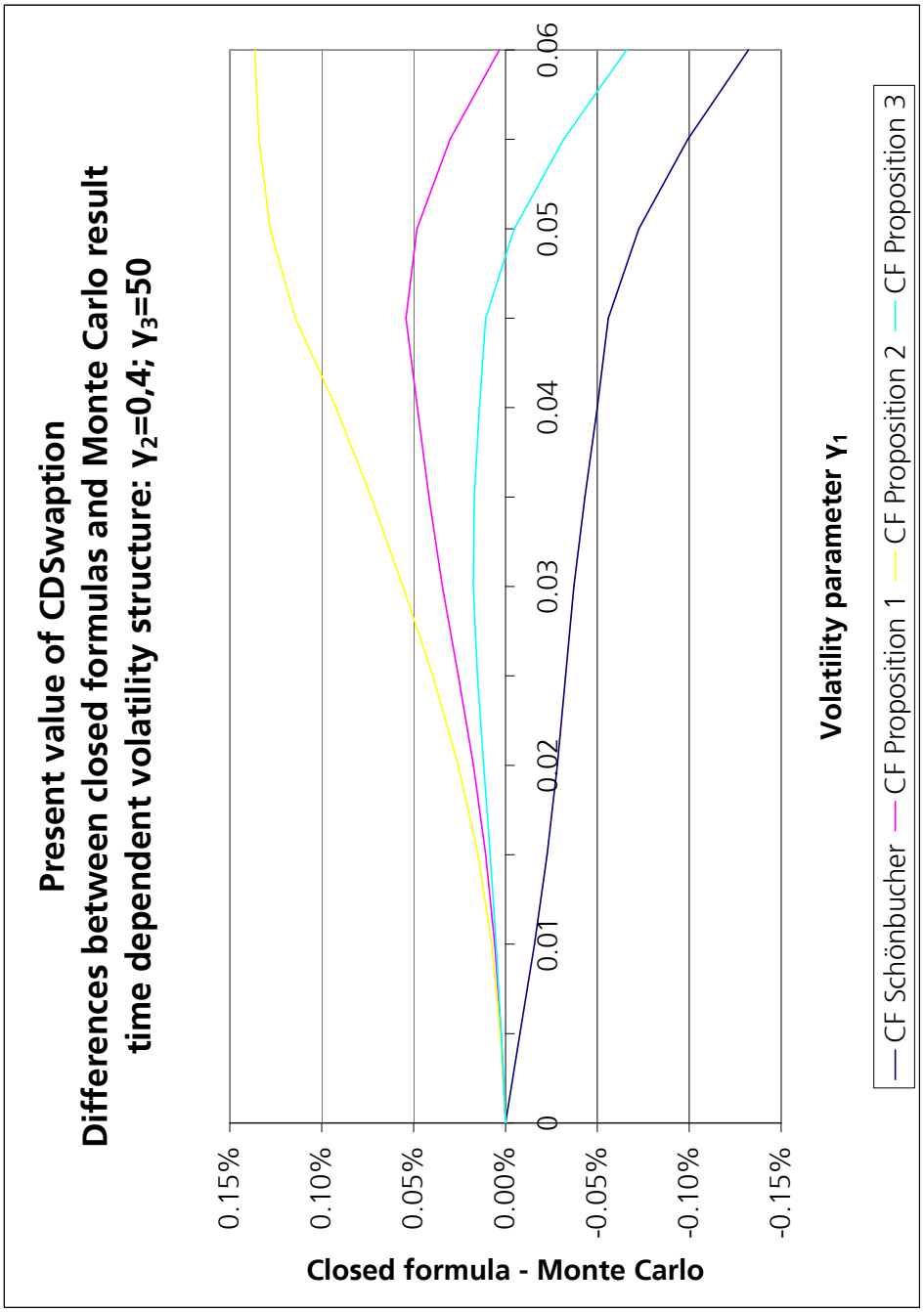

Figure 6 CDSwaption PV — approximation error using $\sigma_n^H(t) = \gamma_1 \exp(-0.4t)(1 + 50t)$

simulations with only 3 intermediate time steps between tenor dates and only 100 simulations for the calculation of the conditional expectation. Pricing of one CDSwaption took about four hours.

Note that the *closed formula* does *not* take into account correlation between interest rates and defaults nor does it depend on volatility of interest rates at all.

The closed formula results are given as 0.694% and 1.417% for the case of $|\sigma^H| = 60\%$ and $|\sigma^H| = 120\%$, respectively. The numerical values of the simulation are summarized in the following table:

$\lvert\sigma^F\rvert$	$\lvert\sigma^H\rvert$	$\rho = -100\%$	$\rho = -50\%$	$\rho = 0\%$	$\rho = +50\%$	$\rho = +100\%$
10%	60%	$0.712\%\pm0.023\%$	$0.692\%\pm0.010\%$	$0.686\%\pm0.001\%$	$0.694\%\pm0.010\%$	$0.721\%\pm0.023\%$
40%	60%	$0.687\%\pm0.023\%$	$0.673\%\pm0.011\%$	$0.686\%\pm0.001\%$	$0.744\%\pm0.010\%$	$0.870\%\pm0.024\%$
10%	120%	$1.684\%\pm0.080\%$	$1.485\%\pm0.041\%$	$1.403\%\pm0.018\%$	$1.517\%\pm0.044\%$	$1.681\%\pm0.083\%$
40%	120%	$1.584\%\pm0.084\%$	$1.441\%\pm0.042\%$	$1.403\%\pm0.018\%$	$1.639\%\pm0.045\%$	$2.067\%\pm0.091\%$

Table 7 MC simulation results for present value of CDSwaption calls depending on correlation of interest rates and volatility of default ρ

We find that CDSwaption PVs increase with increasing positive or negative correlation. The deviation from the uncorrelated case is however in the order of magnitude as the Monte Carlo accuracy. This accuracy might however be increased in reasonable calculation time by exploiting a more refined algorithm for the calculation of conditional expectations.

It is interesting to note, that the deviation from the uncorrelated case is in general smaller for negativ correlations than for positive ones. Moreover for negative correlations, the PV of the CDSwaption first increases with increasing interest rate volatility and then decreases again. Here the effects of rising volatility and decreasing correlation cancel each other to some degree.

5.4 Constant Maturity Credit Default Swaps (CMCDS)

A c-period k-forward Constant Maturity Credit Default Swap (CMCDS) consists of two payment legs:

(1) The premium leg, paying $\overline{s}_{i,i+c+1}(T_i)\delta_i$ at T_{i+1} for all $i = k, \dots, n-1$, if no default happened before T_{i+1}. Here $\overline{s}_{i,i+c+1}$ denotes the $c+1$-period forward swap rate starting at T_i, which was introduced in (23).

(2) The credit or protection leg, pays $(1-R)$ at T_{i+1} for all $i = k, \dots, n-1$, if a default happened between T_i and T_{i+1}.

The value at time t of the premium leg is therefore

$$V^{CMCDS}_{premium}(t) = \sum_{i=k}^{n-1} \delta_i \overline{B}_{i+1}(t) \mathbb{E}^{\overline{\mathbf{P}}_{i+1}}[\overline{s}_{i,i+c+1}(T_i)|\mathcal{F}_t].$$

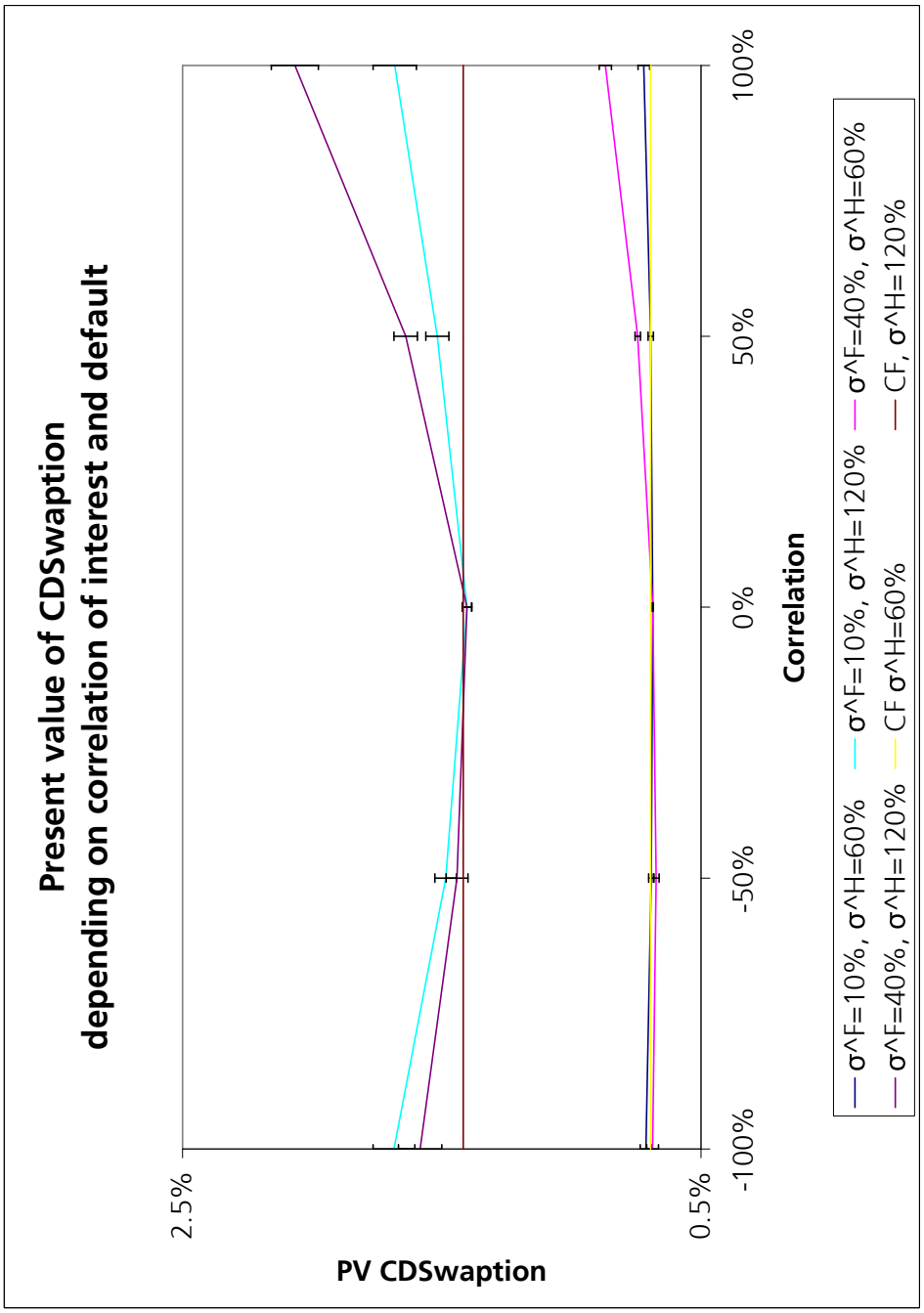

Figure 7 CDSwaption PV depending on correlation between interest rates and default intensities

Moreover, the value of $\overline{s}_{i,i+c+1}(T_i)$ is given in (23) as

$$\overline{s}_{i,i+c+1}(T_i) = (1-R)\frac{\sum_{j=i}^{i+c}\overline{B}_{j+1}(T_i)\mathbb{E}^{\overline{\mathbf{P}}_{j+1}}[h_j(T_j)|\mathcal{F}_i]}{\sum_{j=i}^{i+c}\delta_j\overline{B}_{j+1}(T_i)},$$

so that

$$V_{premium}^{CMCDS}(t) = (1-R)\sum_{i=k}^{n-1}\overline{B}_{i+1}(t)\mathbb{E}^{\overline{\mathbf{P}}_{i+1}}\Big[\delta_i\frac{\sum_{j=i}^{i+c}\overline{B}_{j+1}(T_i)\mathbb{E}^{\overline{\mathbf{P}}_{j+1}}[h_j(T_j)|\mathcal{F}_i]}{\sum_{j=i}^{i+c}\delta_j\overline{B}_{j+1}(T_i)}\Big|\mathcal{F}_t\Big].$$

Using the notation

$$\overline{w}_{i,j}(s) = \frac{\overline{B}_{j+1}(s)}{\sum_{l=i}^{i+c}\delta_l\overline{B}_{l+1}(s)},$$

this abbreviates to

$$V_{premium}^{CMCDS}(t) = (1-R)\sum_{i=k}^{n-1}\overline{B}_{i+1}(t)\mathbb{E}^{\overline{\mathbf{P}}_{i+1}}\Big[\delta_i\sum_{j=i}^{i+c}\overline{w}_{i,j}(T_i)\mathbb{E}^{\overline{\mathbf{P}}_{j+1}}[h_j(T_j)|\mathcal{F}_i]\Big|\mathcal{F}_t\Big].$$

The value at time t of the credit leg was already investigated in (22) and equals

$$V_{credit}(t) = (1-R)\sum_{i=k}^{n-1}\overline{B}_{i+1}(t)\mathbb{E}^{\overline{\mathbf{P}}_{i+1}}[h_i(T_i)|\mathcal{F}_t].$$

Note that the value of the CMCDS given as $V_{CMCDS} = V_{credit} - V_{premium}^{CMCDS}$ equals 0 in the special case $c = 0$.

Also under independence of defaults and interest rates, we have

$$\mathbb{E}^{\overline{\mathbf{P}}_{j+1}}[h_j(T_j)|\mathcal{F}_i] = h_j(T_i),$$
$$\mathbb{E}^{\overline{\mathbf{P}}_{i+1}}[h_i(T_i)|\mathcal{F}_t] = h_i(t),$$

so that we obtain the value of the premium leg in this case as

$$V_{premium}^{CMCDS}(t) = (1-R)\sum_{i=k}^{n-1}\delta_i\overline{B}_{i+1}(t)\mathbb{E}^{\overline{\mathbf{P}}_{i+1}}\Big[\sum_{j=i}^{i+c}\overline{w}_{i,j}(T_i)h_j(T_i)\Big|\mathcal{F}_t\Big].$$

To obtain a control variate for CMCDS valuation, we assume the weights $\overline{w}_{i,j}(t)$ to be constant and the drifts of h_j under $\overline{\mathbf{P}}_{i+1}$ also to be constant. Note that in

the independent case and under constant volatility $\sigma_j^H(t) = \sigma_j^H(0) = \sigma_j^H$ these drifts are

$$\mu_{j,i+1}(t) = \sum_{l=i+1}^{j} \frac{h_l(t)}{1+h_l(t)} \sigma_l^H \sigma_j^H$$

and if they are assumed to be constant between t and T_i

$$\mathbb{E}^{\overline{\mathbf{P}}_{i+1}}\big[h_j(T_i)|\mathcal{F}_t\big] = h_j(t)\exp\big(\mu_{j,i+1}(t)(T_i - t)\big).$$

Proposition: Under the assumptions above it follows that

$$\begin{aligned} V_{premium}^{CMCDS}(t) &= (1-R)\sum_{i=k}^{n-1} \delta_i \overline{B}_{i+1}(t) \sum_{j=i}^{i+c} \overline{w}_{i,j}(t) \mathbb{E}^{\overline{\mathbf{P}}_{i+1}}\big[h_j(T_i)|\mathcal{F}_t\big] \\ &= (1-R)\sum_{i=k}^{n-1} \delta_i \overline{B}_{i+1}(t) \sum_{j=i}^{i+c} \overline{w}_{i,j}(t) h_j(t) \exp\big(\mu_{j,i+1}(t)(T_i - t)\big). \end{aligned}$$

We want to emphasize here that this last formula corresponds to the result derived in (Brigo, 2005, Formula (1) on p. 6) and (Brigo, 2006, Formula (1) on p. 79) in the case of constant volatilities.

Also here, we can relax the assumptions of constant and homogeneous volatilities and derive a formula similar to Brigo's, by assuming that

$$\frac{h_l}{1+h_l}$$

are constant over time for all $l = k, \ldots, n+c-1$ so that

$$\mu_{j,i+1}(s) = \sum_{l=i+1}^{j} \frac{h_l(t)}{1+h_l(t)} \sigma_l^H(s) \sigma_j^H(s)$$

and we obtain

$$\begin{aligned} \mathbb{E}^{\overline{\mathbf{P}}_{i+1}}\big[h_j(T_i)\big|\mathcal{F}_t\big] &= h_j(t)\exp\left(\sum_{l=i+1}^{j} \frac{h_l(t)}{1+h_l(t)} \int_t^{T_i} \rho_{lj}(s)|\sigma_l^H(s)||\sigma_j^H(s)|\,ds\right) \\ &= h_j(t)\exp\left(\sum_{l=i+1}^{j} \frac{h_l(t)}{1+h_l(t)} \sum_{h=k-1}^{i-1} \delta_h \rho_{lj}(T_h)|\sigma_l^H(T_h)||\sigma_j^H(T_h)|\right), \end{aligned}$$

where for the last equality we again assumed constant volatilities and correlations between tenor dates and let $t = T_{k-1}$.

Our Monte Carlo implementation allows us to test the closed formulas with the real values from the model. For numerical examples, we used a five year CMCDS

with quarterly payments starting today for the issuer described in Section **5.2**. The constant maturity length c is chosen to be five years as well, that is $c = 20$.

On page 38 the present value of a CMCDS calculated with a Monte Carlo Simulation and with the closed formula is shown, depending on the (time constant) volatility $|\sigma^H|$ of the default intensities. The standard errors of the MC simulations are given as error bars. As one can see, for intensity volatilities of up to around 60% the approximation error of the closed formula is less than around 10 basis points, however, in contrast to the closed formula in the CDSwaption case, starting at a volatility of 80% the approximation error becomes more and more significant, increasing up to a half of the value of the CMCDS for a default volatility $|\sigma^H|$ of 150%. The precise results of the calculations are given in the table 8.

$\lvert\sigma^H\rvert$	MC result	CF result	$\lvert\sigma^H\rvert$	MC result	CF result
0%	$2.070\%_{\pm 0.000\%}$	2.070%	80%	$3.006\%_{\pm 0.008\%}$	2.452%
10%	$2.075\%_{\pm 0.000\%}$	2.075%	90%	$3.441\%_{\pm 0.013\%}$	2.564%
20%	$2.091\%_{\pm 0.000\%}$	2.092%	100%	$3.962\%_{\pm 0.018\%}$	2.695%
30%	$2.123\%_{\pm 0.000\%}$	2.120%	110%	$4.547\%_{\pm 0.026\%}$	2.847%
40%	$2.179\%_{\pm 0.000\%}$	2.160%	120%	$5.172\%_{\pm 0.037\%}$	3.024%
50%	$2.273\%_{\pm 0.001\%}$	2.212%	130%	$5.813\%_{\pm 0.055\%}$	3.228%
60%	$2.429\%_{\pm 0.003\%}$	2.278%	140%	$6.453\%_{\pm 0.082\%}$	3.463%
70%	$2.669\%_{\pm 0.005\%}$	2.357%	150%	$7.083\%_{\pm 0.123\%}$	3.736%

Table 8 MC simulation results for present value of a CMCDS depending on volatility of default intensity $|\sigma^H|$

Also on page 39 we include a graph of the present value of a CMCDS calculated again with Monte Carlo simulation and closed formula depending on the constant maturity length c, where c runs from 1 to 20 and the volatility of default intensities $|\sigma^H|$ is kept constant at 60%. The standard errors of the MC simulations are given as error bars. Again the precise results of the calculations are collected in a table 9 on page 40.

Summarizing, the closed CMCDS formula always underprices the true CMCDS value, if default intensity volatilities become high, the underpricing is severe especially for longer (5 year) constant maturity periods. Note that usual traded CMCDS are five year CMCDS with five year constant maturities and default intensity volatilities of around 60 to 80% are not unrealistic. So in these cases, we recommend an MC based calculation.

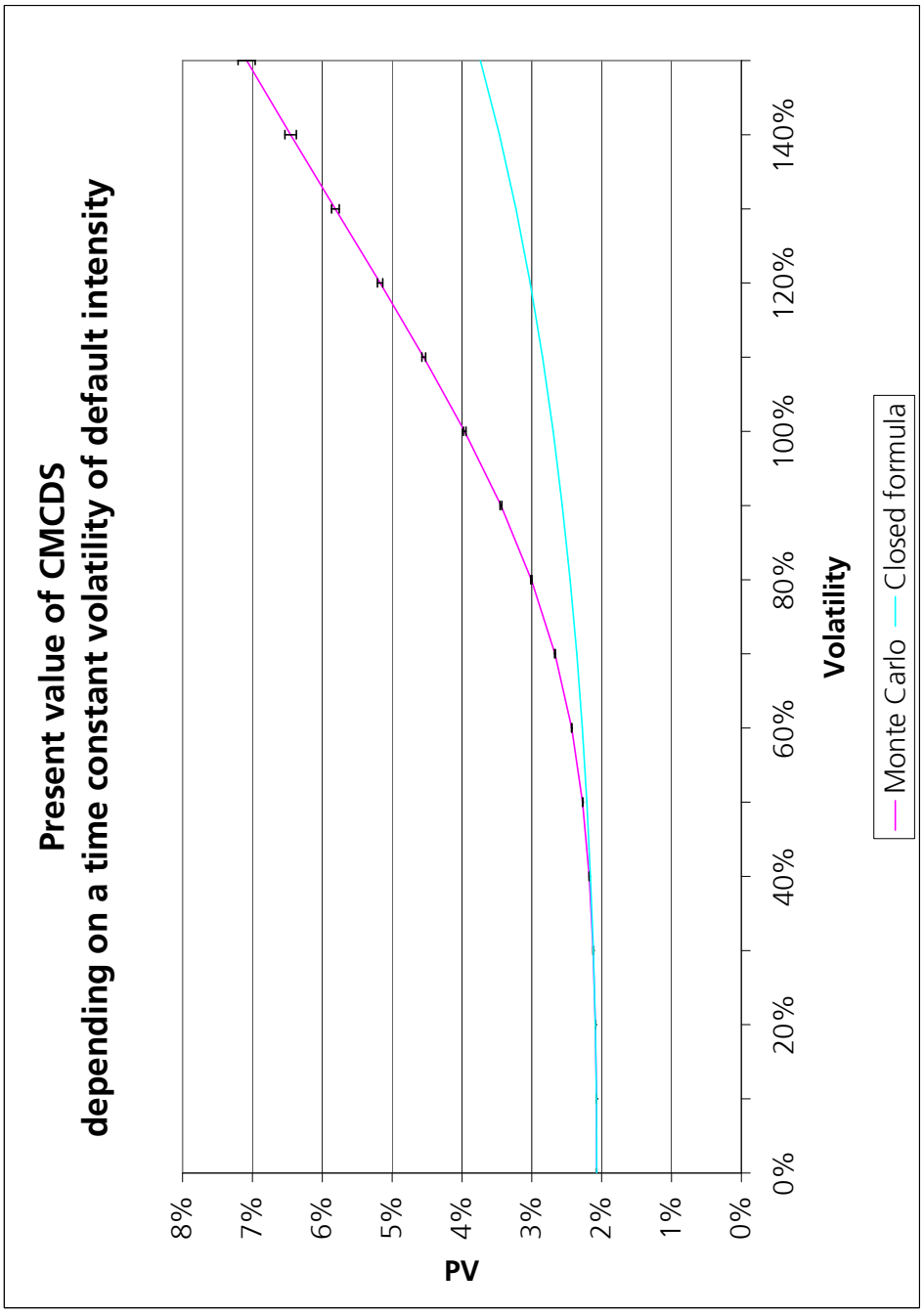

Figure 8 CMCDS PV — approximation error depending on volatility of default intensities

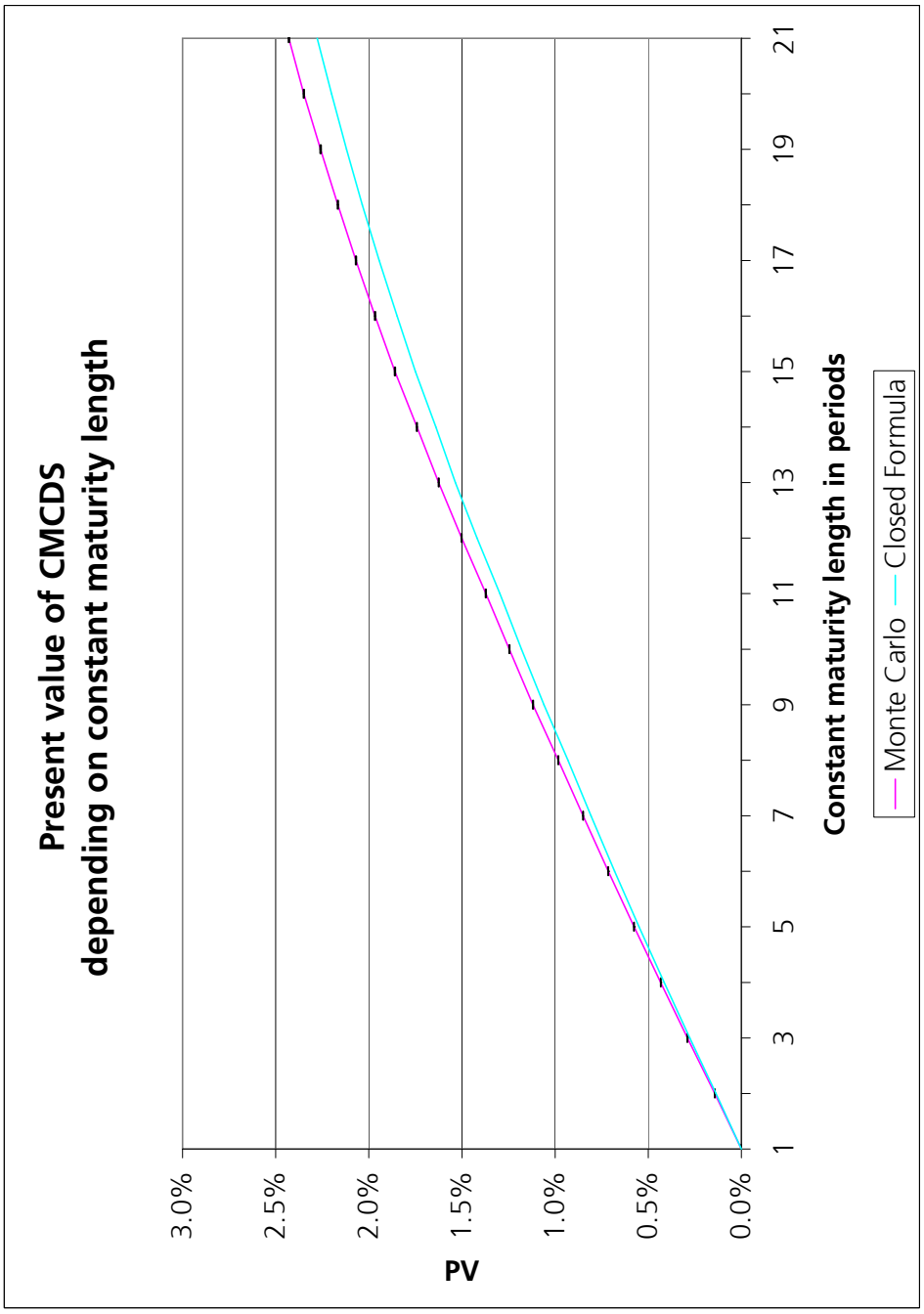

Figure 9 CMCDS PV — approximation error depending constant maturity length

c	MC result	CF result	c	MC result	CF result
0	$0.000\%_{\pm 0.000\%}$	0.000%	10	$1.372\%_{\pm 0.002\%}$	1.296%
1	$0.143\%_{\pm 0.000\%}$	0.136%	11	$1.502\%_{\pm 0.002\%}$	1.419%
2	$0.290\%_{\pm 0.000\%}$	0.277%	12	$1.625\%_{\pm 0.002\%}$	1.535%
3	$0.433\%_{\pm 0.001\%}$	0.414%	13	$1.742\%_{\pm 0.002\%}$	1.640%
4	$0.576\%_{\pm 0.001\%}$	0.550%	14	$1.860\%_{\pm 0.002\%}$	1.750%
5	$0.715\%_{\pm 0.001\%}$	0.680%	15	$1.967\%_{\pm 0.002\%}$	1.849%
6	$0.850\%_{\pm 0.001\%}$	0.808%	16	$2.069\%_{\pm 0.002\%}$	1.945%
7	$0.983\%_{\pm 0.001\%}$	0.931%	17	$2.166\%_{\pm 0.002\%}$	2.035%
8	$1.119\%_{\pm 0.001\%}$	1.060%	18	$2.259\%_{\pm 0.001\%}$	2.120%
9	$1.246\%_{\pm 0.001\%}$	1.180%	19	$2.349\%_{\pm 0.002\%}$	2.200%
			20	$2.429\%_{\pm 0.002\%}$	2.278%

Table 9 MC simulation results for present value of a CMCDS depending on constant maturity length c

6 Conclusion

We consider a Libor market model with integrated default risk. We derived new closed formulas for the valuation of CDSwaptions under decorrelation of the default intensities for different tenor dates.

Next, we implemented a corresponding Monte Carlo model to find present values of Credit Default Swaprates, Credit Default Swaptions and Constant Maturity Credit Default Swaps. Using appropriate control variates makes the implementation efficient in time and accuracy.

We tested the effect of correlation between interest rates and default. We found that correlation has almost no influence on both Credit Default Swaption prices and Credit Default Swaprates. We analyse the market standard formula (see Brigo (2005)) for Constant Maturity Credit Default Swaps and found that it is sufficiently accurate for volatilities of default intensities up to 60%. For higher volatilities however, the formula shows heavy deviations from the true Monte Carlo price. Finally, we found that our closed Credit Default Swaption formulas capture sufficiently accurate the effect of decorrelation.

References

Sarp Kaya Acar, *Optimal capital structure of a firm*. Phd thesis, Technische Universität Kaiserslautern, (2006). 24

Nordine Bennani and Daniel Dahan, An extended market model for credit derivatives. In *Stochastic Finance*, (2004), Autumn School & International Conference. Available from:
`http://nordine.bennani.free.fr/_private/ecmm.pdf`. 10

Damiano Brigo, Constant maturity credit default swap pricing with market

models, (March 2005), 24 pages. Available from: http://www.damianobrigo.it. 1, 36, 40
Damiano Brigo, CMCDS valuation with market models. *Risk*, pp. 78–83, (June 2006). Available from: www.risk.net. 36
Damiano Brigo and Fabio Mercurio, *Interest rate models — theory and practice*. Springer, (2001), ISBN 3-540-41772-9. 25
Edmond Levy, Pricing European average rate currency options. *Journal of Interantional Money and Finance*, **11**, pp. 474–491, (1992). 22
Francis A. Longstaff and Eduardo S. Schwartz, A simple approach to valuing risky fixed and floating rate debt. *The Journal of Finance*, **50** (3), pp. 789–819, (July 1995). 15, 28
Riccardo Rebonato, *Interest-rate option models*. Financial Engineering, John Wiley & Sons, 2nd ed., (1998). 6
Philipp J. Schönbucher, A libor market model with default risk. Bonn Econ Discussion Papers bgse15_2001, University of Bonn, Germany, (December 2000). Available from: http://ideas.repec.org/p/bon/bonedp/bgse15_2001.html. 1, 10, 13, 17
Philipp J. Schönbucher, A note on survival measures and the pricing of options on credit default swaps, (May 2003), working paper, 9 pages. Available from: http://www.math.ethz.ch/~schonbuc/papers/cdsoptions.pdf. 4, 17
Philipp J. Schönbucher, A measure of survival. *Risk*, pp. 79–85, (August 2004). Available from: www.risk.net. 1, 4, 17

Published reports of the Fraunhofer ITWM

The PDF-files of the following reports are available under:
www.itwm.fraunhofer.de/de/zentral__berichte/berichte

1. D. Hietel, K. Steiner, J. Struckmeier

A Finite - Volume Particle Method for Compressible Flows

We derive a new class of particle methods for conservation laws, which are based on numerical flux functions to model the interactions between moving particles. The derivation is similar to that of classical Finite-Volume methods; except that the fixed grid structure in the Finite-Volume method is substituted by so-called mass packets of particles. We give some numerical results on a shock wave solution for Burgers equation as well as the well-known one-dimensional shock tube problem.
(19 pages, 1998)

2. M. Feldmann, S. Seibold

Damage Diagnosis of Rotors: Application of Hilbert Transform and Multi-Hypothesis Testing

In this paper, a combined approach to damage diagnosis of rotors is proposed. The intention is to employ signal-based as well as model-based procedures for an improved detection of size and location of the damage. In a first step, Hilbert transform signal processing techniques allow for a computation of the signal envelope and the instantaneous frequency, so that various types of non-linearities due to a damage may be identified and classified based on measured response data. In a second step, a multi-hypothesis bank of Kalman Filters is employed for the detection of the size and location of the damage based on the information of the type of damage provided by the results of the Hilbert transform.
Keywords: Hilbert transform, damage diagnosis, Kalman filtering, non-linear dynamics
(23 pages, 1998)

3. Y. Ben-Haim, S. Seibold

Robust Reliability of Diagnostic Multi-Hypothesis Algorithms: Application to Rotating Machinery

Damage diagnosis based on a bank of Kalman filters, each one conditioned on a specific hypothesized system condition, is a well recognized and powerful diagnostic tool. This multi-hypothesis approach can be applied to a wide range of damage conditions. In this paper, we will focus on the diagnosis of cracks in rotating machinery. The question we address is: how to optimize the multi-hypothesis algorithm with respect to the uncertainty of the spatial form and location of cracks and their resulting dynamic effects. First, we formulate a measure of the reliability of the diagnostic algorithm, and then we discuss modifications of the diagnostic algorithm for the maximization of the reliability. The reliability of a diagnostic algorithm is measured by the amount of uncertainty consistent with no-failure of the diagnosis. Uncertainty is quantitatively represented with convex models.
Keywords: Robust reliability, convex models, Kalman filtering, multi-hypothesis diagnosis, rotating machinery, crack diagnosis
(24 pages, 1998)

4. F.-Th. Lentes, N. Siedow

Three-dimensional Radiative Heat Transfer in Glass Cooling Processes

For the numerical simulation of 3D radiative heat transfer in glasses and glass melts, practically applicable mathematical methods are needed to handle such problems optimal using workstation class computers. Since the exact solution would require super-computer capabilities we concentrate on approximate solutions with a high degree of accuracy. The following approaches are studied: 3D diffusion approximations and 3D ray-tracing methods.
(23 pages, 1998)

5. A. Klar, R. Wegener

A hierarchy of models for multilane vehicular traffic
Part I: Modeling

In the present paper multilane models for vehicular traffic are considered. A microscopic multilane model based on reaction thresholds is developed. Based on this model an Enskog like kinetic model is developed. In particular, care is taken to incorporate the correlations between the vehicles. From the kinetic model a fluid dynamic model is derived. The macroscopic coefficients are deduced from the underlying kinetic model. Numerical simulations are presented for all three levels of description in [10]. Moreover, a comparison of the results is given there.
(23 pages, 1998)

Part II: Numerical and stochastic investigations

In this paper the work presented in [6] is continued. The present paper contains detailed numerical investigations of the models developed there. A numerical method to treat the kinetic equations obtained in [6] are presented and results of the simulations are shown. Moreover, the stochastic correlation model used in [6] is described and investigated in more detail.
(17 pages, 1998)

6. A. Klar, N. Siedow

Boundary Layers and Domain Decomposition for Radiative Heat Transfer and Diffusion Equations: Applications to Glass Manufacturing Processes

In this paper domain decomposition methods for radiative transfer problems including conductive heat transfer are treated. The paper focuses on semi-transparent materials, like glass, and the associated conditions at the interface between the materials. Using asymptotic analysis we derive conditions for the coupling of the radiative transfer equations and a diffusion approximation. Several test cases are treated and a problem appearing in glass manufacturing processes is computed. The results clearly show the advantages of a domain decomposition approach. Accuracy equivalent to the solution of the global radiative transfer solution is achieved, whereas computation time is strongly reduced.
(24 pages, 1998)

7. I. Choquet

Heterogeneous catalysis modelling and numerical simulation in rarified gas flows Part I: Coverage locally at equilibrium

A new approach is proposed to model and simulate numerically heterogeneous catalysis in rarefied gas flows. It is developed to satisfy all together the following points:
1) describe the gas phase at the microscopic scale, as required in rarefied flows,
2) describe the wall at the macroscopic scale, to avoid prohibitive computational costs and consider not only crystalline but also amorphous surfaces,
3) reproduce on average macroscopic laws correlated with experimental results and
4) derive analytic models in a systematic and exact way.
The problem is stated in the general framework of a non static flow in the vicinity of a catalytic and non porous surface (without aging). It is shown that the exact and systematic resolution method based on the Laplace transform, introduced previously by the author to model collisions in the gas phase, can be extended to the present problem. The proposed approach is applied to the modelling of the EleyRideal and LangmuirHinshelwood recombinations, assuming that the coverage is locally at equilibrium. The models are developed considering one atomic species and extended to the general case of several atomic species. Numerical calculations show that the models derived in this way reproduce with accuracy behaviors observed experimentally.
(24 pages, 1998)

8. J. Ohser, B. Steinbach, C. Lang

Efficient Texture Analysis of Binary Images

A new method of determining some characteristics of binary images is proposed based on a special linear filtering. This technique enables the estimation of the area fraction, the specific line length, and the specific integral of curvature. Furthermore, the specific length of the total projection is obtained, which gives detailed information about the texture of the image. The influence of lateral and directional resolution depending on the size of the applied filter mask is discussed in detail. The technique includes a method of increasing directional resolution for texture analysis while keeping lateral resolution as high as possible.
(17 pages, 1998)

9. J. Orlik

Homogenization for viscoelasticity of the integral type with aging and shrinkage

A multiphase composite with periodic distributed inclusions with a smooth boundary is considered in this contribution. The composite component materials are supposed to be linear viscoelastic and aging (of the nonconvolution integral type, for which the Laplace transform with respect to time is not effectively applicable) and are subjected to isotropic shrinkage. The free shrinkage deformation can be considered as a fictitious temperature deformation in the behavior law. The procedure presented in this paper proposes a way to determine average (effective homogenized) viscoelastic and shrinkage (temperature) composite properties and the homogenized stressfield from known properties of the components. This is done by the extension of the asymptotic homogenization technique known for pure elastic nonhomogeneous bodies to the nonhomogeneous thermoviscoelasticity of the integral nonconvolution type. Up to now, the homogenization theory has not covered viscoelasticity of the integral type. SanchezPalencia (1980), Francfort & Suquet (1987) (see [2], [9]) have considered homogenization for viscoelasticity of the differential form and only up to the first derivative order. The integralmodeled viscoelasticity is more general then the differential one and includes almost all known differential models. The homogenization procedure is based on the construction of an asymptotic solution with respect to a period of the composite structure. This reduces the original problem to some auxiliary boundary value problems of elasticity and viscoelasticity on the unit periodic cell, of the same type as the original non-homogeneous problem. The existence and uniqueness results for such problems were obtained for kernels satisfying some constrain conditions. This is done by the extension of the Volterra integral operator theory to the Volterra operators with respect to the time, whose 1 kernels are space linear operators for any fixed time variables. Some ideas of such approach were proposed in [11] and [12], where the Volterra operators with kernels depending additionally on parameter were considered. This manuscript delivers results of the same nature for the case of the spaceoperator kernels.
(20 pages, 1998)

10. J. Mohring

Helmholtz Resonators with Large Aperture

The lowest resonant frequency of a cavity resonator is usually approximated by the classical Helmholtz formula. However, if the opening is rather large and the front wall is narrow this formula is no longer valid. Here we present a correction which is of third order in the ratio of the diameters of aperture and cavity. In addition to the high accuracy it allows to estimate the damping due to radiation. The result is found by applying the method of matched asymptotic expansions. The correction contains form factors describing the shapes of opening and cavity. They are computed for a number of standard geometries. Results are compared with numerical computations.
(21 pages, 1998)

11. H. W. Hamacher, A. Schöbel

On Center Cycles in Grid Graphs

Finding "good" cycles in graphs is a problem of great interest in graph theory as well as in locational analysis. We show that the center and median problems are NP hard in general graphs. This result holds both for the variable cardinality case (i.e. all cycles of the graph are considered) and the fixed cardinality case (i.e. only cycles with a given cardinality p are feasible). Hence it is of interest to investigate special cases where the problem is solvable in polynomial time. In grid graphs, the variable cardinality case is, for instance, trivially solvable if the shape of the cycle can be chosen freely.
If the shape is fixed to be a rectangle one can analyze rectangles in grid graphs with, in sequence, fixed dimension, fixed cardinality, and variable cardinality. In all cases a complete characterization of the optimal cycles and closed form expressions of the optimal objective values are given, yielding polynomial time algorithms for all cases of center rectangle problems.
Finally, it is shown that center cycles can be chosen as rectangles for small cardinalities such that the center cycle problem in grid graphs is in these cases completely solved.
(15 pages, 1998)

12. H. W. Hamacher, K.-H. Küfer

Inverse radiation therapy planning - a multiple objective optimisation approach

For some decades radiation therapy has been proved successful in cancer treatment. It is the major task of clinical radiation treatment planning to realize on the one hand a high level dose of radiation in the cancer tissue in order to obtain maximum tumor control. On the other hand it is obvious that it is absolutely necessary to keep in the tissue outside the tumor, particularly in organs at risk, the unavoidable radiation as low as possible.
No doubt, these two objectives of treatment planning - high level dose in the tumor, low radiation outside the tumor - have a basically contradictory nature. Therefore, it is no surprise that inverse mathematical models with dose distribution bounds tend to be infeasible in most cases. Thus, there is need for approximations compromising between overdosing the organs at risk and underdosing the target volume.
Differing from the currently used time consuming iterative approach, which measures deviation from an ideal (non-achievable) treatment plan using recursively trial-and-error weights for the organs of interest, we go a new way trying to avoid a priori weight choices and consider the treatment planning problem as a multiple objective linear programming problem: with each organ of interest, target tissue as well as organs at risk, we associate an objective function measuring the maximal deviation from the prescribed doses.
We build up a data base of relatively few efficient solutions representing and approximating the variety of Pareto solutions of the multiple objective linear programming problem. This data base can be easily scanned by physicians looking for an adequate treatment plan with the aid of an appropriate online tool.
(14 pages, 1999)

13. C. Lang, J. Ohser, R. Hilfer

On the Analysis of Spatial Binary Images

This paper deals with the characterization of microscopically heterogeneous, but macroscopically homogeneous spatial structures. A new method is presented which is strictly based on integral-geometric formulae such as Crofton's intersection formulae and Hadwiger's recursive definition of the Euler number. The corresponding algorithms have clear advantages over other techniques. As an example of application we consider the analysis of spatial digital images produced by means of Computer Assisted Tomography.
(20 pages, 1999)

14. M. Junk

On the Construction of Discrete Equilibrium Distributions for Kinetic Schemes

A general approach to the construction of discrete equilibrium distributions is presented. Such distribution functions can be used to set up Kinetic Schemes as well as Lattice Boltzmann methods. The general principles are also applied to the construction of Chapman Enskog distributions which are used in Kinetic Schemes for compressible Navier-Stokes equations.
(24 pages, 1999)

15. M. Junk, S. V. Raghurame Rao

A new discrete velocity method for Navier-Stokes equations

The relation between the Lattice Boltzmann Method, which has recently become popular, and the Kinetic Schemes, which are routinely used in Computational Fluid Dynamics, is explored. A new discrete velocity model for the numerical solution of Navier-Stokes equations for incompressible fluid flow is presented by combining both the approaches. The new scheme can be interpreted as a pseudo-compressibility method and, for a particular choice of parameters, this interpretation carries over to the Lattice Boltzmann Method.
(20 pages, 1999)

16. H. Neunzert

Mathematics as a Key to Key Technologies

The main part of this paper will consist of examples, how mathematics really helps to solve industrial problems; these examples are taken from our Institute for Industrial Mathematics, from research in the Technomathematics group at my university, but also from ECMI groups and a company called TecMath, which originated 10 years ago from my university group and has already a very successful history.
(39 pages (4 PDF-Files), 1999)

17. J. Ohser, K. Sandau

Considerations about the Estimation of the Size Distribution in Wicksell's Corpuscle Problem

Wicksell's corpuscle problem deals with the estimation of the size distribution of a population of particles, all having the same shape, using a lower dimensional sampling probe. This problem was originary formulated for particle systems occurring in life sciences but its solution is of actual and increasing interest in materials science. From a mathematical point of view, Wicksell's problem is an inverse problem where the interesting size distribution is the unknown part of a Volterra equation. The problem is often regarded ill-posed, because the structure of the integrand implies unstable numerical solutions. The accuracy of the numerical solutions is considered here using the condition number, which allows to compare different numerical methods with different (equidistant) class sizes and which indicates, as one result, that a finite section thickness of the probe reduces the numerical problems. Furthermore, the relative error of estimation is computed which can be split into two parts. One part consists of the relative discretization error that increases for increasing class size, and the second part is related to the relative statistical error which increases with decreasing class size. For both parts, upper bounds can be given and the sum of them indicates an optimal class width depending on some specific constants.
(18 pages, 1999)

18. E. Carrizosa, H. W. Hamacher, R. Klein, S. Nickel

Solving nonconvex planar location problems by finite dominating sets

It is well-known that some of the classical location problems with polyhedral gauges can be solved in polynomial time by finding a finite dominating set, i. e. a finite set of candidates guaranteed to contain at least one optimal location.
In this paper it is first established that this result holds for a much larger class of problems than currently considered in the literature. The model for which this result can be proven includes, for instance, location problems with attraction and repulsion, and location-allocation problems.
Next, it is shown that the approximation of general gauges by polyhedral ones in the objective function of our general model can be analyzed with regard to the subsequent error in the optimal objective value. For the approximation problem two different approaches are described, the sandwich procedure and the greedy algorithm. Both of these approaches lead - for fixed epsilon - to polynomial approximation algorithms with accuracy epsilon for solving the general model considered in this paper.
Keywords: Continuous Location, Polyhedral Gauges, Finite Dominating Sets, Approximation, Sandwich Algorithm, Greedy Algorithm
(19 pages, 2000)

19. A. Becker

A Review on Image Distortion Measures

Within this paper we review image distortion measures. A distortion measure is a criterion that assigns a "quality number" to an image. We distinguish between mathematical distortion measures and those distortion measures in-cooperating a priori knowledge about the imaging devices (e. g. satellite images), image processing algorithms or the human physiology. We will consider representative examples of different kinds of distortion measures and are going to discuss them.
Keywords: Distortion measure, human visual system
(26 pages, 2000)

20. H. W. Hamacher, M. Labbé, S. Nickel, T. Sonneborn

Polyhedral Properties of the Uncapacitated Multiple Allocation Hub Location Problem

We examine the feasibility polyhedron of the uncapacitated hub location problem (UHL) with multiple allocation, which has applications in the fields of air passenger and cargo transportation, telecommunication and postal delivery services. In particular we determine the dimension and derive some classes of facets of this polyhedron. We develop some general rules about lifting facets from the uncapacitated facility location (UFL) for UHL and projecting facets from UHL to UFL. By applying these rules we get a new class of facets for UHL which dominates the inequalities in the original formulation. Thus we get a new formulation of UHL whose constraints are all facet–defining. We show its superior computational performance by benchmarking it on a well known data set.
Keywords: integer programming, hub location, facility location, valid inequalities, facets, branch and cut
(21 pages, 2000)

21. H. W. Hamacher, A. Schöbel

Design of Zone Tariff Systems in Public Transportation

Given a public transportation system represented by its stops and direct connections between stops, we consider two problems dealing with the prices for the customers: The fare problem in which subsets of stops are already aggregated to zones and "good" tariffs have to be found in the existing zone system. Closed form solutions for the fare problem are presented for three objective functions. In the zone problem the design of the zones is part of the problem. This problem is NP hard and we therefore propose three heuristics which prove to be very successful in the redesign of one of Germany's transportation systems.
(30 pages, 2001)

22. D. Hietel, M. Junk, R. Keck, D. Teleaga

The Finite-Volume-Particle Method for Conservation Laws

In the Finite-Volume-Particle Method (FVPM), the weak formulation of a hyperbolic conservation law is discretized by restricting it to a discrete set of test functions. In contrast to the usual Finite-Volume approach, the test functions are not taken as characteristic functions of the control volumes in a spatial grid, but are chosen from a partition of unity with smooth and overlapping partition functions (the particles), which can even move along pre- scribed velocity fields. The information exchange between particles is based on standard numerical flux functions. Geometrical information, similar to the surface area of the cell faces in the Finite-Volume Method and the corresponding normal directions are given as integral quantities of the partition functions. After a brief derivation of the Finite-Volume-Particle Method, this work focuses on the role of the geometric coefficients in the scheme.
(16 pages, 2001)

23. T. Bender, H. Hennes, J. Kalcsics, M. T. Melo, S. Nickel

Location Software and Interface with GIS and Supply Chain Management

The objective of this paper is to bridge the gap between location theory and practice. To meet this objective focus is given to the development of software capable of addressing the different needs of a wide group of users. There is a very active community on location theory encompassing many research fields such as operations research, computer science, mathematics, engineering, geography, economics and marketing. As a result, people working on facility location problems have a very diverse background and also different needs regarding the software to solve these problems. For those interested in non-commercial applications (e. g. students and researchers), the library of location algorithms (LoLA can be of considerable assistance. LoLA contains a collection of efficient algorithms for solving planar, network and discrete facility location problems. In this paper, a detailed description of the functionality of LoLA is presented. In the fields of geography and marketing, for instance, solving facility location problems requires using large amounts of demographic data. Hence, members of these groups (e. g. urban planners and sales managers) often work with geographical information too s. To address the specific needs of these users, LoLA was inked to a geographical information system (GIS) and the details of the combined functionality are described in the paper. Finally, there is a wide group of practitioners who need to solve large problems and require special purpose software with a good data interface. Many of such users can be found, for example, in the area of supply chain management (SCM). Logistics activities involved in strategic SCM include, among others, facility location planning. In this paper, the development of a commercial location software tool is also described. The too is embedded in the Advanced Planner and Optimizer SCM software developed by SAP AG, Walldorf, Germany. The paper ends with some conclusions and an outlook to future activities.

Keywords: facility location, software development, geographical information systems, supply chain management

(48 pages, 2001)

24. H. W. Hamacher, S. A. Tjandra

Mathematical Modelling of Evacuation Problems: A State of Art

This paper details models and algorithms which can be applied to evacuation problems. While it concentrates on building evacuation many of the results are applicable also to regional evacuation. All models consider the time as main parameter, where the travel time between components of the building is part of the input and the overall evacuation time is the output. The paper distinguishes between macroscopic and microscopic evacuation models both of which are able to capture the evacuees' movement over time.

Macroscopic models are mainly used to produce good lower bounds for the evacuation time and do not consider any individual behavior during the emergency situation. These bounds can be used to analyze existing buildings or help in the design phase of planning a building. Macroscopic approaches which are based on dynamic network flow models (minimum cost dynamic flow, maximum dynamic flow, universal maximum flow, quickest path and quickest flow) are described. A special feature of the presented approach is the fact, that travel times of evacuees are not restricted to be constant, but may be density dependent. Using multicriteria optimization priority regions and blockage due to fire or smoke may be considered. It is shown how the modelling can be done using time parameter either as discrete or continuous parameter.

Microscopic models are able to model the individual evacuee's characteristics and the interaction among evacuees which influence their movement. Due to the corresponding huge amount of data one uses simulation approaches. Some probabilistic laws for individual evacuee's movement are presented. Moreover ideas to model the evacuee's movement using cellular automata (CA) and resulting software are presented.

In this paper we will focus on macroscopic models and only summarize some of the results of the microscopic approach. While most of the results are applicable to general evacuation situations, we concentrate on building evacuation.

(44 pages, 2001)

25. J. Kuhnert, S. Tiwari

Grid free method for solving the Poisson equation

A Grid free method for solving the Poisson equation is presented. This is an iterative method. The method is based on the weighted least squares approximation in which the Poisson equation is enforced to be satisfied in every iterations. The boundary conditions can also be enforced in the iteration process. This is a local approximation procedure. The Dirichlet, Neumann and mixed boundary value problems on a unit square are presented and the analytical solutions are compared with the exact solutions. Both solutions matched perfectly.

Keywords: Poisson equation, Least squares method, Grid free method

(19 pages, 2001)

26. T. Götz, H. Rave, D. Reinel-Bitzer, K. Steiner, H. Tiemeier

Simulation of the fiber spinning process

To simulate the influence of process parameters to the melt spinning process a fiber model is used and coupled with CFD calculations of the quench air flow. In the fiber model energy, momentum and mass balance are solved for the polymer mass flow. To calculate the quench air the Lattice Boltzmann method is used. Simulations and experiments for different process parameters and hole configurations are compared and show a good agreement.

Keywords: Melt spinning, fiber model, Lattice Boltzmann, CFD

(19 pages, 2001)

27. A. Zemitis

On interaction of a liquid film with an obstacle

In this paper mathematical models for liquid films generated by impinging jets are discussed. Attention is stressed to the interaction of the liquid film with some obstacle. S. G. Taylor [Proc. R. Soc. London Ser. A 253, 313 (1959)] found that the liquid film generated by impinging jets is very sensitive to properties of the wire which was used as an obstacle. The aim of this presentation is to propose a modification of the Taylor's model, which allows to simulate the film shape in cases, when the angle between jets is different from 180°. Numerical results obtained by discussed models give two different shapes of the liquid film similar as in Taylors experiments. These two shapes depend on the regime: either droplets are produced close to the obstacle or not. The difference between two regimes becomes larger if the angle between jets decreases. Existence of such two regimes can be very essential for some applications of impinging jets, if the generated liquid film can have a contact with obstacles.

Keywords: impinging jets, liquid film, models, numerical solution, shape

(22 pages, 2001)

28. I. Ginzburg, K. Steiner

Free surface lattice-Boltzmann method to model the filling of expanding cavities by Bingham Fluids

The filling process of viscoplastic metal alloys and plastics in expanding cavities is modelled using the lattice Boltzmann method in two and three dimensions. These models combine the regularized Bingham model for viscoplastic with a free-interface algorithm. The latter is based on a modified immiscible lattice Boltzmann model in which one species is the fluid and the other one is considered as vacuum. The boundary conditions at the curved liquid-vacuum interface are met without any geometrical front reconstruction from a first-order Chapman-Enskog expansion. The numerical results obtained with these models are found in good agreement with available theoretical and numerical analysis.

Keywords: Generalized LBE, free-surface phenomena, interface boundary conditions, filling processes, Bingham viscoplastic model, regularized models

(22 pages, 2001)

29. H. Neunzert

»Denn nichts ist für den Menschen als Menschen etwas wert, was er nicht mit Leidenschaft tun kann«
Vortrag anlässlich der Verleihung des Akademiepreises des Landes Rheinland-Pfalz am 21.11.2001

Was macht einen guten Hochschullehrer aus? Auf diese Frage gibt es sicher viele verschiedene, fachbezogene Antworten, aber auch ein paar allgemeine Gesichtspunkte: es bedarf der »Leidenschaft« für die Forschung (Max Weber), aus der dann auch die Begeisterung für die Lehre erwächst. Forschung und Lehre gehören zusammen, um die Wissenschaft als lebendiges Tun vermitteln zu können. Der Vortrag gibt Beispiele dafür, wie in angewandter Mathematik Forschungsaufgaben aus praktischen Alltagsproblemstellungen erwachsen, die in die Lehre auf verschiedenen Stufen (Gymnasium bis Graduiertenkolleg) einfließen; er leitet damit auch zu einem aktuellen Forschungsgebiet, der Mehrskalenanalyse mit ihren vielfältigen Anwendungen in Bildverarbeitung, Materialentwicklung und Strömungsmechanik über, was aber nur kurz gestreift wird. Mathematik erscheint hier als eine moderne Schlüsseltechnologie, die aber auch enge Beziehungen zu den Geistes- und Sozialwissenschaften hat.

Keywords: Lehre, Forschung, angewandte Mathematik, Mehrskalenanalyse, Strömungsmechanik

(18 pages, 2001)

30. J. Kuhnert, S. Tiwari

Finite pointset method based on the projection method for simulations of the incompressible Navier-Stokes equations

A Lagrangian particle scheme is applied to the projection method for the incompressible Navier-Stokes equations. The approximation of spatial derivatives is obtained by the weighted least squares method. The pressure Poisson equation is solved by a local iterative procedure with the help of the least squares method. Numerical tests are performed for two dimensional cases. The Couette flow, Poiseuelle flow, decaying shear flow and the driven cavity flow are presented. The numerical solutions are obtained for stationary as well as instationary cases and are compared with the analytical solutions for channel flows. Finally, the driven cavity in a unit square is considered and the stationary solution obtained from this scheme is compared with that from the finite element method.

Keywords: Incompressible Navier-Stokes equations, Meshfree method, Projection method, Particle scheme, Least squares approximation

AMS subject classification: 76D05, 76M28

(25 pages, 2001)

31. R. Korn, M. Krekel

Optimal Portfolios with Fixed Consumption or Income Streams

We consider some portfolio optimisation problems where either the investor has a desire for an a priori specified consumption stream or/and follows a deterministic pay in scheme while also trying to maximize expected utility from final wealth. We derive explicit closed form solutions for continuous and discrete monetary streams. The mathematical method used is classical stochastic control theory.

Keywords: Portfolio optimisation, stochastic control, HJB equation, discretisation of control problems.

(23 pages, 2002)

32. M. Krekel

Optimal portfolios with a loan dependent credit spread

If an investor borrows money he generally has to pay higher interest rates than he would have received, if he had put his funds on a savings account. The classical model of continuous time portfolio optimisation ignores this effect. Since there is obviously a connection between the default probability and the total per-

centage of wealth, which the investor is in debt, we study portfolio optimisation with a control dependent interest rate. Assuming a logarithmic and a power utility function, respectively, we prove explicit formulae of the optimal control.
Keywords: Portfolio optimisation, stochastic control, HJB equation, credit spread, log utility, power utility, non-linear wealth dynamics
(25 pages, 2002)

33. J. Ohser, W. Nagel, K. Schladitz

The Euler number of discretized sets - on the choice of adjacency in homogeneous lattices

Two approaches for determining the Euler-Poincaré characteristic of a set observed on lattice points are considered in the context of image analysis { the integral geometric and the polyhedral approach. Information about the set is assumed to be available on lattice points only. In order to retain properties of the Euler number and to provide a good approximation of the true Euler number of the original set in the Euclidean space, the appropriate choice of adjacency in the lattice for the set and its background is crucial. Adjacencies are defined using tessellations of the whole space into polyhedrons. In R 3 , two new 14 adjacencies are introduced additionally to the well known 6 and 26 adjacencies. For the Euler number of a set and its complement, a consistency relation holds. Each of the pairs of adjacencies (14:1; 14:1), (14:2; 14:2), (6; 26), and (26; 6) is shown to be a pair of complementary adjacencies with respect to this relation. That is, the approximations of the Euler numbers are consistent if the set and its background (complement) are equipped with this pair of adjacencies. Furthermore, sufficient conditions for the correctness of the approximations of the Euler number are given. The analysis of selected microstructures and a simulation study illustrate how the estimated Euler number depends on the chosen adjacency. It also shows that there is not a uniquely best pair of adjacencies with respect to the estimation of the Euler number of a set in Euclidean space.
Keywords: image analysis, Euler number, neighborhod relationships, cuboidal lattice
(32 pages, 2002)

34. I. Ginzburg, K. Steiner

Lattice Boltzmann Model for Free-Surface flow and Its Application to Filling Process in Casting

A generalized lattice Boltzmann model to simulate free-surface is constructed in both two and three dimensions. The proposed model satisfies the interfacial boundary conditions accurately. A distinctive feature of the model is that the collision processes is carried out only on the points occupied partially or fully by the fluid. To maintain a sharp interfacial front, the method includes an anti-diffusion algorithm. The unknown distribution functions at the interfacial region are constructed according to the first order Chapman-Enskog analysis. The interfacial boundary conditions are satisfied exactly by the coefficients in the Chapman-Enskog expansion. The distribution functions are naturally expressed in the local interfacial coordinates. The macroscopic quantities at the interface are extracted from the least-square solutions of a locally linearized system obtained from the known distribution functions. The proposed method does not require any geometric front construction and is robust for any interfacial topology. Simulation results of realistic filling process are presented: rectangular cavity in two dimensions and Hammer box, Campbell box, Sheffield box, and Motorblock in three dimensions. To enhance the stability at high Reynolds numbers, various upwind-type schemes are developed. Free-slip and no-slip boundary conditions are also discussed.
Keywords: Lattice Boltzmann models; free-surface phenomena; interface boundary conditions; filling processes; injection molding; volume of fluid method; interface boundary conditions; advection-schemes; upwind-schemes
(54 pages, 2002)

35. M. Günther, A. Klar, T. Materne, R. Wegener

Multivalued fundamental diagrams and stop and go waves for continuum traffic equations

In the present paper a kinetic model for vehicular traffic leading to multivalued fundamental diagrams is developed and investigated in detail. For this model phase transitions can appear depending on the local density and velocity of the flow. A derivation of associated macroscopic traffic equations from the kinetic equation is given. Moreover, numerical experiments show the appearance of stop and go waves for highway traffic with a bottleneck.
Keywords: traffic flow, macroscopic equations, kinetic derivation, multivalued fundamental diagram, stop and go waves, phase transitions
(25 pages, 2002)

36. S. Feldmann, P. Lang, D. Prätzel-Wolters

Parameter influence on the zeros of network determinants

To a network N(q) with determinant D(s;q) depending on a parameter vector q Î Rr via identification of some of its vertices, a network N^ (q) is assigned. The paper deals with procedures to find N^ (q), such that its determinant D^ (s;q) admits a factorization in the determinants of appropriate subnetworks, and with the estimation of the deviation of the zeros of D^ from the zeros of D. To solve the estimation problem state space methods are applied.
Keywords: Networks, Equicofactor matrix polynomials, Realization theory, Matrix perturbation theory
(30 pages, 2002)

37. K. Koch, J. Ohser, K. Schladitz

Spectral theory for random closed sets and estimating the covariance via frequency space

A spectral theory for stationary random closed sets is developed and provided with a sound mathematical basis. Definition and proof of existence of the Bartlett spectrum of a stationary random closed set as well as the proof of a Wiener-Khintchine theorem for the power spectrum are used to two ends: First, well known second order characteristics like the covariance can be estimated faster than usual via frequency space. Second, the Bartlett spectrum and the power spectrum can be used as second order characteristics in frequency space. Examples show, that in some cases information about the random closed set is easier to obtain from these characteristics in frequency space than from their real world counterparts.
Keywords: Random set, Bartlett spectrum, fast Fourier transform, power spectrum
(28 pages, 2002)

38. D. d'Humières, I. Ginzburg

Multi-reflection boundary conditions for lattice Boltzmann models

We present a unified approach of several boundary conditions for lattice Boltzmann models. Its general framework is a generalization of previously introduced schemes such as the bounce-back rule, linear or quadratic interpolations, etc. The objectives are two fold: first to give theoretical tools to study the existing boundary conditions and their corresponding accuracy; secondly to design formally third- order accurate boundary conditions for general flows. Using these boundary conditions, Couette and Poiseuille flows are exact solution of the lattice Boltzmann models for a Reynolds number Re = 0 (Stokes limit).
Numerical comparisons are given for Stokes flows in periodic arrays of spheres and cylinders, linear periodic array of cylinders between moving plates and for Navier-Stokes flows in periodic arrays of cylinders for Re < 200. These results show a significant improvement of the overall accuracy when using the linear interpolations instead of the bounce-back reflection (up to an order of magnitude on the hydrodynamics fields). Further improvement is achieved with the new multi-reflection boundary conditions, reaching a level of accuracy close to the quasi-analytical reference solutions, even for rather modest grid resolutions and few points in the narrowest channels. More important, the pressure and velocity fields in the vicinity of the obstacles are much smoother with multi-reflection than with the other boundary conditions.
Finally the good stability of these schemes is highlighted by some simulations of moving obstacles: a cylinder between flat walls and a sphere in a cylinder.
Keywords: lattice Boltzmann equation, boudary condistions, bounce-back rule, Navier-Stokes equation
(72 pages, 2002)

39. R. Korn

Elementare Finanzmathematik

Im Rahmen dieser Arbeit soll eine elementar gehaltene Einführung in die Aufgabenstellungen und Prinzipien der modernen Finanzmathematik gegeben werden. Insbesondere werden die Grundlagen der Modellierung von Aktienkursen, der Bewertung von Optionen und der Portfolio-Optimierung vorgestellt. Natürlich können die verwendeten Methoden und die entwickelte Theorie nicht in voller Allgemeinheit für den Schulunterricht verwendet werden, doch sollen einzelne Prinzipien so heraus gearbeitet werden, dass sie auch an einfachen Beispielen verstanden werden können.
Keywords: Finanzmathematik, Aktien, Optionen, Portfolio-Optimierung, Börse, Lehrerweiterbildung, Mathematikunterricht
(98 pages, 2002)

40. J. Kallrath, M. C. Müller, S. Nickel

Batch Presorting Problems: Models and Complexity Results

In this paper we consider short term storage systems. We analyze presorting strategies to improve the effiency of these storage systems. The presorting task is called Batch PreSorting Problem (BPSP). The BPSP is a variation of an assigment problem, i. e., it has an assigment problem kernel and some additional constraints. We present different types of these presorting problems, introduce mathematical programming formulations and prove the NP-completeness for one type of the BPSP. Experiments are carried out in order to compare the different model formulations and to investigate the behavior of these models.
Keywords: Complexity theory, Integer programming, Assigment, Logistics
(19 pages, 2002)

41. J. Linn

On the frame-invariant description of the phase space of the Folgar-Tucker equation

The Folgar-Tucker equation is used in flow simulations of fiber suspensions to predict fiber orientation depending on the local flow. In this paper, a complete, frame-invariant description of the phase space of this differential equation is presented for the first time.
Key words: fiber orientation, Folgar-Tucker equation, injection molding
(5 pages, 2003)

42. T. Hanne, S. Nickel

A Multi-Objective Evolutionary Algorithm for Scheduling and Inspection Planning in Software Development Projects

In this article, we consider the problem of planning inspections and other tasks within a software development (SD) project with respect to the objectives quality (no. of defects), project duration, and costs. Based on a discrete-event simulation model of SD processes comprising the phases coding, inspection, test, and rework, we present a simplified formulation of the problem as a multiobjective optimization problem. For solving the problem (i. e. finding an approximation of the efficient set) we develop a multiobjective evolutionary algorithm. Details of the algorithm are discussed as well as results of its application to sample problems.
Key words: multiple objective programming, project management and scheduling, software development, evolutionary algorithms, efficient set
(29 pages, 2003)

43. T. Bortfeld , K.-H. Küfer, M. Monz, A. Scherrer, C. Thieke, H. Trinkaus

Intensity-Modulated Radiotherapy - A Large Scale Multi-Criteria Programming Problem -

Radiation therapy planning is always a tight rope walk between dangerous insufficient dose in the target volume and life threatening overdosing of organs at risk. Finding ideal balances between these inherently contradictory goals challenges dosimetrists and physicians in their daily practice. Today's planning systems are typically based on a single evaluation function that measures the quality of a radiation treatment plan. Unfortunately, such a one dimensional approach cannot satisfactorily map the different backgrounds of physicians and the patient dependent necessities. So, too often a time consuming iteration process between evaluation of dose distribution and redefinition of the evaluation function is needed.

In this paper we propose a generic multi-criteria approach based on Pareto's solution concept. For each entity of interest - target volume or organ at risk a structure dependent evaluation function is defined measuring deviations from ideal doses that are calculated from statistical functions. A reasonable bunch of clinically meaningful Pareto optimal solutions are stored in a data base, which can be interactively searched by physicians. The system guarantees dynamical planning as well as the discussion of tradeoffs between different entities.

Mathematically, we model the upcoming inverse problem as a multi-criteria linear programming problem. Because of the large scale nature of the problem it is not possible to solve the problem in a 3D-setting without adaptive reduction by appropriate approximation schemes.

Our approach is twofold: First, the discretization of the continuous problem is based on an adaptive hierarchical clustering process which is used for a local refinement of constraints during the optimization procedure. Second, the set of Pareto optimal solutions is approximated by an adaptive grid of representatives that are found by a hybrid process of calculating extreme compromises and interpolation methods.

Keywords: multiple criteria optimization, representative systems of Pareto solutions, adaptive triangulation, clustering and disaggregation techniques, visualization of Pareto solutions, medical physics, external beam radiotherapy planning, intensity modulated radiotherapy

(31 pages, 2003)

44. T. Halfmann, T. Wichmann

Overview of Symbolic Methods in Industrial Analog Circuit Design

Industrial analog circuits are usually designed using numerical simulation tools. To obtain a deeper circuit understanding, symbolic analysis techniques can additionally be applied. Approximation methods which reduce the complexity of symbolic expressions are needed in order to handle industrial-sized problems.

This paper will give an overview to the field of symbolic analog circuit analysis. Starting with a motivation, the state-of-the-art simplification algorithms for linear as well as for nonlinear circuits are presented. The basic ideas behind the different techniques are described, whereas the technical details can be found in the cited references. Finally, the application of linear and nonlinear symbolic analysis will be shown on two example circuits.

Keywords: CAD, automated analog circuit design, symbolic analysis, computer algebra, behavioral modeling, system simulation, circuit sizing, macro modeling, differential-algebraic equations, index

(17 pages, 2003)

45. S. E. Mikhailov, J. Orlik

Asymptotic Homogenisation in Strength and Fatigue Durability Analysis of Composites

Asymptotic homogenisation technique and two-scale convergence is used for analysis of macro-strength and fatigue durability of composites with a periodic structure under cyclic loading. The linear damage accumulation rule is employed in the phenomenological micro-durability conditions (for each component of the composite) under varying cyclic loading. Both local and non-local strength and durability conditions are analysed. The strong convergence of the strength and fatigue damage measure as the structure period tends to zero is proved and their limiting values are estimated.

Keywords: multiscale structures, asymptotic homogenization, strength, fatigue, singularity, non-local conditions

(14 pages, 2003)

46. P. Domínguez-Marín, P. Hansen, N. Mladenovi´c , S. Nickel

Heuristic Procedures for Solving the Discrete Ordered Median Problem

We present two heuristic methods for solving the Discrete Ordered Median Problem (DOMP), for which no such approaches have been developed so far. The DOMP generalizes classical discrete facility location problems, such as the p-median, p-center and Uncapacitated Facility Location problems. The first procedure proposed in this paper is based on a genetic algorithm developed by Moreno Vega [MV96] for p-median and p-center problems. Additionally, a second heuristic approach based on the Variable Neighborhood Search metaheuristic (VNS) proposed by Hansen & Mladenovic [HM97] for the p-median problem is described. An extensive numerical study is presented to show the efficiency of both heuristics and compare them.

Keywords: genetic algorithms, variable neighborhood search, discrete facility location

(31 pages, 2003)

47. N. Boland, P. Domínguez-Marín, S. Nickel, J. Puerto

Exact Procedures for Solving the Discrete Ordered Median Problem

The Discrete Ordered Median Problem (DOMP) generalizes classical discrete location problems, such as the N-median, N-center and Uncapacitated Facility Location problems. It was introduced by Nickel [16], who formulated it as both a nonlinear and a linear integer program. We propose an alternative integer linear programming formulation for the DOMP, discuss relationships between both integer linear programming formulations, and show how properties of optimal solutions can be used to strengthen these formulations. Moreover, we present a specific branch and bound procedure to solve the DOMP more efficiently. We test the integer linear programming formulations and this branch and bound method computationally on randomly generated test problems.

Keywords: discrete location, Integer programming

(41 pages, 2003)

48. S. Feldmann, P. Lang

Padé-like reduction of stable discrete linear systems preserving their stability

A new stability preserving model reduction algorithm for discrete linear SISO-systems based on their impulse response is proposed. Similar to the Padé approximation, an equation system for the Markov parameters involving the Hankel matrix is considered, that here however is chosen to be of very high dimension. Although this equation system therefore in general cannot be solved exactly, it is proved that the approximate solution, computed via the Moore-Penrose inverse, gives rise to a stability preserving reduction scheme, a property that cannot be guaranteed for the Padé approach. Furthermore, the proposed algorithm is compared to another stability preserving reduction approach, namely the balanced truncation method, showing comparable performance of the reduced systems. The balanced truncation method however starts from a state space description of the systems and in general is expected to be more computational demanding.

Keywords: Discrete linear systems, model reduction, stability, Hankel matrix, Stein equation

(16 pages, 2003)

49. J. Kallrath, S. Nickel

A Polynomial Case of the Batch Presorting Problem

This paper presents new theoretical results for a special case of the batch presorting problem (BPSP). We will show tht this case can be solved in polynomial time. Offline and online algorithms are presented for solving the BPSP. Competetive analysis is used for comparing the algorithms.

Keywords: batch presorting problem, online optimization, competetive analysis, polynomial algorithms, logistics

(17 pages, 2003)

50. T. Hanne, H. L. Trinkaus

knowCube for MCDM – Visual and Interactive Support for Multicriteria Decision Making

In this paper, we present a novel multicriteria decision support system (MCDSS), called knowCube, consisting of components for knowledge organization, generation, and navigation. Knowledge organization rests upon a database for managing qualitative and quantitative criteria, together with add-on information. Knowledge generation serves filling the database via e. g. identification, optimization, classification or simulation. For "finding needles in haycocks", the knowledge navigation component supports graphical database retrieval and interactive, goal-oriented problem solving. Navigation "helpers" are, for instance, cascading criteria aggregations, modifiable metrics, ergonomic interfaces, and customizable visualizations. Examples from real-life projects, e.g. in industrial engineering and in the life sciences, illustrate the application of our MCDSS.

Key words: Multicriteria decision making, knowledge management, decision support systems, visual interfaces, interactive navigation, real-life applications.

(26 pages, 2003)

51. O. Iliev, V. Laptev

On Numerical Simulation of Flow Through Oil Filters

This paper concerns numerical simulation of flow through oil filters. Oil filters consist of filter housing (filter box), and a porous filtering medium, which completely separates the inlet from the outlet. We discuss mathematical models, describing coupled flows in the pure liquid subregions and in the porous filter media, as well as interface conditions between them. Further, we reformulate the problem in fictitious regions method manner, and discuss peculiarities of the numerical algorithm in solving the coupled system. Next, we show numerical results, validating the model and the algorithm. Finally, we present results from simulation of 3-D oil flow through a real car filter.

Keywords: oil filters, coupled flow in plain and porous media, Navier-Stokes, Brinkman, numerical simulation

(8 pages, 2003)

52. W. Dörfler, O. Iliev, D. Stoyanov, D. Vassileva

On a Multigrid Adaptive Refinement Solver for Saturated Non-Newtonian Flow in Porous Media

A multigrid adaptive refinement algorithm for non-Newtonian flow in porous media is presented. The saturated flow of a non-Newtonian fluid is described by the continuity equation and the generalized Darcy law. The resulting second order nonlinear elliptic equation is discretized by a finite volume method on a cell-centered grid. A nonlinear full-multigrid, full-approximation-storage algorithm is implemented. As a smoother, a single grid solver based on Picard linearization and Gauss-Seidel relaxation is used. Further, a local refinement multigrid algorithm on a composite grid is developed. A residual based error indicator is used in the adaptive refinement criterion. A special implementation approach is used, which allows us to perform unstructured local refinement in conjunction with the finite volume discretization. Several results from numerical experiments are presented in order to examine the performance of the solver.

Keywords: Nonlinear multigrid, adaptive refinement, non-Newtonian flow in porous media

(17 pages, 2003)

53. S. Kruse

On the Pricing of Forward Starting Options under Stochastic Volatility

We consider the problem of pricing European forward starting options in the presence of stochastic volatility. By performing a change of measure using the asset

price at the time of strike determination as a numeraire, we derive a closed-form solution based on Heston's model of stochastic volatility.
Keywords: Option pricing, forward starting options, Heston model, stochastic volatility, cliquet options
(11 pages, 2003)

54. O. Iliev, D. Stoyanov

Multigrid – adaptive local refinement solver for incompressible flows

A non-linear multigrid solver for incompressible Navier-Stokes equations, exploiting finite volume discretization of the equations, is extended by adaptive local refinement. The multigrid is the outer iterative cycle, while the SIMPLE algorithm is used as a smoothing procedure. Error indicators are used to define the refinement subdomain. A special implementation approach is used, which allows to perform unstructured local refinement in conjunction with the finite volume discretization. The multigrid - adaptive local refinement algorithm is tested on 2D Poisson equation and further is applied to a lid-driven flows in a cavity (2D and 3D case), comparing the results with bench-mark data. The software design principles of the solver are also discussed.
Keywords: Navier-Stokes equations, incompressible flow, projection-type splitting, SIMPLE, multigrid methods, adaptive local refinement, lid-driven flow in a cavity
(37 pages, 2003)

55. V. Starikovicius

The multiphase flow and heat transfer in porous media

In first part of this work, summaries of traditional Multiphase Flow Model and more recent Multiphase Mixture Model are presented. Attention is being paid to attempts include various heterogeneous aspects into models. In second part, MMM based differential model for two-phase immiscible flow in porous media is considered. A numerical scheme based on the sequential solution procedure and control volume based finite difference schemes for the pressure and saturation-conservation equations is developed. A computer simulator is built, which exploits object-oriented programming techniques. Numerical result for several test problems are reported.
Keywords: Two-phase flow in porous media, various formulations, global pressure, multiphase mixture model, numerical simulation
(30 pages, 2003)

56. P. Lang, A. Sarishvili, A. Wirsen

Blocked neural networks for knowledge extraction in the software development process

One of the main goals of an organization developing software is to increase the quality of the software while at the same time to decrease the costs and the duration of the development process. To achieve this, various decisions e.ecting this goal before and during the development process have to be made by the managers. One appropriate tool for decision support are simulation models of the software life cycle, which also help to understand the dynamics of the software development process. Building up a simulation model requires a mathematical description of the interactions between di.erent objects involved in the development process. Based on experimental data, techniques from the .eld of knowledge discovery can be used to quantify these interactions and to generate new process knowledge based on the analysis of the determined relationships. In this paper blocked neuronal networks and related relevance measures will be presented as an appropriate tool for quanti.cation and validation of qualitatively known dependencies in the software development process.
Keywords: Blocked Neural Networks, Nonlinear Regression, Knowledge Extraction, Code Inspection
(21 pages, 2003)

57. H. Knaf, P. Lang, S. Zeiser

Diagnosis aiding in Regulation Thermography using Fuzzy Logic

The objective of the present article is to give an overview of an application of Fuzzy Logic in Regulation Thermography, a method of medical diagnosis support. An introduction to this method of the complementary medical science based on temperature measurements – so-called thermograms – is provided. The process of modelling the physician's thermogram evaluation rules using the calculus of Fuzzy Logic is explained.
Keywords: fuzzy logic,knowledge representation, expert system
(22 pages, 2003)

58. M.T. Melo, S. Nickel, F. Saldanha da Gama

Largescale models for dynamic multi-commodity capacitated facility location

In this paper we focus on the strategic design of supply chain networks. We propose a mathematical modeling framework that captures many practical aspects of network design problems simultaneously but which have not received adequate attention in the literature. The aspects considered include: dynamic planning horizon, generic supply chain network structure, external supply of materials, inventory opportunities for goods, distribution of commodities, facility configuration, availability of capital for investments, and storage limitations. Moreover, network configuration decisions concerning the gradual relocation of facilities over the planning horizon are considered. To cope with fluctuating demands, capacity expansion and reduction scenarios are also analyzed as well as modular capacity shifts. The relation of the proposed modeling framework with existing models is discussed. For problems of reasonable size we report on our computational experience with standard mathematical programming software. In particular, useful insights on the impact of various factors on network design decisions are provided.
Keywords: supply chain management, strategic planning, dynamic location, modeling
(40 pages, 2003)

59. J. Orlik

Homogenization for contact problems with periodically rough surfaces

We consider the contact of two elastic bodies with rough surfaces at the interface. The size of the micro-peaks and valleys is very small compared with the macrosize of the bodies' domains. This makes the direct application of the FEM for the calculation of the contact problem prohibitively costly. A method is developed that allows deriving a macrocontact condition on the interface. The method involves the twoscale asymptotic homogenization procedure that takes into account the microgeometry of the interface layer and the stiffnesses of materials of both domains. The macrocontact condition can then be used in a FEM model for the contact problem on the macrolevel. The averaged contact stiffness obtained allows the replacement of the interface layer in the macromodel by the macrocontact condition.
Keywords: asymptotic homogenization, contact problems
(28 pages, 2004)

60. A. Scherrer, K.-H. Küfer, M. Monz, F. Alonso, T. Bortfeld

IMRT planning on adaptive volume structures – a significant advance of computational complexity

In intensity-modulated radiotherapy (IMRT) planning the oncologist faces the challenging task of finding a treatment plan that he considers to be an ideal compromise of the inherently contradictive goals of delivering a sufficiently high dose to the target while widely sparing critical structures. The search for this a priori unknown compromise typically requires the computation of several plans, i.e. the solution of several optimization problems. This accumulates to a high computational expense due to the large scale of these problems - a consequence of the discrete problem formulation. This paper presents the adaptive clustering method as a new algorithmic concept to overcome these difficulties. The computations are performed on an individually adapted structure of voxel clusters rather than on the original voxels leading to a decisively reduced computational complexity as numerical examples on real clinical data demonstrate. In contrast to many other similar concepts, the typical trade-off between a reduction in computational complexity and a loss in exactness can be avoided: the adaptive clustering method produces the optimum of the original problem. This flexible method can be applied to both single- and multi-criteria optimization methods based on most of the convex evaluation functions used in practice.
Keywords: Intensity-modulated radiation therapy (IMRT), inverse treatment planning, adaptive volume structures, hierarchical clustering, local refinement, adaptive clustering, convex programming, mesh generation, multi-grid methods
(24 pages, 2004)

61. D. Kehrwald

Parallel lattice Boltzmann simulation of complex flows

After a short introduction to the basic ideas of lattice Boltzmann methods and a brief description of a modern parallel computer, it is shown how lattice Boltzmann schemes are successfully applied for simulating fluid flow in microstructures and calculating material properties of porous media. It is explained how lattice Boltzmann schemes compute the gradient of the velocity field without numerical differentiation. This feature is then utilised for the simulation of pseudo-plastic fluids, and numerical results are presented for a simple benchmark problem as well as for the simulation of liquid composite moulding.
Keywords: Lattice Boltzmann methods, parallel computing, microstructure simulation, virtual material design, pseudo-plastic fluids, liquid composite moulding
(12 pages, 2004)

62. O. Iliev, J. Linn, M. Moog, D. Niedziela, V. Starikovicius

On the Performance of Certain Iterative Solvers for Coupled Systems Arising in Discretization of Non-Newtonian Flow Equations

Iterative solution of large scale systems arising after discretization and linearization of the unsteady non-Newtonian Navier–Stokes equations is studied. cross WLF model is used to account for the non-Newtonian behavior of the fluid. Finite volume method is used to discretize the governing system of PDEs. Viscosity is treated explicitely (e.g., it is taken from the previous time step), while other terms are treated implicitly. Different preconditioners (block–diagonal, block–triangular, relaxed incomplete LU factorization, etc.) are used in conjunction with advanced iterative methods, namely, BiCGStab, CGS, GMRES. The action of the preconditioner in fact requires inverting different blocks. For this purpose, in addition to preconditioned BiCGStab, CGS, GMRES, we use also algebraic multigrid method (AMG). The performance of the iterative solvers is studied with respect to the number of unknowns, characteristic velocity in the basic flow, time step, deviation from Newtonian behavior, etc. Results from numerical experiments are presented and discussed.
Keywords: Performance of iterative solvers, Preconditioners, Non-Newtonian flow
(17 pages, 2004)

63. R. Ciegis, O. Iliev, S. Rief, K. Steiner

On Modelling and Simulation of Different Regimes for Liquid Polymer Moulding

In this paper we consider numerical algorithms for solving a system of nonlinear PDEs arising in modeling of liquid polymer injection. We investigate the particular case when a porous preform is located within the mould, so that the liquid polymer flows through a porous medium during the filling stage. The nonlinearity of the governing system of PDEs is due to the non-Newtonian behavior of the polymer, as well as due to the moving free boundary. The latter is related to the penetration front and a Stefan type problem is formulated to account for it. A finite-volume method is used to approximate the given differential problem. Results of numerical experiments are presented.
We also solve an inverse problem and present algorithms for the determination of the absolute preform permeability coefficient in the case when the velocity of the penetration front is known from measurements. In both cases (direct and inverse problems) we emphasize on the specifics related to the non-Newtonian behavior of the polymer. For completeness, we discuss also the Newtonian case. Results of some experimental

measurements are presented and discussed.
Keywords: Liquid Polymer Moulding, Modelling, Simulation, Infiltration, Front Propagation, non-Newtonian flow in porous media
(43 pages, 2004)

64. T. Hanne, H. Neu

Simulating Human Resources in Software Development Processes

In this paper, we discuss approaches related to the explicit modeling of human beings in software development processes. While in most older simulation models of software development processes, esp. those of the system dynamics type, humans are only represented as a labor pool, more recent models of the discrete-event simulation type require representations of individual humans. In that case, particularities regarding the person become more relevant. These individual effects are either considered as stochastic variations of productivity, or an explanation is sought based on individual characteristics, such as skills for instance. In this paper, we explore such possibilities by recurring to some basic results in psychology, sociology, and labor science. Various specific models for representing human effects in software process simulation are discussed.
Keywords: Human resource modeling, software process, productivity, human factors, learning curve
(14 pages, 2004)

65. O. Iliev, A. Mikelic, P. Popov

Fluid structure interaction problems in deformable porous media: Toward permeability of deformable porous media

In this work the problem of fluid flow in deformable porous media is studied. First, the stationary fluid-structure interaction (FSI) problem is formulated in terms of incompressible Newtonian fluid and a linearized elastic solid. The flow is assumed to be characterized by very low Reynolds number and is described by the Stokes equations. The strains in the solid are small allowing for the solid to be described by the Lame equations, but no restrictions are applied on the magnitude of the displacements leading to strongly coupled, nonlinear fluid-structure problem. The FSI problem is then solved numerically by an iterative procedure which solves sequentially fluid and solid subproblems. Each of the two subproblems is discretized by finite elements and the fluid-structure coupling is reduced to an interface boundary condition. Several numerical examples are presented and the results from the numerical computations are used to perform permeability computations for different geometries.
Keywords: fluid-structure interaction, deformable porous media, upscaling, linear elasticity, stokes, finite elements
(28 pages, 2004)

66. F. Gaspar, O. Iliev, F. Lisbona, A. Naumovich, P. Vabishchevich

On numerical solution of 1-D poroelasticity equations in a multilayered domain

Finite volume discretization of Biot system of poroelasticity in a multilayered domain is presented. Staggered grid is used in order to avoid nonphysical oscillations of the numerical solution, appearing when a collocated grid is used. Various numerical experiments are presented in order to illustrate the accuracy of the finite difference scheme. In the first group of experiments, problems having analytical solutions are solved, and the order of convergence for the velocity, the pressure, the displacements, and the stresses is analyzed. In the second group of experiments numerical solution of real problems is presented.
Keywords: poroelasticity, multilayered material, finite volume discretization, MAC type grid
(41 pages, 2004)

67. J. Ohser, K. Schladitz, K. Koch, M. Nöthe

Diffraction by image processing and its application in materials science

A spectral theory for constituents of macroscopically homogeneous random microstructures modeled as homogeneous random closed sets is developed and provided with a sound mathematical basis, where the spectrum obtained by Fourier methods corresponds to the angular intensity distribution of x-rays scattered by this constituent. It is shown that the fast Fourier transform applied to three-dimensional images of microstructures obtained by micro-tomography is a powerful tool of image processing. The applicability of this technique is is demonstrated in the analysis of images of porous media.
Keywords: porous microstructure, image analysis, random set, fast Fourier transform, power spectrum, Bartlett spectrum
(13 pages, 2004)

68. H. Neunzert

Mathematics as a Technology: Challenges for the next 10 Years

No doubt: Mathematics has become a technology in its own right, maybe even a key technology. Technology may be defined as the application of science to the problems of commerce and industry. And science? Science maybe defined as developing, testing and improving models for the prediction of system behavior; the language used to describe these models is mathematics and mathematics provides methods to evaluate these models. Here we are! Why has mathematics become a technology only recently? Since it got a tool, a tool to evaluate complex, "near to reality" models: Computer! The model may be quite old – Navier-Stokes equations describe flow behavior rather well, but to solve these equations for realistic geometry and higher Reynolds numbers with sufficient precision is even for powerful parallel computing a real challenge. Make the models as simple as possible, as complex as necessary – and then evaluate them with the help of efficient and reliable algorithms: These are genuine mathematical tasks.
Keywords: applied mathematics, technology, modelling, simulation, visualization, optimization, glass processing, spinning processes, fiber-fluid interaction, trubulence effects, topological optimization, multicriteria optimization, Uncertainty and Risk, financial mathematics, Malliavin calculus, Monte-Carlo methods, virtual material design, filtration, bio-informatics, system biology
(29 pages, 2004)

69. R. Ewing, O. Iliev, R. Lazarov, A. Naumovich

On convergence of certain finite difference discretizations for 1D poroelasticity interface problems

Finite difference discretizations of 1D poroelasticity equations with discontinuous coefficients are analyzed. A recently suggested FD discretization of poroelasticity equations with constant coefficients on staggered grid, [5], is used as a basis. A careful treatment of the interfaces leads to harmonic averaging of the discontinuous coefficients. Here, convergence for the pressure and for the displacement is proven in certain norms for the scheme with harmonic averaging (HA). Order of convergence 1.5 is proven for arbitrary located interface, and second order convergence is proven for the case when the interface coincides with a grid node. Furthermore, following the ideas from [3], modified HA discretization are suggested for particular cases. The velocity and the stress are approximated with second order on the interface in this case. It is shown that for wide class of problems, the modified discretization provides better accuracy. Second order convergence for modified scheme is proven for the case when the interface coincides with a displacement grid node. Numerical experiments are presented in order to illustrate our considerations.
Keywords: poroelasticity, multilayered material, finite volume discretizations, MAC type grid, error estimates
(26 pages,2004)

70. W. Dörfler, O. Iliev, D. Stoyanov, D. Vassileva

On Efficient Simulation of Non-Newtonian Flow in Saturated Porous Media with a Multigrid Adaptive Refinement Solver

Flow of non-Newtonian in saturated porous media can be described by the continuity equation and the generalized Darcy law. Efficient solution of the resulting second order nonlinear elliptic equation is discussed here. The equation is discretized by a finite volume method on a cell-centered grid. Local adaptive refinement of the grid is introduced in order to reduce the number of unknowns. A special implementation approach is used, which allows us to perform unstructured local refinement in conjunction with the finite volume discretization. Two residual based error indicators are exploited in the adaptive refinement criterion. Second order accurate discretization on the interfaces between refined and non-refined subdomains, as well as on the boundaries with Dirichlet boundary condition, are presented here, as an essential part of the accurate and efficient algorithm. A nonlinear full approximation storage multigrid algorithm is developed especially for the above described composite (coarse plus locally refined) grid approach. In particular, second order approximation around interfaces is a result of a quadratic approximation of slave nodes in the multigrid - adaptive refinement (MG-AR) algorithm. Results from numerical solution of various academic and practice-induced problems are presented and the performance of the solver is discussed.
Keywords: Nonlinear multigrid, adaptive renement, non-Newtonian in porous media
(25 pages, 2004)

71. J. Kalcsics, S. Nickel, M. Schröder

Towards a Unified Territory Design Approach – Applications, Algorithms and GIS Integration

Territory design may be viewed as the problem of grouping small geographic areas into larger geographic clusters called territories in such a way that the latter are acceptable according to relevant planning criteria. In this paper we review the existing literature for applications of territory design problems and solution approaches for solving these types of problems. After identifying features common to all applications we introduce a basic territory design model and present in detail two approaches for solving this model: a classical location–allocation approach combined with optimal split resolution techniques and a newly developed computational geometry based method. We present computational results indicating the efficiency and suitability of the latter method for solving large–scale practical problems in an interactive environment. Furthermore, we discuss extensions to the basic model and its integration into Geographic Information Systems.
Keywords: territory desgin, political districting, sales territory alignment, optimization algorithms, Geographical Information Systems
(40 pages, 2005)

72. K. Schladitz, S. Peters, D. Reinel-Bitzer, A. Wiegmann, J. Ohser

Design of acoustic trim based on geometric modeling and flow simulation for non-woven

In order to optimize the acoustic properties of a stacked fiber non-woven, the microstructure of the non-woven is modeled by a macroscopically homogeneous random system of straight cylinders (tubes). That is, the fibers are modeled by a spatially stationary random system of lines (Poisson line process), dilated by a sphere. Pressing the non-woven causes anisotropy. In our model, this anisotropy is described by a one parametric distribution of the direction of the fibers. In the present application, the anisotropy parameter has to be estimated from 2d reflected light microscopic images of microsections of the non-woven.
After fitting the model, the flow is computed in digitized realizations of the stochastic geometric model using the lattice Boltzmann method. Based on the flow resistivity, the formulas of Delany and Bazley predict the frequency-dependent acoustic absorption of the non-woven in the impedance tube.
Using the geometric model, the description of a non-woven with improved acoustic absorption properties is obtained in the following way: First, the fiber thicknesses, porosity and anisotropy of the fiber system are modified. Then the flow and acoustics simulations are performed in the new sample. These two steps are repeatedc for various sets of parameters. Finally, the set of parameters for the geometric model leading to the best acoustic absorption is chosen.
Keywords: random system of fibers, Poisson line process, flow resistivity, acoustic absorption, Lattice-Boltzmann method, non-woven
(21 pages, 2005)

73. V. Rutka, A. Wiegmann

Explicit Jump Immersed Interface Method for virtual material design of the effective elastic moduli of composite materials

Virtual material design is the microscopic variation of materials in the computer, followed by the numerical evaluation of the effect of this variation on the material's macroscopic properties. The goal of this procedure is an in some sense improved material. Here, we give examples regarding the dependence of the effective elastic moduli of a composite material on the geometry of the shape of an inclusion. A new approach on how to solve such interface problems avoids mesh generation and gives second order accurate results even in the vicinity of the interface.
The Explicit Jump Immersed Interface Method is a finite difference method for elliptic partial differential equations that works on an equidistant Cartesian grid in spite of non-grid aligned discontinuities in equation parameters and solution. Near discontinuities, the standard finite difference approximations are modified by adding correction terms that involve jumps in the function and its derivatives. This work derives the correction terms for two dimensional linear elasticity with piecewise constant coefficients, i. e. for composite materials. It demonstrates numerically convergence and approximation properties of the method.
Keywords: virtual material design, explicit jump immersed interface method, effective elastic moduli, composite materials
(22 pages, 2005)

74. T. Hanne

Eine Übersicht zum Scheduling von Baustellen

Im diesem Dokument werden Aspekte der formalen zeitlichen Planung bzw. des Scheduling für Bauprojekte anhand ausgewählter Literatur diskutiert. Auf allgemeine Aspekte des Scheduling soll dabei nicht eingegangen werden. Hierzu seien als Standard-Referenzen nur Brucker (2004) und Pinedo (1995) genannt. Zu allgemeinen Fragen des Projekt-Managements sei auf Kerzner (2003) verwiesen.
Im Abschnitt 1 werden einige Anforderungen und Besonderheiten der Planung von Baustellen diskutiert. Diese treten allerdings auch in zahlreichen anderen Bereichen der Produktionsplanung und des Projektmanagements auf. In Abschnitt 2 werden dann Aspekte zur Formalisierung von Scheduling-Problemen in der Bauwirtschaft diskutiert, insbesondere Ziele und zu berücksichtigende Restriktionen. Auf eine mathematische Formalisierung wird dabei allerdings verzichtet. Abschnitt 3 bietet eine Übersicht über Verfahren und grundlegende Techniken für die Berechnung von Schedules. In Abschnitt 4 wird ein Überblick über vorhandene Software, zum einen verbreitete Internationale Software, zum anderen deutschsprachige Branchenlösungen, gegeben. Anschließend werden Schlussfolgerungen gezogen und es erfolgt eine Auflistung der Literaturquellen.
Keywords: Projektplanung, Scheduling, Bauplanung, Bauindustrie
(32 pages, 2005)

75. J. Linn

The Folgar–Tucker Model as a Differential Algebraic System for Fiber Orientation Calculation

The Folgar–Tucker equation (FTE) is the model most frequently used for the prediction of fiber orientation (FO) in simulations of the injection molding process for short–fiber reinforced thermoplasts. In contrast to its widespread use in injection molding simulations, little is known about the mathematical properties of the FTE: an investigation of e. g. its phase space M_{FT} has been presented only recently [12]. The restriction of the dependent variable of the FTE to the set M_{FT} turns the FTE into a differential algebraic system (DAS), a fact which is commonly neglected when devising numerical schemes for the integration of the FTE. In this article we present some recent results on the problem of trace stability as well as some introductory material which complements our recent paper [12].
Keywords: fiber orientation, Folgar–Tucker model, invariants, algebraic constraints, phase space, trace stability
(15 pages, 2005)

76. M. Speckert, K. Dreßler, H. Mauch, A. Lion, G. J. Wierda

Simulation eines neuartigen Prüfsystems für Achserprobungen durch MKS-Modellierung einschließlich Regelung

Testing new suspensions based on real load data is performed on elaborate multi channel test rigs. Usually, wheel forces and moments measured during driving maneuvers are reproduced by the test rig. Because of the complicated interaction between test rig and suspension each new rig configuration has to prove its efficiency with respect to the requirements and the configuration might be subject to optimization.
This paper deals with mathematical and physical modeling of a new concept of a test rig which is based on two hexapods. The model contains the geometric configuration as well as the hydraulics and the controller. It is implemented as an ADAMS/Car template and can be combined with different suspension models to get a complete assembly representing the entire test rig. Using this model, all steps required for a real test run such as controller adaptation, drive file iteration and simulation can be performed. Geometric or hydraulic parameters can be modified easily to improve the setup and adapt the system to the suspension and the given load data.
The model supports and accompanies the introduction of the new rig concept and can be used to prepare real tests on a virtual basis. Using both a front and a rear suspension the approach is described and the potentials coming with the simulation are pointed out.
Keywords: virtual test rig, suspension testing, multibody simulation, modeling hexapod test rig, optimization of test rig configuration
(20 pages, 2005)
In deutscher Sprache; bereits erschienen in: VDI-Berichte Nr. 1900, VDI-Verlag GmbH Düsseldorf (2005), Seiten 227-246

77. K.-H. Küfer, M. Monz, A. Scherrer, P. Süss, F. Alonso, A. S. A. Sultan, Th. Bortfeld, D. Craft, Chr. Thieke

Multicriteria optimization in intensity modulated radiotherapy planning

Inverse treatment planning of intensity modulated radiothrapy is a multicriteria optimization problem: planners have to find optimal compromises between a sufficiently highdose intumor tissuethat garantuee a high tumor control, and, dangerous overdosing of critical structures, in order to avoid high normal tissue complcication problems.
The approach presented in this work demonstrates how to state a flexible generic multicriteria model of the IMRT planning problem and how to produce clinically highly relevant Pareto-solutions. The model is imbedded in a principal concept of Reverse Engineering, a general optimization paradigm for design problems. Relevant parts of the Pareto-set are approximated by using extreme compromises as cornerstone solutions, a concept that is always feasible if box constraints for objective funtions are available. A major practical drawback of generic multicriteria concepts trying to compute or approximate parts of the Pareto-set is the high computational effort. This problem can be overcome by exploitation of an inherent asymmetry of the IMRT planning problem and an adaptive approximation scheme for optimal solutions based on an adaptive clustering preprocessing technique. Finally, a coherent approach for calculating and selecting solutions in a real-timeinteractive decision-making process is presented. The paper is concluded with clinical examples and a discussion of ongoing research topics.
Keywords: multicriteria optimization, extreme solutions, real-time decision making, adaptive approximation schemes, clustering methods, IMRT planning, reverse engineering
(51 pages, 2005)

78. S. Amstutz, H. Andrä

A new algorithm for topology optimization using a level-set method

The levelset method has been recently introduced in the field of shape optimization, enabling a smooth representation of the boundaries on a fixed mesh and therefore leading to fast numerical algorithms. However, most of these algorithms use a HamiltonJacobi equation to connect the evolution of the levelset function with the deformation of the contours, and consequently they cannot create any new holes in the domain (at least in 2D). In this work, we propose an evolution equation for the levelset function based on a generalization of the concept of topological gradient. This results in a new algorithm allowing for all kinds of topology changes.
Keywords: shape optimization, topology optimization, topological sensitivity, level-set
(22 pages, 2005)

79. N. Ettrich

Generation of surface elevation models for urban drainage simulation

Traditional methods fail for the purpose of simulating the complete flow process in urban areas as a consequence of heavy rainfall and as required by the European Standard EN-752 since the bi-directional coupling between sewer and surface is not properly handled. The methodology, developed in the BMBF/EUREKA-project RisUrSim, solves this problem by carrying out the runoff on the basis of shallow water equations solved on high-resolution surface grids. Exchange nodes between the sewer and the surface, like inlets and manholes, are located in the computational grid and water leaving the sewer in case of surcharge is further distributed on the surface.
So far, it has been a problem to get the dense topographical information needed to build models suitable for hydrodynamic runoff calculation in urban areas. Recent airborne data collection methods like laser scanning, however, offer a great chance to economically gather densely sampled input data. This paper studies the potential of such laser-scan data sets for urban water hydrodynamics.
Keywords: Flooding, simulation, urban elevation models, laser scanning
(22 pages, 2005)

80. H. Andrä, J. Linn, I. Matei, I. Shklyar, K. Steiner, E. Teichmann

OPTCAST – Entwicklung adäquater Strukturoptimierungsverfahren für Gießereien Technischer Bericht (KURZFASSUNG)

Im vorliegenden Bericht werden die Erfahrungen und Ergebnisse aus dem Projekt **OptCast** zusammengestellt. Das Ziel dieses Projekts bestand (a) in der Anpassung der Methodik der automatischen Strukturoptimierung für Gussteile und (b) in der Entwicklung und Bereitstellung von gießereispezifischen Optimierungstools für Gießereien und Ingenieurbüros.
Gießtechnische Restriktionen lassen sich nicht auf geometrische Restriktionen reduzieren, sondern sind nur über eine Gießsimulation (Erstarrungssimulation und Eigenspannungsanalyse) adäquat erfassbar, da die lokalen Materialeigenschaften des Gussteils nicht nur von der geometrischen Form des Teils, sondern auch vom verwendeten Material abhängen. Wegen dieser Erkenntnis wurde ein neuartiges iteratives Topologieoptimierungsverfahren unter Verwendung der Level-Set-Technik entwickelt, bei dem keine variable Dichte des Materials eingeführt wird. In jeder Iteration wird ein scharfer Rand des Bauteils berechnet. Somit ist die Gießsimulation in den iterativen Optimierungsprozess integrierbar.
Der Bericht ist wie folgt aufgebaut: In Abschnitt 2 wird der Anforderungskatalog erläutert, der sich aus der Bearbeitung von Benchmark-Problemen in der ersten Projektphase ergab. In Abschnitt 3 werden die Benchmark-Probleme und deren Lösung mit den im Projekt entwickelten Tools beschrieben. Abschnitt 4 enthält die Beschreibung der neu entwickelten Schnittstellen und die mathematische Formulierung des Topologieoptimierungsproblems. Im letzten Abschnitt wird das neue Topologieoptimierungsverfahren, das die Simulation des Gießprozesses einschließt, erläutert.
Keywords: Topologieoptimierung, Level-Set-Methode, Gießprozesssimulation, Gießtechnische Restriktionen, CAE-Kette zur Strukturoptimierung
(77 pages, 2005)

81. N. Marheineke, R. Wegener

Fiber Dynamics in Turbulent Flows Part I: General Modeling Framework

The paper at hand deals with the modeling of turbulence effects on the dynamics of a long slender elastic fiber. Independent of the choice of the drag model, a general aerodynamic force concept is derived on the basis of the velocity field for the randomly fluctuating component of the flow. Its construction as centered differentiable Gaussian field complies thereby with the requirements of the stochastic k-ε turbulence model and Kolmogorov's universal equilibrium theory on local isotropy.

Keywords: fiber-fluid interaction; Cosserat rod; turbulence modeling; Kolmogorov's energy spectrum; double-velocity correlations; differentiable Gaussian fields

Part II: Specific Taylor Drag

In [12], an aerodynamic force concept for a general air drag model is derived on top of a stochastic k-ε description for a turbulent flow field. The turbulence effects on the dynamics of a long slender elastic fiber are particularly modeled by a correlated random Gaussian force and in its asymptotic limit on a macroscopic fiber scale by Gaussian white noise with flow-dependent amplitude. The paper at hand now presents quantitative similarity estimates and numerical comparisons for the concrete choice of a Taylor drag model in a given application.

Keywords: flexible fibers; k-ε turbulence model; fiber-turbulence interaction scales; air drag; random Gaussian aerodynamic force; white noise; stochastic differential equations; ARMA process

(38 pages, 2005)

82. C. H. Lampert, O. Wirjadi

An Optimal Non-Orthogonal Separation of the Anisotropic Gaussian Convolution Filter

We give ananalytical and geometrical treatment of what it means to separate a Gaussian kernel along arbitrary axes in R^n, and we present a separation scheme that allows to efficiently implement anisotropic Gaussian convolution filters in arbitrary dimension. Based on our previous analysis we show that this scheme is optimal with regard to the number of memory accesses and interpolation operations needed.

Our method relies on non-orthogonal convolution axes and works completely in image space. Thus, it avoids the need for an FFT-subroutine. Depending on the accuracy and speed requirements, different interpolation schemes and methods to implement the one-dimensional Gaussian (FIR, IIR) can be integrated. The algorithm is also feasible for hardware that does not contain a floating-point unit.

Special emphasis is laid on analyzing the performance and accuracy of our method. In particular, we show that without anyspecial optimization of the source code, our method can perform anisotropic Gaussian filtering faster than methods relying on the Fast Fourier Transform.

Keywords: Anisotropic Gaussian filter, linear filtering, orientation space, nD image processing, separable filters

(25 pages, 2005)

83. H. Andrä, D. Stoyanov

Error indicators in the parallel finite element solver for linear elasticity DDFEM

This report discusses two approaches for a posteriori error indication in the linear elasticity solver DDFEM: An indicator based on the Richardson extrapolation and Zienkiewicz-Zhu-type indicator.

The solver handles 3D linear elasticity steady-state problems. It uses own input language to de-scribe the mesh and the boundary conditions. Finite element discretization over tetrahedral meshes with first or second order shape functions (hierarchical basis) has been used to resolve the model. The parallelization of the numerical method is based on the domain decomposition approach. DDFEM is highly portable over a set of parallel computer architectures supporting the MPI-standard.

Keywords: linear elasticity, finite element method, hierarchical shape functions, domain decom-position, parallel implementation, a posteriori error estimates

(21 pages, 2006)

84. M. Schröder, I. Solchenbach

Optimization of Transfer Quality in Regional Public Transit

In this paper we address the improvement of transfer quality in public mass transit networks. Generally there are several transit operators offering service and our work is motivated by the question how their timetables can be altered to yield optimized transfer possibilities in the over-all network. To achieve this, only small changes to the timetables are allowed.

The set-up makes it possible to use a quadratic semi-assignment model to solve the optimization problem. We apply this model, equipped with a new way to assess transfer quality, to the solu-tion of four real-world examples. It turns out that improvements in overall transfer quality can be determined by such optimization-based techniques. Therefore they can serve as a first step to-wards a decision support tool for planners of regional transit networks.

Keywords: public transit, transfer quality, quadratic assignment problem

(16 pages, 2006)

85. A. Naumovich, F. J. Gaspar

On a multigrid solver for the three-dimensional Biot poroelasticity system in multilayered domains

In this paper, we present problem-dependent prolongation and problem-dependent restriction for a multigrid solver for the three-dimensional Biot poroelasticity system, which is solved in a multilayered domain. The system is discretized on a staggered grid using the finite volume method. During the discretization, special care is taken of the discontinuous coefficients. For the efficient multigrid solver, a need in operator-dependent restriction and/or prolongation arises. We derive these operators so that they are consistent with the discretization. They account for the discontinuities of the coefficients, as well as for the coupling of the unknowns within the Biot system. A set of numerical experiments shows necessity of use of the operator-dependent restriction and prolongation in the multigrid solver for the considered class of problems.

Keywords: poroelasticity, interface problem, multigrid, operator-dependent prolongation

(11 pages, 2006)

86. S. Panda, R. Wegener, N. Marheineke

Slender Body Theory for the Dynamics of Curved Viscous Fibers

The paper at hand presents a slender body theory for the dynamics of a curved inertial viscous Newtonian fiber. Neglecting surface tension and temperature dependence, the fiber flow is modeled as a three-dimensional free boundary value problem via instationary incompressible Navier-Stokes equations. From regular asymptotic expansions in powers of the slenderness parameter leading-order balance laws for mass (cross-section) and momentum are derived that combine the unrestricted motion of the fiber center-line with the inner viscous transport. The physically reasonable form of the one-dimensional fiber model results thereby from the introduction of the intrinsic velocity that characterizes the convective terms.

Keywords: curved viscous fibers; fluid dynamics; Navier-Stokes equations; free boundary value problem; asymptotic expansions; slender body theory

(14 pages, 2006)

87. E. Ivanov, H. Andrä, A. Kudryavtsev

Domain Decomposition Approach for Automatic Parallel Generation of Tetrahedral Grids

The desire to simulate more and more geometrical and physical features of technical structures and the availability of parallel computers and parallel numerical solvers which can exploit the power of these machines have lead to a steady increase in the number of grid elements used. Memory requirements and computational time are too large for usual serial PCs. An a priori partitioning algorithm for the parallel generation of 3D nonoverlapping compatible unstructured meshes based on a CAD surface description is presented in this paper. Emphasis is given to practical issues and implementation rather than to theoretical complexity. To achieve robustness of the algorithm with respect to the geometrical shape of the structure authors propose to have several or many but relatively simple algorithmic steps. The geometrical domain decomposition approach has been applied. It allows us to use classic 2D and 3D high-quality Delaunay mesh generators for independent and simultaneous volume meshing. Different aspects of load balancing methods are also explored in the paper. The MPI library and SPMD model are used for parallel grid generator implementation. Several 3D examples are shown.

Key words: Grid Generation, Unstructured Grid, Delaunay Triangulation, Parallel Programming, Domain Decomposition, Load Balancing

(18 pages, 2006)

88. S. Tiwari, S. Antonov, D. Hietel, J. Kuhnert, R. Wegener

A Meshfree Method for Simulations of Interactions between Fluids and Flexible Structures

We present the application of a meshfree method for simulations of interaction between fluids and flexible structures. As a flexible structure we consider a sheet of paper. In a twodimensional framework this sheet can be modeled as curve by the dynamical Kirchhoff-Love theory. The external forces taken into account are gravitation and the pressure difference between upper and lower surface of the sheet. This pressure difference is computed using the Finite Pointset Method (FPM) for the incompressible Navier-Stokes equations. FPM is a meshfree, Lagrangian particle method. The dynamics of the sheet are computed by a finite difference method. We show the suitability of the meshfree method for simulations of fluidstructure interaction in several applications

Key words: Meshfree Method, FPM, Fluid Structure Interaction, Sheet of Paper, Dynamical Coupling

(16 pages, 2006)

89. R. Ciegis , O. Iliev, V. Starikovicius, K. Steiner

Numerical Algorithms for Solving Problems of Multiphase Flows in Porous Media

In this paper we discuss numerical algorithms for solving the system of nonlinear PDEs, arising in modelling of two-phase ows in porous media, as well as the proper object oriented implementation of these algorithms. Global pressure model for isothermal two-phase immiscible flow in porous media is considered in this paper. Finite-volume method is used for the space discretization of the system of PDEs. Different time stepping discretizations and linearization approaches are discussed. The main concepts of the PDE software tool MfsolverC++ are given. Numerical results for one realistic problem are presented.

Keywords: nonlinear algorithms, finite-volume method, software tools, porous media, flows

(16 pages, 2006)

90. D. Niedziela, O. Iliev, A. Latz

On 3D Numerical Simulations of Viscoelastic Fluids

In this work we present and solve a class of non–Newtonian viscoelastic fluid flow problems. Models for non-Newtonian fluids can be classified into three large groups depending on the type of the constitutive relation used: algebraic, differential and integral. The first type of models are most simple one, the last are the most physically adequate ones. Here we consider some models from the first and the third groups, and present robust and efficient algorithms for their solution. We present new mathematical model, which belongs to the class of generalized Newtonian models and is able to account for the anisotropy of the viscosity tensor observed in many real liquids. In particular, we discuss a unified model that captures both shear thinning and extensional thickening for complex flows. The resulting large variations of the viscosity tensor in space and time are leading to a strong numerical coupling of the momentum equations due to the appearance of mixed derivatives in the discretization. To treat this strong coupling appropriately, we present two modifications of classical projection methods (like e.g. SIMPLE). In the first modification all momentum equations are solved coupled (i.e. mixed derivative are discretized implicitly) but still iterations are performed between the momen-

tum equations and the continuity equation. The second one is a fully coupled method, where momentum and continuity equation are solved together using a proper preconditioner. The models involving integral constitutive relation which accounts for the history of deformations, result in a system of integro-differential equations. To solve it, we suggest a proper splitting scheme, which treats the integral and the differential parts consecutively. Integral Oldroyd B and Doi Edwards models are used to simulate flows of dilute and concentrated polymer solutions, respectively.
Keywords: non–Newtonian fluids, anisotropic viscosity, integral constitutive equation
(18 pages, 2006)

91. A. Winterfeld

Application of general semi-infinite Programming to Lapidary Cutting Problems

We consider a volume maximization problemarising in gemstone cutting industry. The problem is formulated as a general semi-infnite program(GSIP)and solved using an interior point method developed by Stein. It is shown, that the convexity assumption needed for the convergence of the algorithm can be satisfied by appropriate model-ling. Clustering techniques are used to reduce the number of container constraints, which is necessary to make the subproblems practically tractable. An iterative process consisting of GSIP optimization and adaptive refinement steps is then employed to obtain an optimal solution which is also feasible for the original problem. Some numeri-cal results based on real world data are also presented.
Keywords: large scale optimization, nonlinear programming, general semi-infinite optimization, design centering, clustering
(26 pages, 2006)

92. J. Orlik, A. Ostrovska

Space-Time Finite Element Approximation and Numerical Solution of Hereditary Linear Viscoelasticity Problems

In this paper we suggest a fast numerical approach to treat problems of the hereditary linear viscoelasticity, which results in the system of elliptic partial differential equations in space variables, who's coefficients are Volterra integral operators of the second kind in time. We propose to approximate the relaxation kernels by the product of purely time- and space-dependent terms, which is achieved by their piecewisepolynomial space-interpolation. A priori error estimate was obtained and it was shown, that such approximation does not decrease the convergence order, when an interpolation polynomial is chosen of the same order as the shape functions for the spatial finite element approximation, while the computational effort is significantly reduced.
Keywords: hereditary viscoelasticity; kern approximation by interpolation; space-time finite element approximation, stability and a priori estimate
(24 pages, 2006)

93. V. Rutka, A. Wiegmann, H. Andrä

EJIIM for Calculation of effective Elastic Moduli in 3D Linear Elasticity

The Explicit Jump Immersed Interface Method solves boundary value problems by embedding arbitrary domains in rectangular parallelepipeds and extending the boundary value problem to such a domain. Now the boundary conditions become jump conditions, and separate equations for the discretized solution of the pde and for the jump conditions are written. In thefirst set of equations, the jumps correct standard difference formulas, in the second set of equations solution values from interior grid points are used to compute quantities on the interface. For constant coefficient pde, the first set can be solved very efficiently by direct Fast Fourier transform inversion, and this is used to efficiently evaluate the smaller Schur-complement matrix-vector multiplication in a conjugate gradient approach to find the jumps. Here this approch is applied to the three-dimensional equations of linear elasticity. The resulting method is second order convergent for the displacements in the maximum norm as the grid is refined. It is applied to calculate the effective elastic moduli of fibrous and porous microstructures in three dimensions using the strain energy equivalence principle. From these effective moduli, best estimates under various symmetry assumptions are calculated.
Keywords: Elliptic PDE, linear elasticity, irregular domain, finite differences, fast solvers, effective elastic moduli
(24 pages, 2006)

94. A. Wiegmann, A. Zemitis

EJ-HEAT: A Fast Explicit Jump Harmonic Averaging Solver for the Effective Heat Conductivity of Composite Materials

The stationary heat equation is solved with periodic boundary conditions in geometrically complex composite materials with high contrast in the thermal conductivities of the individual phases. This is achieved by harmonic averaging and explicitly introducing the jumps across the material interfaces as additional variables. The continuity of the heat flux yields the needed extra equations for these variables. A Schur-complent formulation for the new variables is derived that is solved using the FFT and BiCGStab methods.
The EJ-HEAT solver is given as a 3-page Matlab program in the Appendix. The C++ implementation is used for material design studies. It solves 3-dimensional problems with around 190 Mio variables on a 64-bit AMD Opteron desktop system in less than 6 GB memory and in minutes to hours, depending on the contrast and required accuracy.
The approach may also be used to compute effective electric conductivities because they are governed by the stationary heat equation.
Keywords: Stationary heat equation, effective thermal conductivity, explicit jump, discontinuous coefficients, virtual material design, microstructure simulation, EJ-HEAT
(21 pages, 2006)

95. A. Naumovich

On a finite volume discretization of the three-dimensional Biot poroelasticity system in multilayered domains

In this paper we propose a finite volume discretization for the threedimensional Biot poroelasticity system in multilayered domains. For the stability reasons, staggered grids are used. The discretization accounts for discontinuity of the coefficients across the interfaces between layers with different physical properties. Numerical experiments, based on the proposed discretization showed second order convergence in the maximum norm for the primary as well as flux unknowns of the system. A certain application example is presented as well.
Keywords: Biot poroelasticity system, interface problems, finite volume discretization, finite difference method.
(21 pages, 2006)

96. M. Krekel, J. Wenzel

A unified approach to Credit Default Swaption and Constant Maturity Credit Default Swap valuation

In this paper we examine the pricing of arbitrary credit derivatives with the Libor Market Model with Default Risk. We show, how to setup the Monte Carlo-Simulation efficiently and investigate the accuracy of closed-form solutions for Credit Default Swaps, Credit Default Swaptions and Constant Maturity Credit Default Swaps. In addition we derive a new closed-form solution for Credit Default Swaptions which allows for time-dependent volatility and abitrary correlation structure of default intensities.
Keywords: LIBOR market model, credit risk, Credit Default Swaption, Constant Maturity Credit Default Swap-method.
(43 pages, 2006)

Status quo: October 2006